Universität Rostock

Traditio et Innovatio

Investigation of heavy petroleum-derived material with thermogravimetry coupled to high resolution Fourier transform ion cyclotron resonance mass spectrometry

KUMULATIVE DISSERTATION

ZUR ERLANGUNG DES AKADEMISCHEN GRADES EINES

DOCTOR RERUM NATURALIUM (DR. RER. NAT.)

DER MATHEMATISCH-NATURWISSENSCHAFTLICHEN FAKULTÄT

DER UNIVERSITÄT ROSTOCK

VORGELEGT VON

ANIKA NEUMANN

GEB. AM 29.NOVEMBER 1991 IN BRAUNSCHWEIG

ROSTOCK, November 2020

https://doi.org/10.18453/rosdok_id00002988

GUTACHTER:

Prof. Dr. Ralf Zimmermann, Universität Rostock, Institut für Chemie

Dr. habil. Pierre Giusti, Total Research and Technology Gonfreville TRTG

JAHR DER EINREICHUNG: 2020

JAHR DER VERTEIDIGUNG: 2021

"Imagination
is more important than knowledge,
because knowledge
is limited."

(Albert Einstein)

Acknowledgement

At first, I would like to thank Prof. Dr. Ralf Zimmermann that I could join his working group for my Bachelor thesis, Master thesis, and also for the four and a half years, which I needed to finally write my PhD thesis. I am very glad that I will be allowed to be further a part of your group!

I would particularly like to thank Martin Sklorz, who supported me in my scientific work and who I could always ask for help, when I had any (technical) problems. I would like to express here my admiration for his enormous, broad knowledge and all the small details, which he can keep in mind.

Furthermore, special thanks go to Christopher Rüger. He was my mentor in so many different things and he rapidly became one of my best friends. Over the years of our teamwork, he taught me many of the knowledge I needed to finally write this thesis. I really look forward to our future collaborations!

In addition, I would like to thank all my colleagues from Rostock and Munich, who created a very nice working atmosphere and with who I really liked to spend some free time. I thank Andrea Schaarschmidt who managed many orderings and conducted smaller laboratory work for me. Furthermore, I thank Sabine Haack for preparing me well for supervising our students during the laboratory internships and for nice chats about sewing. I thank Christin Kühl for her kindness and cooperativeness, helping me in all my organising questions. Special thanks go to Julian Schade, who is the best colleague I can think of. He is always cooperative and a good friend. I would be very glad, if we could still work together in the future.

Moreover, I would like to thank my best friends. I would particularly like to thank Johanna Claus, who will be named Johanna Meyer soon, for our great, longstanding friendship, which lasts since the second semester. Without her, I would have given up many times on this way. Furthermore, I thank Lise Oberem, Anne Paland, Jessica Schulz and Julia Steinsiek who have always supported me and who are great friends. I would like to thank Vanessa Stock as well, because she provided me refuge in her small store during the intensive writing phase when I really needed relief. She became a kind friend for me.

In the end, I would like to thank my mother and my father. They let me find my own way, although I know, that it was very hard especially for my mom. Nevertheless, I could ask them for help whenever I needed to. Thank you so much for that!

Danksagung

Zu allererst möchte ich mich bei Prof. Dr. Ralf Zimmermann für die herzliche Aufnahme in die Arbeitsgruppe bedanken, in der ich nun neben Bachelorarbeit und Masterarbeit nun auch die viereinhalb Jahre meiner Promotion verbringen konnte. Ich freue mich sehr, dass ich auch noch weiterhin Teil dieser Gruppe bleiben darf!

Mein besonderer Dank gilt Martin Sklorz, da er mich stets bei meinem wissenschaftlichen Arbeiten unterstützt hat und ich ihn immer bei (technischen) Problemen aller Art um Hilfe bitten konnte. Ich bewundere besonders sein immenses, breit aufgestelltes Wissen und die vielen Details, die er sich einfach so merken kann.

Ganz besonders möchte ich mich auch bei Christopher Rüger bedanken, der in so vielen verschiedenen Punkten mein Mentor war und auch schnell zu einem meiner besten Freunde wurde. Er hat mich über die Jahre unserer Zusammenarbeit viele der Dinge gelehrt, die ich brauchte, um diese Arbeit anfertigen zu können. Ich freue mich sehr, dass wir auch in Zukunft weiterhin zusammenarbeiten können!

Auch bedanke ich mich herzlich bei all meinen Rostocker und Münchner Kollegen, die eine sehr angenehme Arbeitsatmosphäre geschaffen haben und mit denen es stets Spaß gemacht Zeit zu verbringen. Ich danke Andrea Schaarschmidt für die vielen Bestellungen und kleinen Laborarbeiten, die sie mir abgenommen hat. Des Weiteren bedanke ich mich bei Sabine Haack für die tolle Vorbereitung auf die Praktikumsbetreuung und die vielen schönen Plausche übers Nähen. Ich danke Christin Kühl für ihre stete Freundlichkeit und Hilfsbereitschaft bei allen möglichen organisatorischen Fragen. Besonders möchte ich mich auch bei Julian Schade bedanken, dem besten Kollegen, den man sich wünschen kann! Er ist stets hilfsbereit und ein guter Freund. Ich würde mich freuen, wenn wir auch noch in Zukunft hier zusammen arbeiten können.

Zudem möchte ich mich bei meinen besten Freundinnen bedanken. Ganz besonders bedanke ich mich bei Johanna Claus, die bald Johanna Meyer heißen wird, für unsere langjährige, beständige Freundschaft, die eigentlich schon seit dem zweiten Semester besteht. Ohne sie hätte ich unterwegs auf diesem Weg bestimmt schon öfter aufgegeben. Des Weiteren bedanke ich mich bei Lise Oberem, Jessica Schulz, Anne Paland und Julia Steinsiek, die mich auch immer unterstützt haben und tolle Freundinnen sind. Auch möchte ich mich bei Vanessa Stock bedanken, die mir gerade in der letzten Zeit des intensiven Schreibens dieser Arbeit oft in ihrem kleinen Laden Zuflucht gewährt hat, wenn ich dringend etwas Ablenkung brauchte. Sie ist eine liebe Freundin für mich geworden.

Zuletzt bedanke ich mich bei meiner Mutter und meinem Vater. Sie haben mich meinen eigenen Weg gehen lassen, auch wenn das besonders meiner Mama immer schwer gefallen ist. Trotzdem konnte ich sie immer um Hilfe bitten, wenn ich wirklich welche brauchte. Vielen Dank dafür!

Content

Abbreviations ii
Summary iv
Zusammenfassung v
1 Motivation and aim 1
2 Introduction to petroleum derived materials 2
2.1 Petroleum 2
2.1.1 The Continuum Model of Petroleum 3
2.1.2 Petroleum refining 3
2.2 Polyethylene terephthalate 4
2.3 Bitumen 5
2.4 SARA-fractionation and Asphaltenes 6
3 Fundamentals of the applied techniques 7
3.1 Separation techniques 7
3.1.1 Thermogravimetry 7
3.1.2 Comprehensive two-dimensional gas chromatography 8
3.2 Mass spectrometry 9
3.2.1 Atmospheric pressure ionisation 10
3.2.1.1 Atmospheric pressure chemical ionisation 11
3.2.1.2 Atmospheric pressure photo ionisation 11
3.2.1.3 Atmospheric pressure laser ionisation 12
3.2.2 Fourier transform ion cyclotron resonance mass spectrometry 12
3.2.2.1 Instrumentation 12
3.2.2.2 Cyclotron motion 13
3.2.2.3 Measurement principle 14
3.2.2.4 Petroleomics 15
3.2.3 Time-of-flight mass spectrometry 17
4 Results 19
4.1 Evolved gas analysis coupled to FT-ICR MS and method integration for the analysis of complex mixtures 20
4.2 Application of evolved gas analysis high resolution mass spectrometry 23
4.2.1 Investigation of pyrolysis products of polyethylene terephthalate 23
4.2.2 Understanding the aging effects in bitumen at the molecular level 24
4.2.3 Chemical characterization of occluded material and pyrolysis products of asphaltenes 28

4.3 Development of new analysis techniques for the investigation of complex mixtures 33
4.3.1 Xe/Kr-atmospheric pressure photo ionisation 33
4.3.2 Atmospheric pressure single photon laser ionisation 35
5 Conclusion and Outlook 40
6 References 41
Appendix 52
Curriculum Vitae 52
Conference Contribution 53
Declaration on the contribution to the manuscripts for cumulative thesis 54
Publications for the cumulative thesis 56

Abbreviations

AEBP	atmospheric equivalent boiling point
AFM	atomic force microscopy
APCI	atmospheric pressure chemical ionisation
API	American Petroleum Institute
APLI	atmospheric pressure laser ionisation
APMPLI	atmospheric pressure multi-photon laser ionisation
APPI	atmospheric pressure photoionisation
APSPLI	atmospheric pressure single-photon laser ionisation
BC	boiling cut
C_5	n-pentane
C6	n-hexane
C_7	n-heptane
CID	collision induced dissociation
DBE	(ring) double bond equivalent
DCM	dichloromethane
DTG	derivative thermogravimetric signal
EGA	evolved gas analysis
EI	electron ionisation
ESI	electrospray ionisation
FID	Free induction decay
FT	Fourier transform
GC	gas chromatography
GC×GC	two-dimensional gas chromatography
HDM	hydrodemetallation
HDN	hydrodenitrofication
HDS	hydrodesulfuration
HFO	heavy fuel oil
HR	high-resolution
ICR	ion cyclotron resonance
IR	infra-red
L^2MS	two-step laser ionisation mass spectrometry
LC	liquid chromatography
m/z	mass over charge ratio
MeOH	methanol
MGO	marine gas oil
MS	mass spectrometry
NMR	nuclear magnetic resonance
PAH	polyaromatic hydrocarbon
PAV	pressure aging vessel
PE	polyethylene
PET	polyethylene terephthalate
PP	polypropylene
REMPI	resonance-enhanced multi photon ionisation
RF	radio frequency
RFT	rotating flask test
RP	resolving power
RT	retention time

RTFOT	rolling thin film oven test
SARA	saturates, aromatics, resins, asphaltenes
SPI	single photon ionisation
TA	thermal analysis
TG	thermogravimetry
TGA	thermal gravimetric analysis
THF	tetrahydrofuran
TIC	total ion chromatogram
TOF	time-of-flight
Tol	toluene
UV	ultraviolet
VGO	vacuum gas oil

Summary

This PhD thesis addresses the chemical characterization of heavy petroleum-derived materials at the molecular level by thermogravimetry coupled to high-resolution Fourier transform ion cyclotron resonance mass spectrometry (TG-FT-ICR MS). High-resolution mass spectrometry is able to simultaneously detect thousands of signals in a single mass spectrum and enables their sum formula attribution. Thermogravimetry serves as temperature-resolved sample introduction technique for evolved gas analysis of highly complex mixtures. Volatile and semi-volatile compounds are intactly volatilized, whereas high-molecular weight compounds are pyrolysed. However, although TG-FT-ICR MS has been shown to be a powerful analytical tool for the chemical description of heavy petroleum materials, its analytical capabilities can be expanded by the application of different ionisation techniques, sample fractionation, or data integration with other analytical techniques. Consequently, this PhD thesis also present further developments of ionisation techniques to enhance the chemical description of ultra-complex mixtures.

TG-FT-ICR MS was applied in this thesis in different petroleum related research fields, such as waste upgrading of polyethylene terephthalate, the investigation of bitumen aging as binder in road construction, or the chemical characterization of asphaltenes often related to several crude oil refining and production problems. Bitumen short-term aging was investigated by combining the strength of atmospheric pressure chemical ionisation (APCI) TG-FT-ICR MS, which sensitively ionises semi-polar to polar species, with two-dimensional gas chromatography high-resolution time-of-flight mass spectrometry (GC×GC-HR-TOF MS), which enabled the structural elucidation of volatile to semi-volatile compounds. The data integration of both methods provide insights into aging-related alterations: the abundance of oxygen-containing compounds, such as the O_1-, O_2-, S_1O_1-, and N_1O_1-class as well as distinct chemical functionalities, such as fluorenones and sulfoxides, were found to increase. The concentration of non-aromatic sulphur-containing compounds, including thiolanes, as well as aromatic nitrogen-containing compounds, such as acridines, were found to strongly decrease during aging. TG-FT-ICR MS further revealed valuable information on the most complex fraction of crude oil, the asphaltenes. With this technique, insights into precipitation effects of asphaltenes could be revealed. It could be shown, that the precipitation solvent strongly affects the composition of occluded material. Furthermore, highly purified asphaltenes were shown to release occluded material after extrography fractionation, which was most probably bonded in cooperative aggregates. The detection of pyrolysis fragments added information concerning the critical debate on the asphaltene structural motifs. The combination of different evolved analysis techniques, several ionisation methods as well as mass spectrometric analysers further enabled a recombination suggestion of an average, archipelago-type asphaltene molecule.

The further development of ionisation techniques helps to address a selected chemical space simplifying ultra-complex mixtures and reduce matrix effects. In the context of this PhD work, atmospheric pressure photoionisation applying a Xenon-discharge lamp (8.4 and 9.6 eV) was introduced, which enabled the efficient ionisation of highly aromatic compounds as radical cations. Moreover, a new ionisation technique was developed by using single photon laser ionisation under atmospheric pressure conditions (APSPLI). The concentration of oxygen was shown to be a crucial parameter in APSPLI with respect to VUV-induced dissociation of oxygen, which produces oxidised ionisation artefacts. However, artefacts could be reduced by applying O_2/H_2O filter cartridges to further purify the nitrogen supply, high nitrogen flow rates, and the ionisation of the analytes immediately after being introduced to the ionisation chamber. Furthermore, APSPLI was successfully applied to complex petroleum-derived mixtures introduced by thermogravimetry or gas chromatography coupling. In comparison to multi-photon based APLI, APSPLI highlights especially sulphur-containing compounds and covers therefore a broader chemical space.

Zusammenfassung

Diese Doktorarbeit adressiert die chemische Charakterisierung von schweren, erdölverwandten Materialien auf molekularer Ebene unter Verwendung von Thermogravimetrie gekoppelt an Fouriertransformation Ionenzyklotronresonanz-Massenspektrometrie (TG-FT-ICR MS). Hochauflösende Massenspektrometrie kann tausende Signale in einem Einzelspektrum gleichzeitig detektieren und Summenformeln zu ihnen zuweisen. Thermogravimetrie dient als temperaturaufgelöste Probenaufgabetechnik zur Emissionsgasanalyse von hochkomplexen Mischungen. Flüchtige und semi-flüchtige Komponenten werden intakt verdampft, wohingegen hochmolekulare Spezies pyrolysiert werden. Obwohl gezeigt wurde, dass TG-FT-ICR MS ein starkes analytisches Werkzeug für die chemische Beschreibung von schweren Erdölmaterialien ist, kann diese Methode durch den Einsatz verschiedener Ionisationstechniken, Probenfraktionierung oder der Zusammenführung verschiedener Datensätze anderer analytischer Techniken erweitert werden. Folglich zeigt diese Doktorarbeit auch die Weiterentwicklung von Ionisationstechniken, mit denen die chemische Beschreibung von ultra-komplexen Mischungen erweitert werden kann.

TG-FT-ICR MS wurde in dieser Arbeit für verschiedene erdölrelevante Forschungsgebiete, wie Abfallverwertung von Polyethylenterephthalat (PET), der Untersuchung von Alterung von Bitumen als Bindungsmaterial im Straßenbau und die chemische Charakterisierung von Asphaltenen, welche häufig mit verschiedenen Problemen der Erdölraffination und –produktion in Zusammenhang stehen, angewendet. Bitumen-Kurzzeitalterung wurde mittels der Kombination von Atmosphärendruck chemischer Ionisation (APCI) TG-FT-ICR MS, welche sensitiv semi- bis polare Komponenten ionisiert, und zweidimensionaler Gaschromatographie gekoppelt mit hochauflösender Flugzeit-Massenspektrometrie (GC×GC-HR-TOF MS), welche die strukturelle Aufklärung von flüchtigen und semi-flüchtigen Verbindungen ermöglicht. Die Zusammenführung der Datensätze beider Methoden bietet Einblicke in alterungsbezogene Änderungen: Die Häufigkeit von sauerstoffhaltigen Verbindungen, wie die O_1-, O_2-, S_1O_1-, und N_1O_1-Klasse sowie bestimmte chemische Funktionalitäten, wie Fluorenone und Sulfoxide, ist angestiegen. Die Konzentration von nicht-aromatischen schwefelhaltigen Verbindungen, wie Thiolane, und stickstoffhaltigen Verbindungen, wie Acridine, hat durch die Alterung abgenommen. TG-FT-ICR MS konnte außerdem wertvolle Informationen zu der komplexesten Fraktion von Erdöl, den Asphaltenen, beitragen. Mit dieser Technik konnten Einblicke in Fällungseffekte von Asphaltenen gewonnen werden. Es konnte gezeigt werden, dass das Fällungssolvent einen großen Einfluss auf die Zusammensetzung des okkludierten Materials hat. Des Weiteren wurde gezeigt, dass stark aufgereinigte Asphaltene nach Extrographie-Fraktionierung weiteres okkludiertes Material freisetzen, welches zuvor höchst wahrscheinlich in zusammenwirkenden Aggregaten gebunden war. Die Detektion von Pyrolysefragmenten konnte Informationen zu der Debatte um die molekulare Architektur von Asphaltenen beitragen. Die Kombination von verschiedenen Emissionsgasanalysetechniken, unterschiedlichen Ionisationstechniken und Massenanalysatoren erlaubte weiterhin einen Vorschlag für ein rekombiniertes, durchschnittliches Asphaltenemolekül der Archipelagostruktur.

Die Weiterentwicklung von Ionisationsmethoden hilft dabei, einen selektiven chemischen Bereich anzusprechen und dadurch ultra-komplexe Mischungen zu vereinfachen und Matrixeffekte zu reduzieren. Im Rahmen dieser Doktorarbeit wurde die Atmosphärendruck-Photoionisation mit einer Xenon-Gasentladungslampe (8.4 und 9.6 eV) eingeführt, welche die effiziente Ionisation von hocharomatischen Komponenten als Radikalkationen ermöglicht. Des Weiteren wurde eine neue Ionisationstechnik entwickelt, die Atmosphärendruck-Einphotonen-Laserionisierung (APSPLI). Die Konzentration von Restsauerstoff ist ein entscheidender Parameter in APSPLI mit Hinblick auf VUV-induzierte Dissoziation von Sauerstoff, welche zu oxidierten Ionisationsartefakten führt. Diese Artefakte können jedoch durch den Einsatz von O_2/H_2O-Filterkartuschen (Aufreinigung des Stickstoffzuflusses), hohen Stickstofffluss und der Ionisation sofort nach dem Eintreten der Substanzen in die Ionenquelle reduziert werden. APSPLI wurde auch erfolgreich zur Analyse von komplexen erdölverwandten Materialien eingesetzt, welche über thermogravimetrische und gaschromatographische Kopplung aufgegeben wurden. Im Vergleich zu der Multiphotonenionisation APLI, hebt APSPLI besonders schwefelhaltige Komponenten hervor und deckt somit einen breiteren chemischen Bereich ab.

1 Motivation and aim

Petroleum can be numbered among the most important resources of modern mankind. Due to its extensive usage during the last century, light crude oil reservoirs and easy to access petroleum reserves are mostly depleted. Heavy crude oils as well as unconventional oil reservoirs therefore raise in importance. However, due to the higher complexity and chemical diversity related with heavier feedstocks, petroleum production, transportation, storing, and refining are faced to increasing challenges. Heavy petroleum-derived material is often related to the formation of deposits or catalyst poisoning during the upgrading process. Similarly to the increasing problems during the production and processing, the chemical and compositional characterisation of those highly complex mixtures remain an analytical challenge.[1, 2]

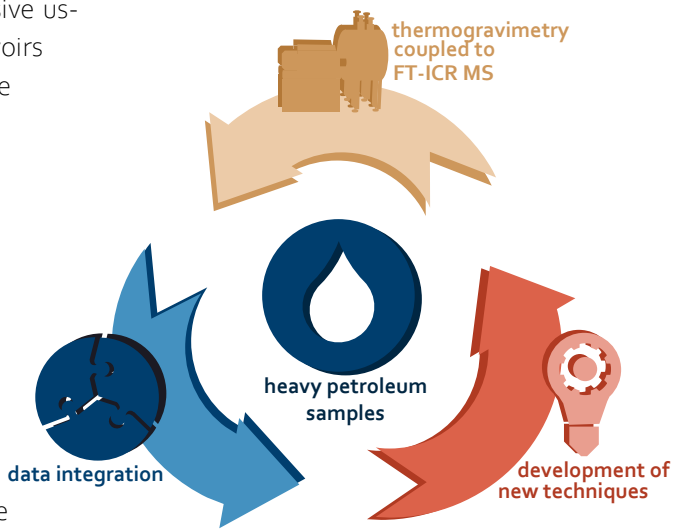

In the last decades, the analytical capabilities in the field of petroleum analysis drastically expanded. Especially, high-resolution Fourier transform ion cyclotron resonance mass spectrometry (FT-ICR MS) added valuable information at the molecular level due to its unbeaten resolving power and mass accuracy, which enables the calculation of sum formulae on the basis of the measured mass-to-charge ratio. However, only the combination of different analytical approaches with FT-ICR MS, such as several ionisation methods, fragmentation techniques, fractionation, or chromatographic separation, addresses the comprehensive chemical description of heavy petroleum derived material. [1, 3] Despite the continuous advances in analytical technology, the "petroleome" of crude oil is still not completely unravelled.

This PhD thesis aimed to comprehensively characterize heavy petroleum-derived material at the molecular level and addresses different petroleum related research fields such as polymer waste upgrading, aging of bitumen as binder in road construction, or asphaltenes often causing problems during the production and refining cycle of crude oil. In the context of this PhD work, the combination of FT-ICR MS and evolved gas analysis has been shown to provide valuable information on the most complex constituents of petroleum. Besides that, data integration strategies are presented combining the strengths of FT-ICR MS with different ionisation methods selectively ionising a specific compositional space. To integrate further structural information, mass spectrometric fragmentation techniques were applied and FT-ICR MS data were further supported by gas chromatographic information. I further aimed in this PhD work to expand the analytical capabilities for petroleum analysis by improving and extending selective and sensitive ionisation techniques. Within this context, I introduced atmospheric pressure photoionisation using xenon discharge lamps for ionisation, which leads to a simplification of the received spectra. Furthermore, atmospheric pressure single photon laser ionisation was introduced, aiming for a selective and sensitive ionisation of low- to semi-polar compounds.

2 Introduction to petroleum derived materials

The following section focuses on different petroleum derived materials investigated in this PhD work. Since petroleum is one of the most complex mixtures in the world, its complete and comprehensive chemical description remain an analytical challenge. This work primarily focusses on the investigation of the most complex fractions of crude oil, such as bitumen and asphaltenes, at the molecular level.

2.1 Petroleum

Petroleum or crude oil is a naturally occurring, highly complex mixture of hydrocarbons containing considerable amounts of sulphur, nitrogen, and oxygen as well as trace amounts of metals. The main components of the hydrocarbons are paraffins with 15-60 wt.-%, cycloalkanes (naphthenes) with 30-60 wt.-%, and aromatics with 3-30 wt.-%. [4] With respect to the elemental composition, crude oils are generally composed of 83 to 87 wt.-% carbon, 10 to 14 wt.-% hydrogen, 0.1 to 2 wt.-% nitrogen, 0.05 to 1.5 wt.-% oxygen, 0.05 to 6.0 wt.-% sulphur. Metals are contained as vanadium, nickel, copper and iron, which are often bound in porphyrin complexes. [4] Paraffins are present in crude oils as linear or branched alkanes, whereas naphthenes are mainly found as cyclo-pentane or cyclo-hexane units, which can occur as fused ring systems in heavier petroleum fractions. Aromatics are present as single or polyaromatic hydrocarbon (PAH) ring systems. Sulphur is incorporated in chemical functionalities forming mercaptans, thiols, sulfides, and thiophenes. Nitrogen occurs in pyridinic or pyrrolic structures as well as in more complex porphyrins. Oxygen is present as aliphatic/naphthenic/aromatic carboxylic acids, phenols, esters, ketones, or furans. However, acidic oxygen compounds are more abundant than non-acidic species. The actual composition of crude oils varies by their geological origin, but also between oil wells in the same field and even between different depths in the same well. The differences can be ascribed to variations in both molecular weight and types of molecules. [1, 5]

Crude oil originates from organic sediments, which were partially degraded by microbes under anaerobic conditions and matured over million years under elevated temperature and pressure. During the genesis, the partially degraded organic sediments form the source rock of the crude oil. After subsidence in deeper regions, the biomass is converted at elevated temperatures to solid, high-molecular weight hydrocarbons, which is called kerogen. During further maturation (katagenesis and metagenesis), the kerogen is transformed into natural gas, crude oil, and bitumen. From matured source rocks, natural gases and crude oil can migrate into porous rocks (primary migration). Due to their comparatively low density, the petroleum molecules migrate upwards until an impermeable rock is reached, leading to an enrichment of the petroleum in the rock below, which serves as reservoir rock. [3, 6]

Naturally occurring fossil materials can be divided into several subgroups, such as natural gas, crude oils, bitumen, asphaltites, asphaltoids, oil shale, natural waxes, kerogen, or coal. The individual subfractions can be further divided on chemical basis into saturated hydrocarbons, aromatics, resins, and asphaltenes. [1] Crude oils can be further classified very generally in terms of physical properties into light (conventional), heavy and extra heavy oils. A parameter commonly used for classification into the afore-mentioned categories is the American Petroleum Institute (API) gravity. API gravity is a measure of how light or heavy a petroleum-derived material is in comparison to water. Light and medium oils are in general attributed with an API gravity between 35° and 20°, heavy oils below 20°, and extra heavy oils below 10°. Bituminous materials range between 5° to 10°, whereas atmospheric residues are determined by 10° to 15° API and vacuum residues by 2° to 8° API. [1, 7]

2.1.1 The Continuum Model of Petroleum

In general, the heavier a crude oil or a distillation cut, the higher is its compositional and structural complexity. In the 1980s, Mieczyslaw M. Boduszynski introduced a Continuum Model of Petroleum, which addressed the compositional progression of petroleum-derived materials. Remarkably, the model was only based on the atmospheric equivalent boiling point (AEBP) trends of light petroleum fractions, molecular weight distributions, elemental analysis, gas chromatography of light distillation cuts as well as field desorption/ionisation low-resolution mass spectrometry. [8–10] The Boduszynski model proposes that different compounds with similar molecular weight cover a broad boiling point range, which in turn means that even narrow boiling cuts reveal a high chemical diversity [11]. Figure 1 illustrates the effect of the molecular weight and structure on the AEBP, as proposed by Boduszynski. For each homologues row, the boiling point increases as a function of the molecular weight. The steepest function is revealed for paraffins, whereas homologues containing naphthenic, aromatic or heteroatomic moieties exhibit an offset to higher boiling points. For a given AEBP, species with the highest molecular weight will be therefore paraffins, followed by naphthenes, aromatics, and heteroatom-containing compounds. [11] Approximately 30 years after its introduction, the Boduszynski model was proven for high boiling fractions and residues by ultra-high-resolution mass spectrometry explained in detail below. It was demonstrated, that carbon number, aromaticity, heteroatom content and complexity, continuously increase as a function of boiling point for petroleum. [12–14]

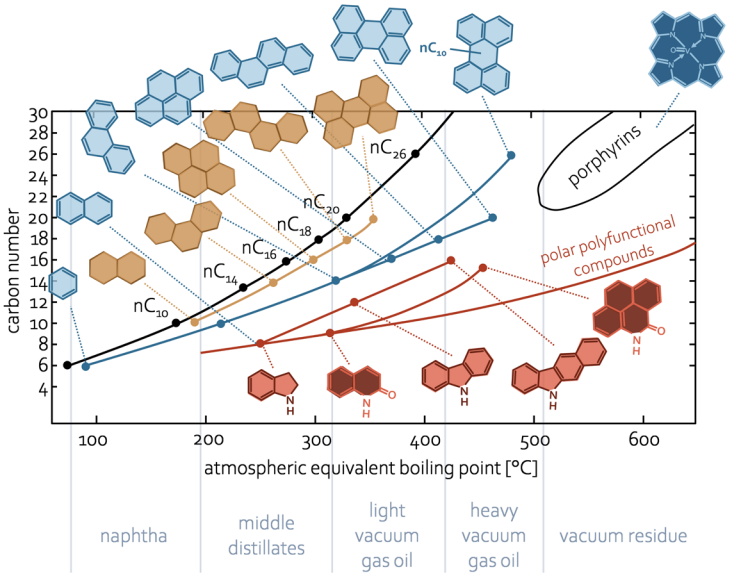

Figure 1: The effect of molecular structure and weight on the atmospheric equivalent boiling point.

2.1.2 Petroleum refining

After the production of crude oil from conventional or unconventional oil fields, the petroleum material is refined into products with maximum economic value. The refinery process involves at first a pre-treatment of the feedstock crude, such as desalting or separation from small gases and water. In the following, a variety of upgrading processes take place to convert low valuable components best possible into high value petroleum products, such as naphtha, gasoline, kerosene, and diesel. Figure 2 schematically introduce different steps of petroleum distillation and upgrading. Atmospheric distillation is the first process for the separation of crude oil feedstocks, in which light and valuable distillation cuts are obtained. The heavier fractions in the atmospheric distillation residue are further distilled under low pressure conditions during vacuum distillation. The two main products obtained are vacuum gas oil (VGO) and vacuum residue. Heavy petroleum cuts are feedstock for different conversion techniques, which aim to improve the yield of high value petroleum products. Thermal cracking, visbreaking, steam cracking, or catalytic cracking and reforming are examples for common upgrading methods. After the conversion of heavy residues

into lighter fractions, the products need to be further/ parallel treated to remove high amounts of heteroatoms and metals present in high boiling petroleum cuts. Processes which reduce the content of heteroatoms involve for example hydrodemetallation (HDM), hydrodesulfuration (HDS) or hydrodenitrification (HDN). [1, 3, 5]

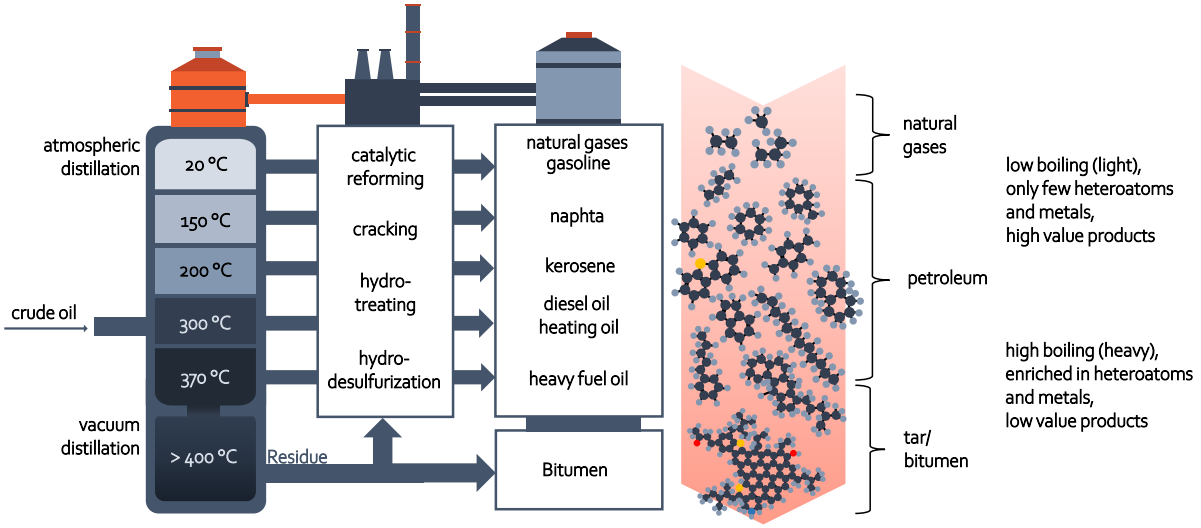

Figure 2: Simplified sheme of crude oil refining. The crude oil feedstocks are separated by atmospheric distillation followed by vacuum distillation. Heavy residues are converted to lighter fractions during different conversion processes.

2.2 Polyethylene terephthalate

The main applications for petroleum refinery products are for transportation (45 %) and for heating/ energy (42 %) purpose. However, approximately 4 wt.-% of the refinery products are used to synthesize different types of polymers, such as polypropylene (PP), polyethylene (PE), or polyethylene terephthalate (PET). [15, 16] After PP and PE, PET is the third most commonly consumed polymer in Europe [17]. The thermoplastic polymer is used for example in fibres for clothing, plastic packaging for liquids and foods or for engineering resins. [17, 18] As global polymer production rapidly increases over the last decade, the rising demand in polymers also caused an accumulation of waste [19]. Different recycling methods were developed to reduce the percentage of plastic disposal in landfills. Another possibility to convert plastic waste into a valuable resource is realised by pyrolysis of the polymers into gas, pyrolysis oil and char, which can be again used as feedstocks in refinery. PET was also explored as potential feed for pyrolysis processes yielding between 23-40 wt.-% liquid and 52-77 wt.-% gaseous pyrolysis products [19, 20]. Due to its potential as energy source, the investigation of the pyrolysis products of PET is of great interest. Conventional analytical methods, such as gas chromatography mass spectrometry (GC-MS) or liquid chromatography (LC), are applied to investigate the composition of pyrolysis mixture offline [21–23]. For online monitoring of the pyrolysis process, the application of thermal analysis (TA) coupled to other analytical techniques, such as infrared spectroscopy (IR) or mass spectrometry, is widely used to investigate polymer pyrolysis products. [24, 25]

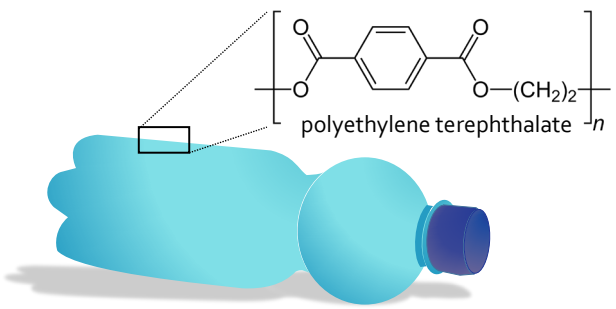

Figure 3: Polyethylene terephthalate (PET) is often applied for plastic packaging or clothing fibres, which causes a high amount of plastic waste.

2.3 Bitumen

Bitumen is characterized by its high viscosity as well as high compositional and structural complexity, containing high amounts of heteroatoms such as sulphur, nitrogen, oxygen, and metals. During the refinery process, bitumen is obtained as residue from vacuum distillation. [26, 27] Mixed with mineral aggregates, bitumen is used as binder to create asphalt concrete for application as pavement in road construction. Modifiers, such as elastomers, plastomers, or crumb rubber, can be added to improve and design the properties of binders. The additives can adjust viscosity, elasticity, hardness, or prolong the lifetime of the pavement. [28–30] During the service time of the pavement, the asphalt experiences hardening and embrittlement caused by different aging effects, which leads to cracking of the material. [31] Aging of the binder occurs during mixing, transportation, and paving, which is termed short-term aging, as well as during the pavement's service time, then referred to as long-term aging. Short-term aging is characterized by high temperatures of 150-160 °C as well as a high specific surface, which is exposed to air. Long-term aging is triggered by climatic conditions, void content, oxidation by atmospheric oxygen, and ultra-violet irradiation. Figure 4 illustrates both aging pathways. To investigate the effects of aging on bitumen, different aging methods were developed to age bitumen in small, laboratory scale. Short-term laboratory aging is simulated for example by the rolling thin film oven test (RTFOT) or the rotating flask test (RFT), while the latter was used under modified conditions in this PhD work in detail described in section 4.2.2. Long-term laboratory aging most often is performed in a pressure aging vessel (PAV) and usually carried out after RTFOT-conditioning. [32–35] Different aging mechanisms lead to alterations in the properties of bitumen. Oxidation is described as permanent and most severe hardening effect of bitumen and occurs during both, short-term and long-term aging. Oxidation causes the formation of polar functional groups, such as sulfoxides, anhydrides, carboxylic acids, and carbonyls, while the reaction is determined by temperature. [26, 27] Other aging mechanisms are known from the evaporation of volatile bitumen constituents, the phase separation of the binder by absorption of oily components into the mineral aggregates, or physical hardening caused by molecular rearrangement. Commonly, aging effects in bitumen are investigated by the determination of physical properties providing insights into mechanical characteristics [34, 36–40]. Due to the high complexity of bitumen, chemical analyses are often limited to SARA-fractionation

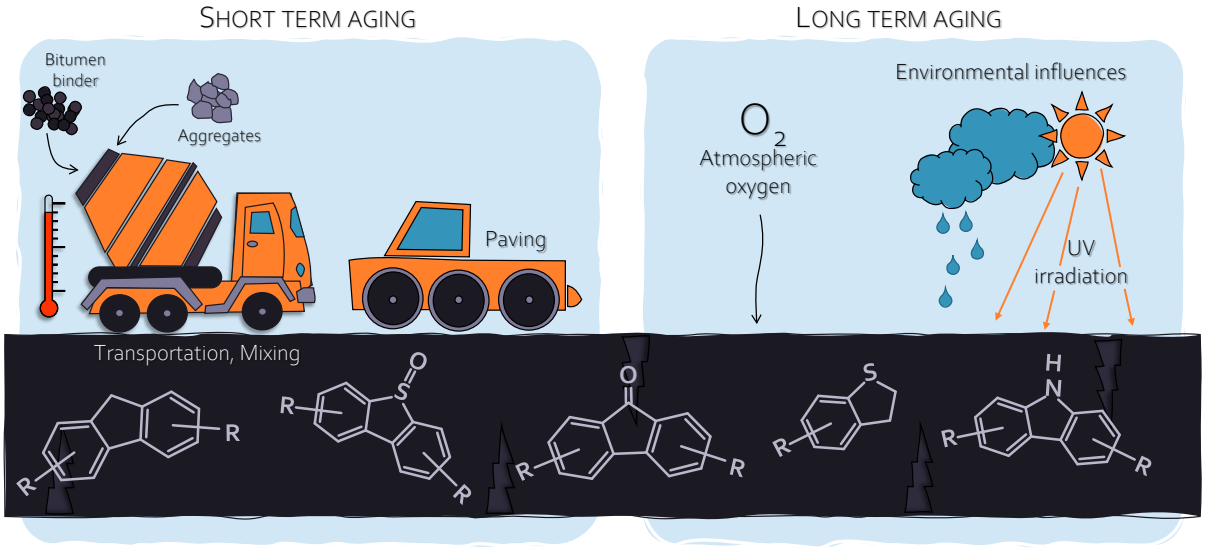

Figure 4: Aging pathways of bitumen. Short-term aging occurs during the mixing of mineral aggregates and bitumen binder under elevated temperatures and high specific surface. Long term aging occurs during the service time of the binder and is influenced by climatic conditions and oxidation.

[41] or bulk analysis of chemical functionalities by infra-red spectroscopy [28, 42–44]. Thus, the comprehensive molecular description of aging effects in bitumen could be strongly promoted by this PhD work [45].

2.4 SARA-fractionation and Asphaltenes

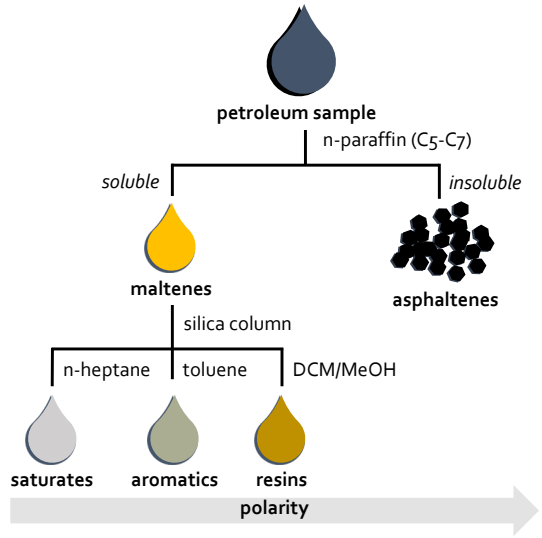

Figure 5: Scheme of SARA-fractionation into saturates, aromatics, resins, and asphaltenes.

Fractionation of crude oil derived material reduces its enormous complexity, which enables the detailed investigation of its subfractions. Commonly, advantage is taken of differences in solubility of various chemical compound classes present in petroleum. The fractionation into saturates, aromatics, resins and asphaltenes (SARA-fractionation) is the most widely applied fractionation technique. [46–48] Figure 5 presents a scheme of the SARA-fractionation procedure. In a first step, the asphaltene fraction is precipitated by adding a n-paraffinic solvent, such as n-pentane (C5), n-/cyclo-hexane (C6), or n-heptane (C7). The soluble fraction is referred to as maltene fraction and is further separated on silica into saturates (n-heptane), aromatics (toluene), and resins (DCM:MeOH). [49, 50] In refinery design and operation, the weight percentages of each fraction are used as quality criterion and helps to improve refinery conditions.

Asphaltenes are regarded as the most complex fraction of petroleum and are often related to problems during crude oil production, transportation, storing, and refinery. Asphaltenes tend to form deposits, are related to catalyst fouling and destabilization of crude oil mixtures. [2, 51–55] Due to their definition by solubility, the asphaltene fraction is composed of highly polar, high molecular weight compounds, which are enriched in heteroatoms as well as metals, such as vanadium and nickel [2]. The high aggregation tendency of asphaltenes led to debates on the weight of asphaltene monomers for decades. Meanwhile, researchers mostly agree on a mass range of 200-1500 Da with an average molecular weight of 500-800 Da. [56–60] Besides the molecular weight, the asphaltene molecular architecture is still subject of investigation. Two different structural motifs are under discussion: The island structural motif (single-core) versus the archipelago structural motif (multi-core). Island-type asphaltenes are thought to be composed of a highly aromatic, peri-condensed aromatic core with peripheral alky side chains, whereas archipelago-type asphaltenes are likely composed of smaller aromatic cores linked by alkyl bridges [61–63]. The island structural motif was introduced in the early 1960s by Yen et al. [64] and was later enhanced by Mullins and co-workers [65]. The island model was supported by a variety of analytical techniques, such as atomic force microscopy (AFM) [66–69], nuclear magnetic resonance (NMR) spectroscopy [62, 70, 71], or laser desorption laser ionisation mass spectrometry (L²MS) [72, 73]. Although the island model serves to describe some asphaltene

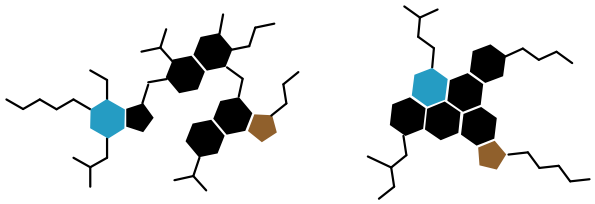

Figure 6: asphaltene architecture: archipelago and island structural motif.

properties, it is incongruent for example to products observed after thermal cracking or pyrolysis of asphaltenes. The presence of alkylated, small aromatic core structures observed in the newly formed maltene fraction or pyrolysis effluent can be better explained by the existence of archipelago-type asphaltenes. [61, 74–81] In the last two decades, high resolution mass spectrometry contributed valuable information to the asphaltene structural debate. [13, 63, 78, 82–84] It was shown by including fractionation and fragmentation techniques, that asphaltenes are composed of both structural motifs. The abundance of each motif differs by the origin of the asphaltenes as well as the molecular weight of the asphaltene compounds within one sample. [84–89] Aggregation was further revealed to be a major issue, which distorts mass spectrometric measurements by highlighting island-type asphaltenes, which are characterized by high monomer ion yield. [85–87, 90, 91]

3 Fundamentals of the applied techniques

In the following section, the fundamentals of analytical techniques primarily applied the in this PhD work are introduced. Thermal gravimetry (TG) coupled to high resolution Fourier transform ion cyclotron resonance mass spectrometry (FT-ICR MS) was predominantly used to obtain the herein presented data. The set-up enabled detailed evolved gas analysis (EGA) at the molecular level of highly viscous as well as solid petroleum-derived material. As ionisation techniques, atmospheric pressure chemical ionisation (APCI), atmospheric pressure photo ionisation (APPI) as well as atmospheric pressure laser ionisation (APLI) were applied. Two-dimensional gas chromatography (2D-GC×GC) coupled to time-of-flight mass spectrometry (TOF-MS) used as supporting technique to validate the FT-ICR MS data and to obtain structural information.

3.1 Separation techniques

3.1.1 Thermogravimetry

Thermogravimetry (TG) enables tracing the mass loss in real time as a function of temperature or heating time as depicted in Figure 7 a). The differential thermogravimetric signal (DTG) reveals the mass loss rate. Generally, physical and chemical processes can be investigated, such as desorption, thermal decomposition or oxidation. [92] For petroleum-derived material, thermogravimetric analysis (TGA) is frequently applied to determine bulk parameters such as mass loss or coke yield [78, 82, 93, 94]. A typical thermogravimetric device is composed of a precise analytical balance, whose sample holder is located in a furnace. Sample material is introduced in a small aluminium (max. temp. 600 °C) or alumina (max. temp. 1000 °C) crucible. For pyrolysis experiments, the furnace volume is purged with nitrogen providing an inert atmosphere, while air is introduced for the investigation of oxidation processes.

The investigation of gases and vaporized material during thermal analysis is referred to as evolved gas analysis (EGA). Therefore, a thermobalance or another thermal analysis device is coupled to an additional analytical technique over a heated transferline, which is most commonly infrared spectroscopy (IR) or mass spectrometry (MS) [95]. IR enables general information on functional groups present in the evolved molecules as well as the quantification of small gases. EGA coupled to mass spectrometry is widely used

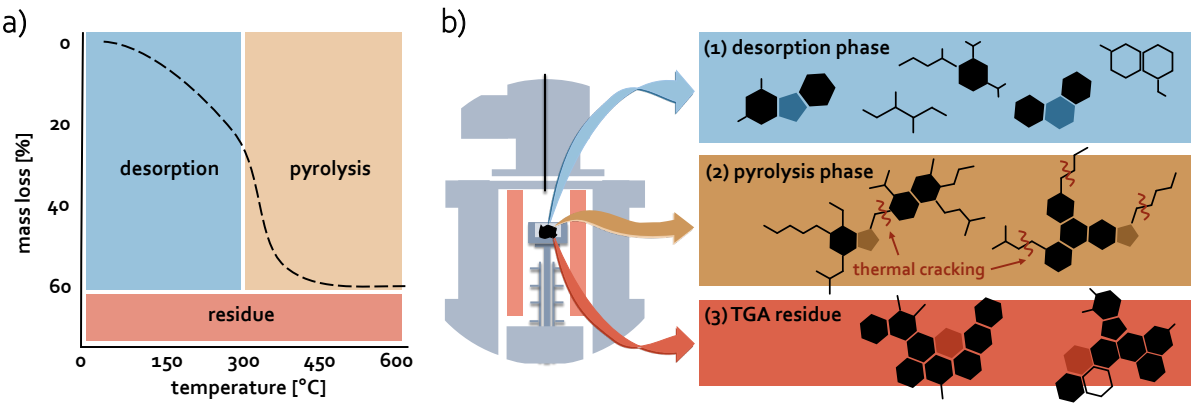

Figure 7: a) Typical mass loss diagram obtained by thermogravimetric measurements. The TG process can be divided into two phases, the desorption and the pyrolysis phase, whereas non-evaporables remain as residue. b) The three main pathways petroleum derived material undergoes during thermal gravimetric analysis. Smaller components are intactly desorbed, while high-molecular compounds are decomposed into smaller pyrolysis fragments. Non-evaporable material remains as coke in the TGA residue.

in the field of thermal degradation of polymers [96–98], but also applied for the chemical characterization of the evolved gas mixture of petroleum-derived materials [99–102]. Unfortunately, commonly applied mass spectrometric analysers, such as time-of-flight or quadrupole systems, lack in mass spectral resolution when heavy petroleum distillation cuts are investigated. Recently, the hyphenation of high resolution mass spectrometry to thermogravimetry was introduced by our working group enabling the evolved gas analysis of highly complex mixtures [103].

When petroleum-derived material is analysed by TG-MS, the evaporation process can be separated into two different phases, the desorption and pyrolysis phase, as illustrated in Figure 7 a). Non-evaporable material remains as residue. Typically, predominant desorption is observed up to 300 °C, while pyrolysis starts between 300-350 °C [104]. Due to its temperature profile, the TG process can be seen as separation method reducing the complexity of the spectra compared to direct infusion inlets. Figure 7 b) illustrates the three main pathways petroleum derived material undergoes during TGA. During the desorption phase, smaller, low molecular weight molecules are intactly evaporated, which occur in the order of their boiling points with increasing temperature. Nonetheless, due to the simple evaporation process, the separation is strongly limited. In the pyrolysis phase, high-molecular weight compounds are thermally cracked [78]. Species composed of several building blocks are likely cracked at their aliphatic linkers bridging the aromatic cores [63, 79]. Compounds, which contain one highly aromatic core are known to cleave of their alkyl side chains during thermal degradation [79, 105, 106]. If the pyrolysis fragments are evaporable, they will be detected during evolved gas analysis, otherwise, highly aromatised compounds remain as coke in the TGA residue [79, 105, 107].

3.1.2 Comprehensive two-dimensional gas chromatography

Gas chromatography (GC) is a widely used analytical technique to separate mixtures of volatile to semi-volatile compounds enabling determination of their chemical structure. For the analysis, the compounds are volatilized and transferred to a separation column, which operates as stationary phase. Separation columns are generally made from fused silica coated with a thin film adapted for the polarity of the analytes. The analytes are transferred through the GC column by a continuous gas stream, which operates as mobile phase. Most often, helium, hydrogen or nitrogen are applied as mobile phases. The chromatographic separation principle relies on the distribution constant of an analyte in both phases. Depending

on the polarity and volatility, the analytes interact differently with the stationary phase resulting in a separated elution of the compounds from the column. The time period spent on the column by the analyte is referred to as retention time (RT). The separation column is placed inside an oven enabling the application of a temperature gradient to enhance separation or to speed up the chromatographic process. At higher temperatures, the analytes' distribution in both phases is shifted to the mobile phase. Therefore, the quality of the separation process depends on the column material, temperature gradient as well as flow rate. [108] The hyphenation of GC to mass spectrometry enables the identification of eluting compounds not only on the basis of their retention time, but also by comparing their fragmentation pattern (EI-MS) with data-bases. [109]

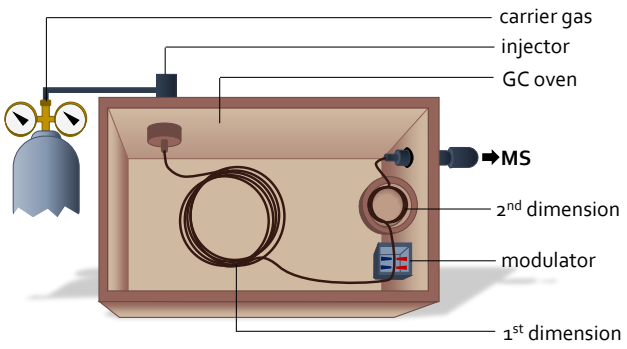

Figure 8: General set-up for two-dimensional gas chromatography. Analytes are first introduced to the 1st dimension column. During the heating program of the main oven, eluting analytes are trapped and reinjected by a modulator into the 2nd dimension column. As detector, commonly TOF-MS systems are applied.

Due to the chemical complexity of higher petroleum cuts, one-dimensional GC-MS rapidly reaches its peak capacity, which results in insufficient separation and co-eluting signals. To overcome this problem, a second dimension can be added, which is realized by a second column most often placed in a separate oven. The general setup of a two-dimensional GC system (GC×GC) is presented in Figure 8. The sample is first injected to the 1st dimension GC column. While the temperature program of the main oven proceeds, the effluent from the 1st column is continuously collected and re-injected to the 2nd column by a modulator. Modulation between the two chromatographic dimensions is the most crucial step. Flow modulators, but also cryogenic modulators are one of the most applied modulators, trapping the effluent by rapid cooling, while re-injection is realized by rapid heating. [110–112] Due to the refocussing of the analytes, chromatographic peak widths are only between 50 to 400 ms. In particular, time-of-flight mass spectrometric systems, introduced in detail below, are suitable because of their high acquisition rate enabling the collection of a sufficient amount of data points per chromatographic peak. [113, 114]

For comprehensive analysis, the analytes are subjected to two stationary phases with orthogonal polarity. Most commonly, a non-polar column is applied for the 1st dimension, which separates the analytes based on their boiling point, while for the 2nd dimension, a polar column is applied separating the analytes by polar interactions. [112] If the afore described column combination is used, analytes occurring in the lower space of the 2D chromatogram express less polar interactions with the 2nd column, while highly polar compounds occur in the upper part. With regard to petroleum-derived material, the naturally present high amount of isomers line up as small narrow bands, while homologues series are found in separated regions. [112]

3.2 Mass spectrometry

Mass spectrometry (MS) is one of the most versatile analytical techniques therefore applied in several fields of science. It enables the detection of the analytes' molecular mass and provides structural information by typical fragmentation patterns. Depending on the MS method, few analytes up to complex mixtures can be investigated in one mass spectrum. However, all mass spectrometric techniques have in

common that analytes need to be present as ions for their investigation. In the following, ionisation techniques as well as mass spectrometric methods essential for this PhD work are introduced in more detail. [115]

3.2.1 Atmospheric pressure ionisation

Classically, electron ionisation (EI) is commonly applied as ionisation technique in mass spectrometry. As hard ionisation method, EI causes fragmentation of the analytes, which is on the one hand beneficial for structural elucidation but may lead on the other hand to the loss of the molecular ion information. In EI, ions are typically produced by high energetic electrons (70 eV) hitting the neutral analytes and causing their ionisation by removing an electron. The high excess energy leads to fragmentation of the produced ions. Due to its universal ionisation ability, EI needs to be conducted under reduced pressure to avoid the absorption of the ionising electrons by surrounding gases. [108, 115] Since the 1970s, ionisation under atmospheric pressure is applied to softly ionize the analytes [116]. In the following decades, several atmospheric pressure ionisation (API) techniques emerged basing on a variety of ionisation schemes. The soft ionisation results – depending on the method – in molecular radical cations [$M^{\bullet+}$] or quasi-molecular ions, which are protonated $[M+H]^+$, deprotonated $[M-H]^-$ or which formed adducts with solvent $[M+S]^+$ or dopant $[M+D]^+$ molecules. [115]

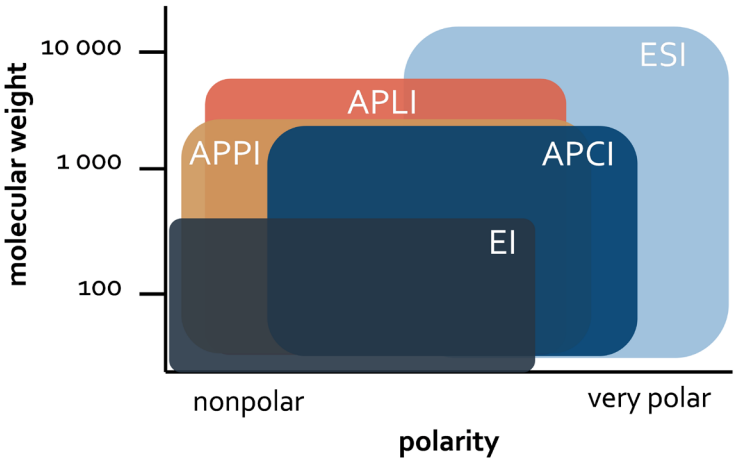

Figure 9: Overview on the covered mass range as well as polarity of the investigated analytes by different ionisation techniques. Although EI is a universal ionisation technique, the investigation of high molecular structures is limit due its high fragmentation behaviour. ESI is capable of highly polar compounds including compounds with high molecular weight. APPI, APCI and APLI cover a similar mass range, however, due to the differences in ionisation pathways, different chemical minorities are addressed.

In contrast to the universal ionisation technique EI, atmospheric pressure ionisation covers a smaller, more specific range of ionisable analytes strongly depending on the applied method. Figure 9 illustrates an overview on the mass and polarity range addressed by different ionisation techniques. Although it was stated beforehand that EI operates for any kind of analyte, the addressable chemical space is limited due to its high fragmentation tendency. Electrospray ionisation (ESI) is suitable for highly polar, acidic, or basic analytes and covers the broadest mass range enabling the ionisation of macromolecules (e.g. proteins) as multiple charged ions as well [117, 118]. A smaller mass range, but a broader polarity up to non-polar aromatic compounds is covered by atmospheric chemical ionisation (APCI), atmospheric pressure photoionization (APPI) as well as atmospheric pressure laser ionisation (APLI). In contrast to ESI ionizing analytes in solution only, the afore-named ionisation techniques are able to ionize compounds in the gas phase. In this PhD work, APPI, APLI and, in particular, APCI revealed great advantages by being coupled to evolved gas analysis and will be therefore introduced in more detail in the following. [115, 119]

3.2.1.1 Atmospheric pressure chemical ionisation

The first APCI ion source was introduced by Horning et al. in 1973. [116] For this initial approach, electrons provided by a radioactive source were used for the ionisation process. [116, 120] In modern APCI, ionisation is carried out by a corona discharge, which is created by a high potential difference of 2-3 kV between a discharge needle and the mass spectrometer inlet. [115, 120] The corona discharge induces plasma region, which causes the ionisation of surrounding gases. Two main ionisation mechanisms occur, which are depicted in Figure 10. With regard to the ion source atmosphere, nitrogen is the initial reactant forming radical cations of $N_2^{\bullet+}$ or $N_4^{\bullet+}$. These ions can further react with the analyte to produce (1) molecular radical cations [$M^{\bullet+}$] by charge transfer or (2) protonated quasi-molecular ions $[M+H]^+$ by several reaction steps with traces of water. [116, 119, 120] In general, the APCI ionisation scheme is able to ionise analytes with mid to high polarity and sufficient thermal stability for vaporization. In theory, also alkenes and naphthenes can be ionised by APCI, but those compounds are not observed due combating ionisation and matrix effects. [121]

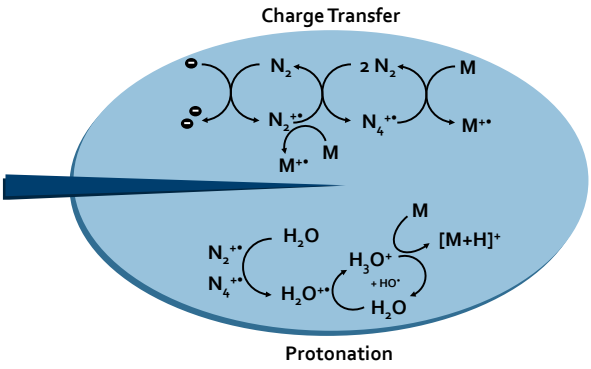

Figure 10: Schematic APCI ionisation. Corona discharge leads to two ionisation pathways. The first pathway is by charge transfer from nitrogen radical cations to the analyte molecule. In the protonation pathway, water is involved by transferring a proton to the analyte.

3.2.1.2 Atmospheric pressure photo ionisation

APPI covers a comparable compositional space to APCI, but low-polar compounds such as aromatic hydrocarbons and sulphur-containing species are more pronounced. [121] In APPI, ionisation is carried out by ultraviolet (UV) light provided by gas discharge lamps. Most commonly, Krypton lamps are applied emitting photons with 10.0 (124 nm) and 10.6 eV (117 nm). [122, 123] Figure 11 illustrates the different ionisation mechanisms involved in the APPI process. The initial mechanism includes a direct photo ionisation process resulting in molecular radical cations of the analytes [$M^{\bullet+}$] or solvent molecules [$S^{\bullet+}$]. In the gaseous phase, further reactions can now take place. If the ionisation energy (IE) of the solvent molecule is higher than the one of the analyte, the charge is transferred to the analyte. The same is observed if the proton affinity (PA) of the analyte is higher; then the solvent molecule transfers a proton to the analyte and a protonated molecular ion is formed $[M+H]^+$.[124, 125] By adding a dopant such as toluene, the protonation mechanisms can be strongly enhanced increasing the molecular ion yield. [125]

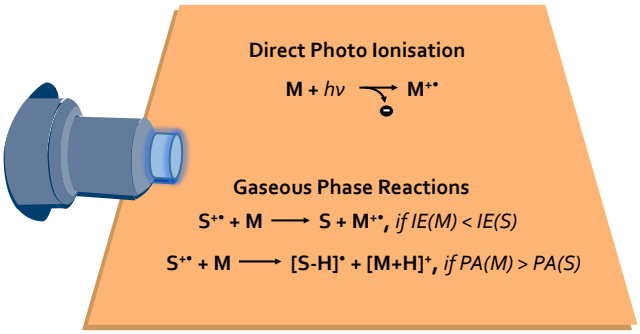

Figure 11: APPI ionisation scheme. The UV-photons provided in APPI are able to directly ionise analytes with ionisation energies below the photon energy. Further gaseous phase reactions can occur between solvent and analyte molecules leading to charge or proton transfer.

3.2.1.3 Atmospheric pressure laser ionisation

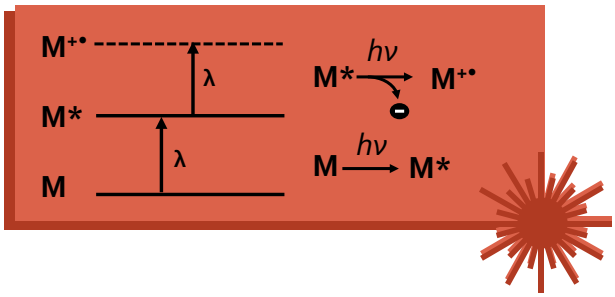

Figure 12: APLI ionisation scheme. Analytes are ionised in a two-step mechanism. In the first step, the analyte is excited by the absorption of the first photon. In the second step, the analyte is ionised by the absorption of an additional photon. Only molecules with a long-lasting excitation state, such as aromatics, can be ionised by APLI.

In 1999, APLI was firstly introduced by Benter and co-workers as a new analytical technique for sensitive and selective detection of specific analytes in the gas phase by mass spectrometry. [126] In the following years, APLI was successfully applied as ionisation technique for liquid chromatography (LC)-MS [127, 128] and GC-MS [129]. In contrast to APPI, where ion formation is induced by single photon ionisation, APLI is based on a multiphoton process. Typically, KrF excimer lasers (248 nm) or Nd:YAG lasers (266 nm) are applied as photon sources. [128] APLI is closely related to resonance enhanced multiphoton ionisation (REMPI) but is conducted under atmospheric pressure instead of vacuum conditions. In both cases, the analyte absorbs in a first step one photon leading to the excitation of the molecule [M*]. In a second step, the excited analyte is ionised by the absorption of another photon or several photons forming a radical cation [$M^{\bullet+}$]. [119, 127] A scheme of the ionisation mechanism is given in Figure 12. Due to the two steps needed for ionisation, only compounds with a long-living excitation state can be ionised efficiently leading to their selective ionisation. In principle, the required resonant intermediate state is only provided by systems rich in π-electrons present in aromatic compounds. [130] In comparison to APPI, APLI reveals an increased sensitivity towards the detection of aromatic compounds caused by the increased photon density in the laser beam compared to the unfocussed light cone of the APPI lamp. [119]

3.2.2 Fourier transform ion cyclotron resonance mass spectrometry

Fourier transform ion cyclotron resonance mass spectrometry (FT-ICR MS) impresses by its unbeaten high resolving power and mass accuracy superior to any other mass spectrometric technique. It can be operated with almost all ionisation techniques commonly applied in mass spectrometry, while atmospheric pressure ionisation rose in importance in particular. Especially for highly complex matrices composed of thousands of components, FT-ICR MS has become an essential analytical tool. Its versatile applicability helped to achieve numerous advances in many fields of science, such as metabolomics, proteomics, environmental chemistry, forensics, petroleomics, foodomics and more. [131, 132]

3.2.2.1 Instrumentation

The basic concept of ICR was developed by Lawrence in the early 1930s by investigating the acceleration of protons in a magnetic field [133, 134]. Two decades later, it was first combined with mass spectrometry by Sommer et al. [135]. Another two and a half decades elapsed until Comisarov and Marshall introduced Fourier transformation for ICR-MS in 1974 [136]. Since then, lots of technical progresses were achieved and the field of application was drastically expanded with the result that high level modern analytics may not be managed without FT-ICR MS. [137] Modern FT-ICR mass spectrometers, as schematically depicted in Figure 13 a), are composed of six main components. The first essential part is an ion source, nowadays mostly operated under atmospheric pressure conditions. A large variety of atmospheric pressure ionisation techniques can be combined with FT-ICR MS. Ionisation methods of interest for this PhD work are

introduced in detail above. The second part is an ion focussing, guidance, preselection, and accumulation system. In the accumulation trap, ions can be stored and fragmentation experiments, such as collision induced dissociation (CID), can be conducted before transferring the ions into the third main component, the analyser cell. Several designs exist, but the most commonly used ICR cells are the infinity cell [138] and the more recently developed dynamically harmonized ParaCell [139–141]. The former was applied for the acquisition of the data presented in this work and is schematically depicted in Figure 13 b). The infinity cell is of cylindrical shape composed of three pairs of electrodes: trapping electrodes retain the ions inside the ICR cell in the horizontal z-dimension. Excitation electrodes are essential to increase the cyclotron orbit explained in detail below, while the ICR signal is recorded as free induction decay (FID) by the detection plates. The fourth part is a superconducting magnet of commonly 7-15 T, but up to 21 T [142, 143], which surrounds the ICR cell providing a strong, homogeneous magnetic field. The differentially pumped vacuum system can be regarded as fifth main part. For high performance, nominal pressure is needed in the analyser cell to avoid collision between ions and neutral molecules. The last but equally important part is a sophisticated data system essential for the acquisition as well as processing of the signal. [115, 131, 132]

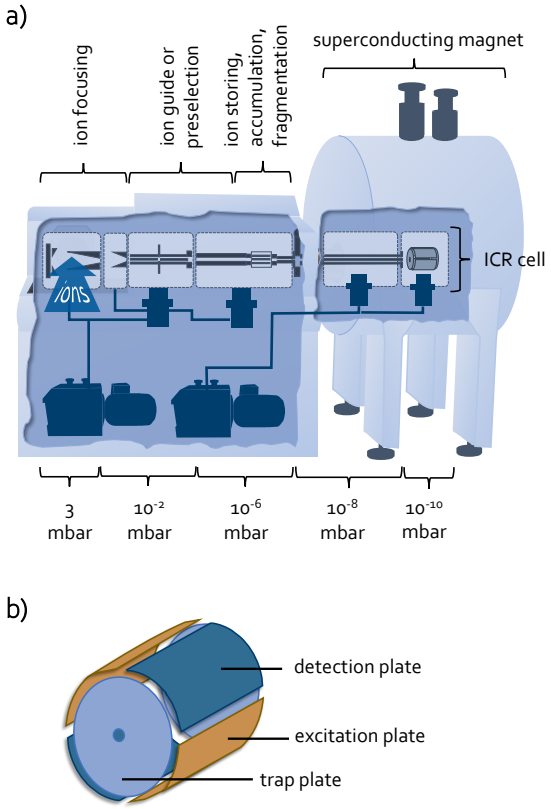

Figure 13: a) Schematic setup of an FT-ICR mass spectrometer. The instrument is composed of six main components: an ionisation source, an ion guidance/accumulation system, the ICR analyser cell, a superconducting magnet, a differentially pumped vacuum system, and a sophisticated data system. b) Scheme of an Infinity ICR cell. The cell is composed of three pairs of electrodes: excitation plates, detection plates, and trapping plates.

3.2.2.2 Cyclotron motion

The fundamental principle of ICR is based on the motion of charged ions in a magnetic field. If an ion of charge **q** and velocity **v** enters a magnetic field **B** perpendicular to the magnetic field lines, the Lorentz force **F** leads to a circular motion, which is called Cyclotron motion depicted in Figure 14 a). The cyclotron motion is carried out with a specific frequency, the Cyclotron frequency f_c, dependent on the charge and mass of the ion as well as the strength of the magnetic field. [132, 144, 145]

$$f_c = \frac{q\,B}{2\,\pi\,m} \qquad (1)$$

In FT-ICR MS, the magnetic field is held constant, and therefore, the cyclotron frequency is directly related to the mass-to-charge ratio of an ion. Further, equation (1) shows that the cyclotron frequency is independent of the ions' velocity and their orbit radii, which in turn means that f_c is not influenced by the kinetic energy of the ions. The angular frequency ω_c, however, is defined as the ratio of the ions' velocity to radius and corresponds to the cyclotron frequency f_c by a factor of 2π as given in equation (2). Since the cyclotron frequency is constant for a given m/q value, the radius of the cyclotron orbit scales directly with velocity,

or with the square root of kinetic energy. This property is used for ion detection in the analyser cell of a FT-ICR MS instrument as explained in detail below.

$$f_c 2\pi = \omega_c = \frac{v}{r} \quad (2)$$

The ion motion is not only determined by the cyclotron motion in the magnetic field, but also influenced by electric potentials trapping the ions in the ICR cell resulting in two additional motions of the ions. The first motion occurs due to the parabolic-like shape of the trapping potential in a cylindrical ICR cell. The ion packages drift in a circular motion along the electric field gradient. This drift motion is called magnetron motion and is depicted in Figure 14 b) in view of the yz-plane. Magnetron frequencies are in the order of 1-100 Hz and therefore much lower than cyclotron frequencies (kHz-MHz). In the ICR analyser cell, the ion package is trapped by the magnetic field in the xy-plane as well as between two electrodes along the z-axis. The trapping of the ions between the back and front trap plate results in a harmonic oscillation between the trapping plates along the magnetic field axis. This second additional motion between the trapping electrodes is called trapping motion. In Figure 14 c), the trapping motion is illustrated in combination with the magnetron motion as black, solid line. The resulting ion motion (blue line) is therefore a combination of the cyclotron motion, the trapping motion and the magnetron motion, which is called the reduced cyclotron frequency. [115, 132, 144]

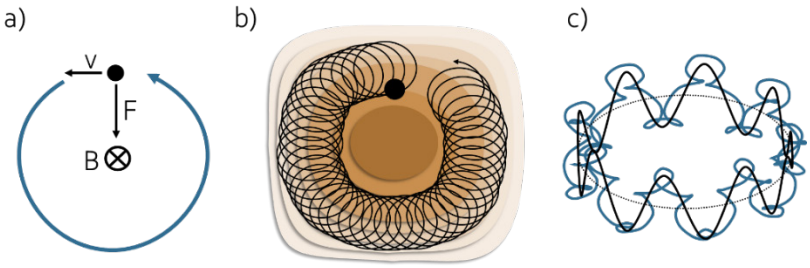

Figure 14: Ion cyclotron motion. a) The fundamental principle of the cyclotron motion. b) Cyclotron motion and magnetron motion initiated by a gradient electric field potential. c) Magnetron motion (black dotted line), trapping motion (black line) and resulting cyclotron motion (blue line).

3.2.2.3 Measurement principle

The motion ions undergo in the ICR analyser cell is comparatively small resulting in an ion package with comparable low radii. Due to the fact that the cyclotron frequency is independent of the cyclotron orbit, the ion packages can be broad to higher orbits without changing the characteristic frequency. In Figure 15 a), a scheme of the measurement principle is given. Before detection, the ion packages are commonly excited to higher orbits by a radio frequency (RF) sweep as illustrated in Figure 15 b). Excitation plates on opposite sides generate an alternating electrical field, which accelerates the ion packages in a spiral motion resulting in an increased cyclotron radius. During detection, the ion packages cycling near the detection plates induce a weak image current on the electrodes (regard Figure 15 c)), which is amplified in the following. Due to inhomogeneity of the magnetic field, the collision with remaining neutral particles and incoherence of the ion packages, the signal is damped over time. Fourier transform is applied to transfer the signal from the time domain to the frequency domain resulting in a Lorentz peak shape caused by the transient signal. Because of the connection of cyclotron frequency with mass and charge of a given ion, the frequency spectrum can be converted to the mass spectrum. [115, 132]

Frequencies can be measured with high accuracy in turn resulting in extremely exact *m/z* values. For the accuracy of the frequency measurements, the observation period of the transient signal is an essential parameter. The longer the transient, the more cycles of the ion packages can be detected enhancing the

accuracy of the frequency measurement. Typical transient lengths differ between 0.5 – 4 s. The highest frequency is determined by the Nyquist criterion. The obtained accuracy of the frequencies is limited by several factors, such as space charge effects between the ions. Electrostatic repulsion causes incoherence of the ion packages, which results in frequency shifts. To decrease space charge effects, the number of ions entering the analyser cell can be reduced. Furthermore, a higher magnetic field strength increases the critical maximum number of ions by B^2, before considerable negative effects are caused by space charge effects. [146]

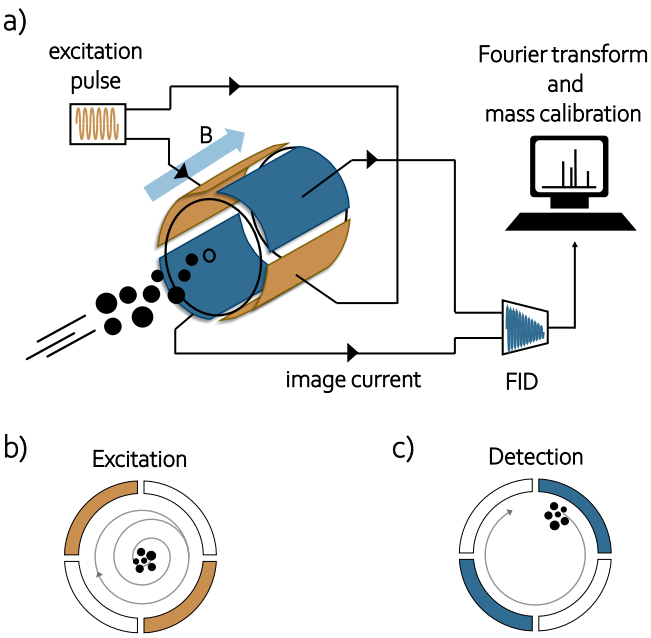

Figure 15: a) Scheme of the measurement principle in FT-ICR MS. Ions, which entered the ICR cell are excited by an RF-pulse to higher cyclotron orbits prior to detection. b) The excitation process. c) Motion of the ion packages during detection mode.

Due to the FID signal, which is not completely damped to zero, Fourier transform of the transient results in a Lorentz peak shape of the signals accompanied by smaller sidebands. Those sideband signals can be reduced by further processing. Apodization of the signal can be carried out by typically multiplying the transient with sin(x) or $\sin^2(x)$ functions. Zero filling smooths the peak shape by increasing the number of data points per *m/z*-interval because of adding zeros to the end of the transient function. During post-processing of the resulting mass spectrum, the mass accuracy can be enhanced by external or internal calibration. External calibration is carried out measuring a standard mixture with the same instrumental parameters and applying the same calibration function to the analyte spectrum. Internal calibration can enhance the mass accuracy by an order of magnitude in comparison to external calibration. [144]

One of the key features of FT-ICR MS, besides high mass accuracy, is its unbeaten high resolving power. Typical resolution achieved in broadband mode for the measurement of complex petroleum samples differs between 300,000 and 600,000 at *m/z* 400 [115], but also extreme high resolution of over 1,000,000 was achieved for large biomolecules and is state of the art for newly developed FT-ICR MS instruments [146]. In FT-ICR MS, resolving power (RP) is defined as shown in equation (3). $\Delta m/z$ is usually defined as the full width at half maximum peak height. [147]

$$RP = \frac{m/z}{\Delta m/z} \tag{3}$$

The resolving power of a FT-ICR MS instrument is at low pressures directly proportional to the length of the transient signal [148] as well as the magnetic field strength [148, 149].

3.2.2.4 Petroleomics

FT-ICR MS has been applied to the analysis of petroleum-derived material for two decades. This field of research is called *Petroleomics* highlighting the attempt to analyse these complex mixtures at the molec-

ular level and to unravel the "petroleome". Due to the extremely complex nature of petroleum, which results in high resolution mass spectra with more than 10,000 *m/z* signals [150, 151], automated data analysis routines as well as data reduction and visualisation are key parameters for its investigation.

Except for the ^{12}C isotope, which has by definition the mass of exact 12 Da, each element differs by a characteristic mass defect from the nominal mass [152]. In Figure 16, the mass defects for selected isotopes relevant in Petroleomics are given. [153] Each combination of $C_cH_hN_nO_oS_s$ therefore results in a unique *m/z* ratio. High resolution mass spectrometry is able to resolve the molecular mass on the lower mDa level enabling the calculation of sum formulae on the basis of the accurately measured m/z ratio. As indicated above, high resolution mass spectra of heavy petroleum fractions contain thousands of different m/z ratios. Due to the isotopic fine structure of each signal, very narrow peak distances occur, which are referred to as characteristic mass splits. One of the most challenging mass splits occurring in petroleum is the difference between isobars only varying in elemental composition by C_3 versus SH_4, which results in a mass difference of solely 3.4 mDa [147]. Even more challenging is the difference between C_4 and $^{13}CH_3S$ accounting for only 1.1 mDa, which can solely addressed by FT-ICR MS. Although the isotopic fine structure additionally increases the complexity of the spectra, the isotopic pattern is helpful to verify calculated sum formulae [154]. Figure 17 provides an impression of the ultra-high complexity of heavy petroleum materials. The zoom-in on the right hand side underlines the high resolving power of FT-ICR MS with regard to very narrow mass splits as well as the large chemical diversity present on one nominal mass. [153]

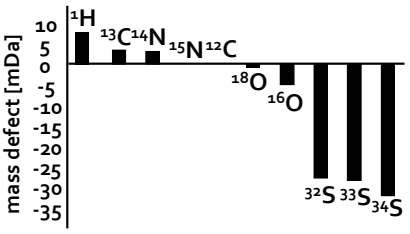

Figure 16: Mass defect of selected isotopes. Each combination of $C_cH_hN_nO_oS_s$ results in a unique m/z ratio.

In Petroleomics, characteristic values calculated from the assigned sum formulae as well as fingerprint plots are applied to reduce the complexity and to illustrate the mass spectrometric information. For a general overview, different species are grouped into compound classes on the basis of the calculated sum formulae. For example, species containing one oxygen-atom are grouped into the O1-class, compounds with one oxygen- and one sulphur-atom are part of the S1O1-class and hydrocarbons composed of only carbon and hydrogen are combined in the CH-class. Figure 18 a) shows a typical example for a compound class distribution found in a light crude oil. The compound class distribution only provides a macroscopic overview, while typical fingerprint plots presented in the following allow an investigation on molecular level. [153, 155]

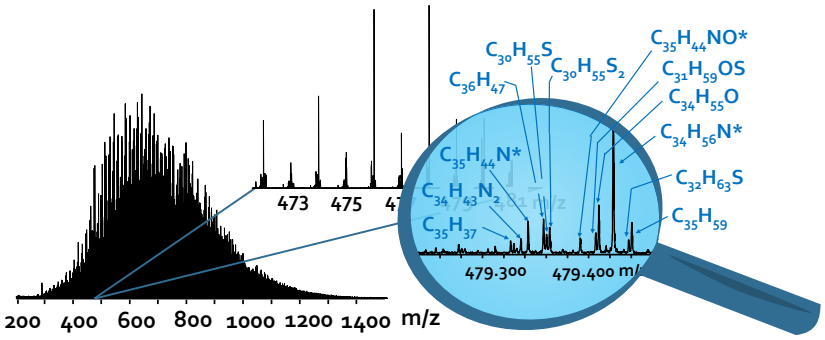

Figure 17: Direct infusion FT-ICR MS spectrum of a heavy petroleum sample. The zoom-in reveals the high complexity in heavy petroleum derived material present on only one nominal mass. Due to the high mass accuracy and resolving power, sum formulae can be calculated based on the measured m/z-value.

From sum formula assignments, the H/C, O/C, S/C, and N/C ratio can be calculated. The H/C ratio of petroleum-derived material provides evidence of the aromaticity of a given molecule or the average aromaticity of the whole sample. Typical values for the H/C ratio are 0.4 (highly aromatic) to 2.4 (highly saturated). O/C, N/C and S/C ratios are often calculated to track processes such as oxidation, desulfuration as well as denitrogenation. Van Krevelen diagrams were introduced in 1957 to determine the maturation of

petroleum deposits [156]. The typical van Krevelen-diagram is spanned by H/C versus O/C, but other heteroatom/C ratios are applied as well. In Figure 18 b), a van Krevelen-diagram of H/C versus S/C is shown. Each dot represents molecular formulae with a certain H/C and S/C ratio, while the size of the dots is linked to the absolute abundance. Species occurring in the upper half of the diagram are more saturated, while compounds in the lower half are increased in aromaticity. Characteristic lines are formed by homologues series. [153, 157]

Aromaticity is not only addressed by the H/C ratio, also the degree of unsaturation, i.e. the ring and doubled bond equivalent (DBE), is a widely applied parameter. The DBE is calculated as follows for the easiest case with only CHNSO. #C represents the number of carbon atoms in one molecule, #H the number of hydrogen atoms and #N the number of nitrogen atoms:

$$DBE = \#C - \frac{\#H}{2} + \frac{\#N}{2} \tag{4}$$

Each ring and each double bond present in a molecule increase the DBE of +1. For example, the benzene molecule, which is composed of one ring and three double bonds, has a DBE of 4. For investigating different compound classes at the molecular level, DBE versus carbon number plots are ideal, because the compositional space is spanned by aromaticity as well as the molecular weight. However, each compound class needs an individual diagram to avoid superimposition. As shown for the van Krevelen-diagram, the dots representing a molecular formula can be colour- and/or size-coded by the absolute intensity. [153, 158]

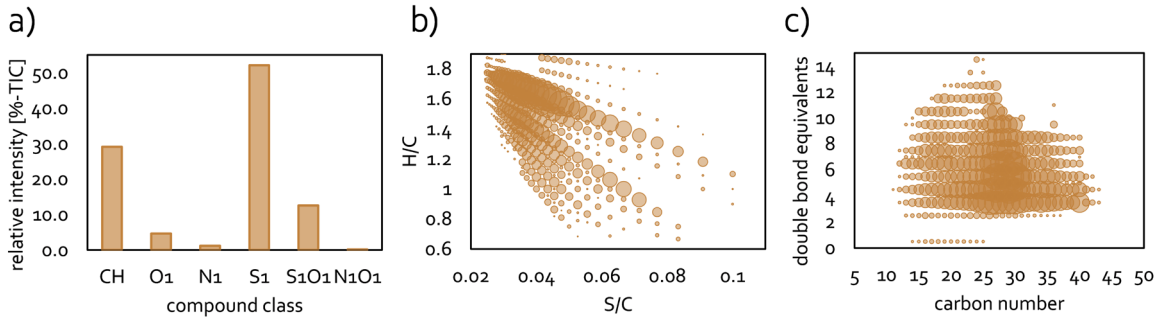

Figure 18 a) Typical compound class distribution of a light crude oil. Compounds containing only C and H in their sum formulae are grouped in the CH-class, species containing one oxygen atom are grouped in the O1-class, etc. b) Van Krevelen-diagram of sulphur containing species. Van Krevelen diagrams are spanned by H/C versus a heteroatom/C ratio. c) DBE versus #C diagram for the S1-class of a light crude oil. DBE versus #C diagrams span chemical space by weight of the molecule (#C) versus aromaticity (DBE).

3.2.3 Time-of-flight mass spectrometry

The measurement principle of time-of-flight mass spectrometry (TOF-MS) is very different from the before discussed FT-ICR MS. In TOF-MS, ions are accelerated by a constant electric field into a free drift region resulting in a separation by their m/z ratio because of their differences in flight time. The entrance of the ions to the drift region needs to be pulsed to define the starting time and location of the time-of-flight measurement. The pulsing can be realized either by pulsed extraction of the ions from the acceleration region or by applying a pulsed ionisation technique. For narrow peak widths, it is necessary that ions enter the drift region with similar kinetic energies. The energy spread, caused for example by electron ionisation, single photon or multiphoton ionisation with a pulsed laser system, is hardly compensable in a linear TOF system. [108, 115]

The integration of a reflection of the ions is used in reflectron TOF systems to reduce differences in kinetic energy focussing the ion packages. A scheme of the general setup is given in Figure 19.The accelerated ions enter in the free drift region the electric field of the reflectron. Depending on their mass and kinetic energy, the penetration depth into the electric field varies. For example, if two ions of the same m/z ratio but different in kinetic energy enter the reflectron, the ion with the higher energy will penetrate deeper in the electric field. Therefore, the covered distance of the faster ion is longer, which compensates its higher velocity. Hence, both ions arrive at the detector at the same time. This focus effect of the ions leads to an increase in time resolution and therefore mass resolution as well. [115, 159]

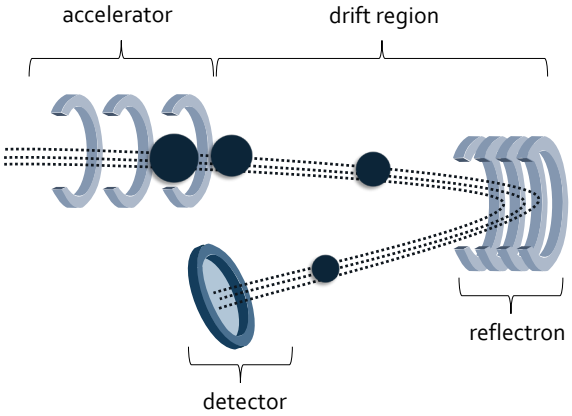

Figure 19: Scheme of a reflectron time of flight mass spectrometer. Kinetic energy spread is refocussed by the reflectron. Ions with the same m/z value but different kinetic energies reveal different penetration depth into the electric field. Ions with higher kinetic energy penetrate deeper, which results in an elongation of the flight pass. Due to this adjustment, ions with the same m/z-value are refocussed leading to smaller deviations in flight time.

The mass resolving power of a TOF system is defined by its ability to differentiate between flight times of ions with different m/z ratios. The total flight time is increased by elongation of the flight path, leading to an enhanced separation of ions with different m/z ratios. The elongation of the flight pass can be achieved by multi reflections of the ions, as applied in multiple-reflection TOF-MS. Such instruments can achieve a resolving power up to 50,000 with an acquisition rate of approximately 100 Hz. [160, 161] A common feature of all time of flight instruments is their high acquisition rate necessary to determine the very short distances between the µs flight times of the ions. TOF-MS is able to detect hundreds of full spectra per second, which is especially adequate for hyphenation to gas chromatography. [115]

4 Results

This PhD work aimed to deepen the chemical characterization of heavy petroleum derived material by the application of high-resolution Fourier transform ion cyclotron resonance mass spectrometry coupled to thermal gravimetry (TG-FT-ICR MS). In Figure 20, all publications summarized in this dissertation are presented in chronological order. In publication 1-5, TG-FT-ICR MS was shown to provide great advantages for the chemical description of the evolved gas mixture of heavy petroleum-derived materials. To broaden the chemical description, TG-FT-ICR MS was combined with different analytical techniques aiming for a comprehensive characterisation at the molecular level. Publication 2 extended TG-FT-ICR MS by the application of different ionisation techniques as well as the integration of data from other mass spectrometric and chromatographic approaches. Mostly the same combination of analytical techniques was also applied in publication 3 for the characterization of PET thermal decomposition products released during pyrolysis.

Figure 20: Chronological order of publications presented in this PhD work. Publication 4, 5 and 6 shaded in darker colour are the first-authorship and the shared first authorship contributions of my thesis.

The application of TG-FT-ICR MS enabled valuable insights into the thermal decomposition behaviour of asphaltenes in Publication 1, 2 and 5, revealing information on occluded compounds and dominant structural motifs. Furthermore, in combination with two-dimensional gas chromatography MS, detailed insights into effects occurring during short-term aging of bitumen could be revealed at the molecular level, which are presented in publication 4. However, the needed integration of data from different ionisation and separation methods with FT-ICR MS information proves that further development of analytical techniques may help in accessing comprehensive description of extremely high complex organic mixtures. Publication 6 aimed for increasing the field of ionisation techniques by presenting single photon ionisation under atmospheric pressure coupled to FT-ICR MS. In the last section, additional unpublished data of the application of different discharge lamps for APPI are presented.

4.1 Evolved gas analysis coupled to FT-ICR MS and method integration for the analysis of complex mixtures

High boiling point petroleum mixtures, such as asphaltenes or bitumen, remain an analytical challenge due to their enormous compositional and structural complexity. Even FT-ICR MS, which is known for its unbeaten mass resolving power and mass accuracy, is limited by the applied ionisation technique, matrix effects or in providing information on structure and distinct chemical functionalities. Publication 1, 2 and 4 especially aimed to widen the analytical approach for the comprehensive investigation of highly complex petroleum-derived materials by the combination of different ionisation methods as well as analytical techniques.

In publication 1-5, we showed the value of combining thermal gravimetry and high-resolution mass spectrometry for the investigation of high complex petroleum derived mixtures. In contrast to direct infusion mass spectrometric techniques, TG-FT-ICR MS provides an additional dimension of information, which enables the temperature-resolved investigation of solid and highly viscous materials at the molecular level. [103] During the evolved gas analysis, low molecular weight petroleum molecules are intactly desorbed and transferred to the gas phase, whereas the pyrolysis of high molecular structures provides information on their thermal fragments. In Figure 21 a), a scheme of the applied set-up is presented. Briefly, the sample is introduced in a small crucible to the thermobalance. Under nitrogen atmosphere, the sample is heated with a defined heating program. In this PhD work, heating rates of 5 K/min to 10 K/min were

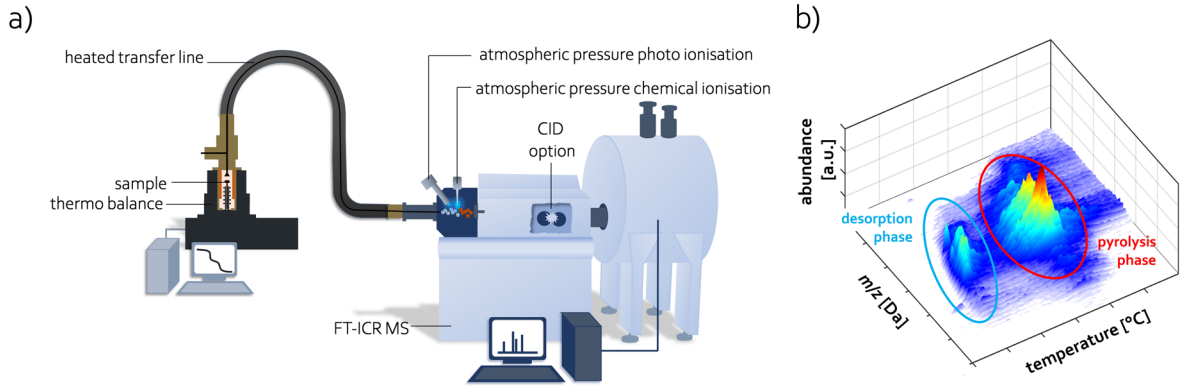

Figure 21 a) Schematic set-up of TG-FT-ICR MS. The thermobalance is coupled to the ionisation source of the FT-ICR MS by a heated transferline. For ionisation, any atmospheric pressure gas phase ionisation technique can be applied. Alternating collision induced dissociation reveals information on core structures. b) Temperature resolved mass spectrum. The spectrum can be divided into the desorption phase (below 300 °C) and the pyrolysis phase (starting between 300-350 °C).

applied. The evolved gas mixture is then transferred over a heated transfer line into the ion source. Ionisation can be carried out by any technique able to ionise molecules in the gas phase under atmospheric pressure, such as APCI (Publication 1-5), APPI (Publication 2) or APLI (Publication 6). As mentioned in the section 3.2.1, each ionisation technique ionises a specific compositional space, highlighting specific chemical functionalities. At slow heating rates, collision induced dissociation (CID) enables the investigation of aromatic core structures in alternation with the detection of regular FT-ICR MS spectra. During the CID process, primarily alkyl side chains are cleaved off leaving the aromatic core intact. [45, 78, 82] Figure 21b) presents a typical temperature-resolved mass spectrum for heavy petroleum material measured by TG-FT-ICR MS. The temperature is plotted on the X-axis, whereas m/z is plotted on the Y-axis. The abundance is applied to the Z-axis and further expressed by colour-coding. The diagram reveals two distinct phases. The first phase occurs below 300°C and is referred to as the desorption phase, in which species are intactly desorbed. The second phase, termed pyrolysis phase, starts between 300 °C and 350 °C. During this

phase, high molecular weight species start to decompose, which leads to the release of smaller pyrolysis products in the gas phase or which initiates coke production.

Publication 1 introduces TG-APCI-FT-ICR MS in combination with CID for SARA-fractions of a heavy fuel oil (HFO), heavy oils and especially asphaltenes. SARA-fractions could be differentiated with respect to their variation in the total ion chromatograms (TIC) as well as on the basis of their different compound class distributions. Heavy oils and asphaltenes from different geological origin revealed smaller differences but could be differentiated at molecular level by combining the mass spectral information of the intact and fragmentation spectra. TG-FT-ICR MS was shown to provide additional and complementary data to the information obtained by gas chromatographic methods, liquid chromatography, or even direct infusion FT-ICR MS. Nonetheless, publication 1 already indicated that the combination of different methodologies will provide a more comprehensive view on highly complex petroleum samples, such as asphaltenes.

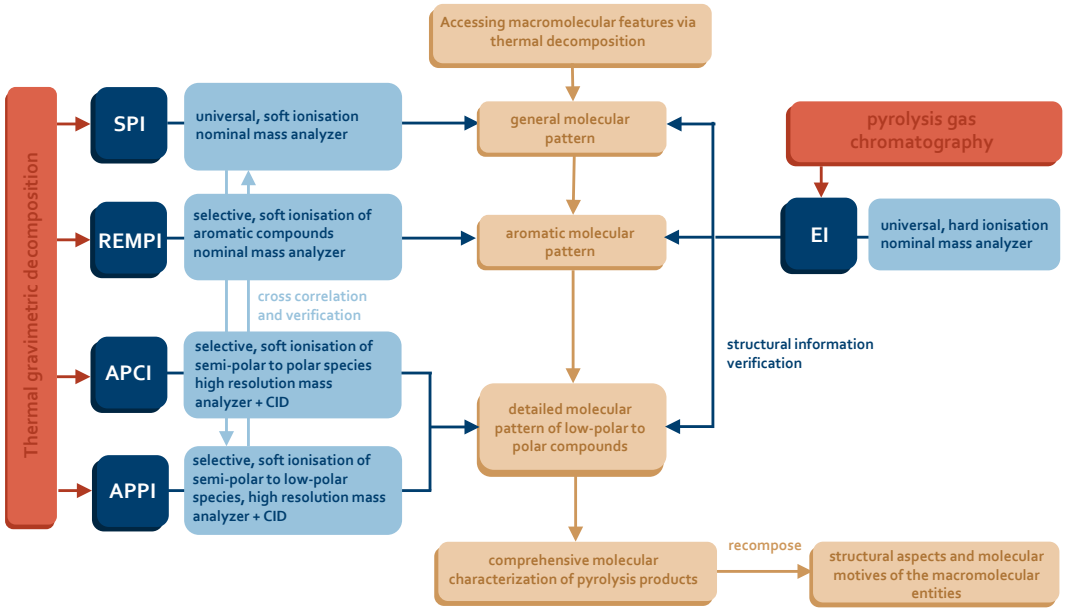

Figure 22: Flowchart for the integration of the TG-MS data and verification by GC-MS. For a comprehensive description of asphaltene pyrolysis products, three different mass spectrometric techniques as well as 5 different ionisation techniques were applied. The comprehensive molecular characterization of the pyrolysis products enabled the recomposition of structural aspects as well as suggesting an average molecular motif for the PetroPhase 2017 asphaltene.

The extreme complex chemical nature of asphaltenes is hardly accessible by any analytical technique alone. Even the application of TG-APCI-FT-ICR MS combined with CID fragmentation is limited by the applied ionisation technique, coke formation by non-evaporable material and limited structural information provided by CID fragmentation. Publication 2 was part of the "Asphaltene Characterization Interlaboratory Study" for the PetroPhase 2017 Conference and aims to overcome analytical limitations by combing the data of three different mass spectrometric analysers, five ionisation techniques, thermal gravimetric and gas chromatographic information as well as elemental analysis. Figure 22 illustrates the data integration strategy. Different TG-MS hyphenations were applied to investigate the thermal decomposition products of asphaltene macromolecules. Several ionisation techniques were involved to access a broad chemical space. Single photon ionisation (SPI) provides the general molecular pattern by universal and soft ionisation. Resonance enhanced multi-photon ionisation (REMPI) enables the soft and selective ionisation of aromatic moieties. APCI and APPI in combination with high resolution FT-ICR MS provide a detailed molecular pattern of low-polar to polar compounds. Additional fragmentation with CID offers information on core structures. Structural estimations from TG-MS techniques were to a certain extent

verified by conventional pyrolysis-GC-MS, which uses EI as a universal, but hard ionisation technique. The comprehensive molecular characterization of the pyrolysis products enabled the recomposing of an average molecular structure of asphaltene molecules present in the PetroPhase 2017 asphaltene.

One-dimensional GC-MS, as applied in Publication 2, rapidly reaches its limits in separation for highly

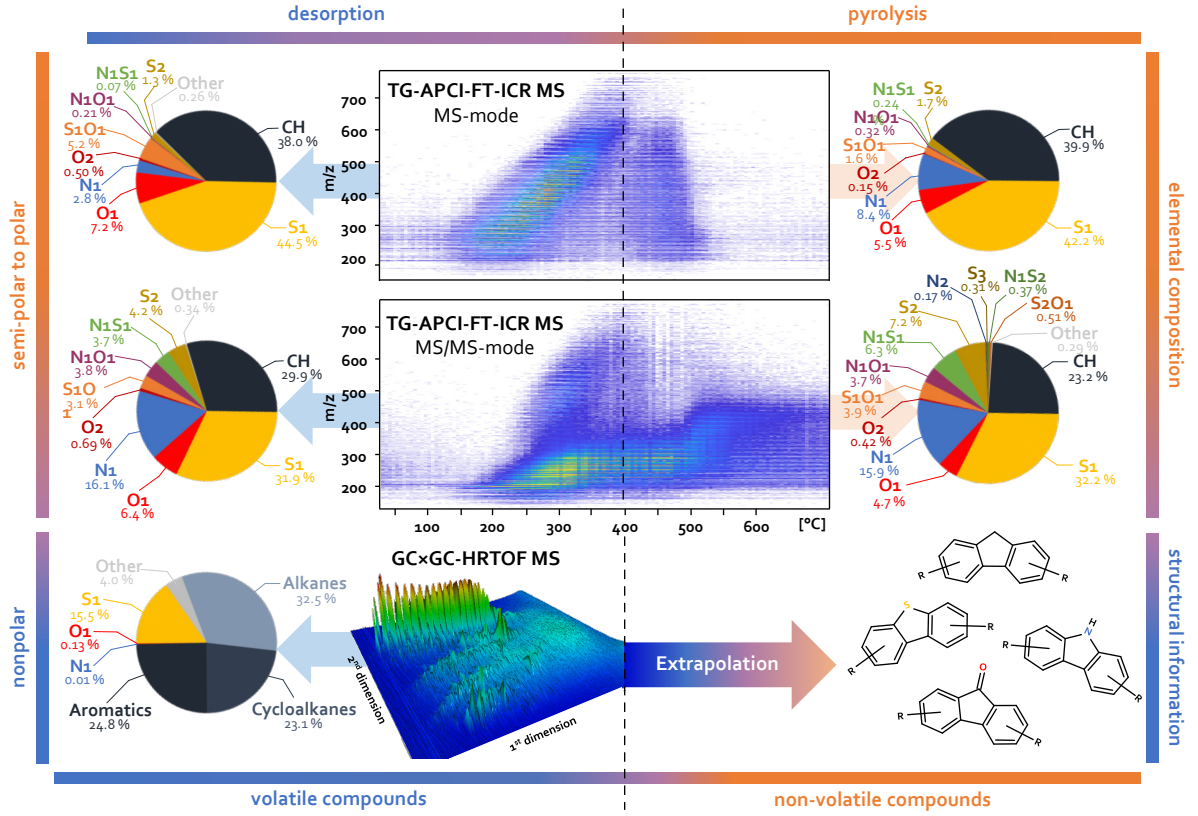

Figure 23: Data integration of TG-APCI-FT-ICR MS and 2D GC×GC-EI-HRTOF MS. TG-FT-ICR MS enables the investigation of intactly desorbable species as well as thermally decomposed fragments of high molecular weight species during the pyrolysis phase. Alternating CID provides information on aromatic core structures. The applied ionisation technique APCI highlights semi-polar to polar compounds as can be seen from the compound class distribution given on the left (desorption phase) and on the right side (pyrolysis phase) of the temperature-resolved mass spectra. 2D GC×GC-EI-HRTOF MS enables structural elucidation of evaporable compounds. The temperature regime covered by 2D GC×GC is mostly congruent with the desorption phase of TG-FT-ICR MS data. Universal EI ionisation also enables the detection of nonpolar components such as alkanes and cycloalkanes.

complex petroleum samples. In publication 4, I aimed to widen the structural description to higher molecular weight compounds to support molecular assignments from FT-ICR MS data. Thus, TG-APCI-FT-ICR MS with CID was combined with two-dimensional gas chromatography high-resolution time-of-flight mass spectrometry (2D GC×GC-HRTOF MS) using EI as ionisation technique. The combination of FT-ICR MS and GC×GC was prior shown to be a valuable analytical tool for the description of petroleum-derived material [162]. In this PhD thesis, the data integration of both techniques was shown to successfully access the compositional space of heavy petroleum fractions at the molecular level. Figure 23 gives a schematic representation of the chemical and structural information addressed by the applied techniques. Temperature-resolved FT-ICR MS spectra can be divided into the desorption phase (evaporation of intactly desorbed compounds) and the pyrolysis phase (release of thermal fragments of high molecular weight compounds). Due to APCI, semi-polar to polar compounds are highlighted. CID (MS/MS-mode) enables the detection of aromatic core structures in alternation with the recording of regular spectra (MS-mode). The pie charts presented on the left hand side of the mass spectra show the chemical class distribution assigned for the desorption phase, whereas diagrams on the right hand side present the revealed composition of the pyrolysis phase. At the bottom of Figure 23, a 2D GC×GC chromatogram is depicted. Due to the ionisation with EI, non-polar compounds present in petroleum-derived material could be accessed as

well. The pie chart in the bottom left corner highlights, that TG-APCI-FT-ICR MS addresses only a minor part of the chemical space, whereas GC×GC-EI-HRTOF MS is able to access non-polar species, such as alkanes and cycloalkanes, and low molecular weight compounds as well. Because of the temperature limits in gas chromatography, the accessed chemical space is mostly equal to the desorption phase of the TG-FT-ICR MS spectra. However, with respect to the Continuum Model of Petroleum (Boduszynski-Model), the obtained structural information can be extrapolated to a certain extent to higher molecular structures.

4.2 Application of evolved gas analysis high resolution mass spectrometry

In this PhD work, evolved gas analysis FT-ICR MS was shown to generate valuable information for a wide range of petroleum-related applications. As common approach for the investigation of polymers, thermogravimetry was applied to PET for the characterization of the pyrolysis products (publication 3). However, in this PhD thesis, I could broaden the application field of TG-FT-ICR MS from polymers to heavy petroleum residues. In publication 4, its value for the characterization of aging products in bitumen was demonstrated. Furthermore, TG-FT-ICR MS provided valuable information for the chemical characterization of asphaltenes and their occluded compounds in publication 1,2 and 5. Especially in publication 5, my results contributed to the debate on asphaltenes' molecular architecture.

4.2.1 Investigation of pyrolysis products of polyethylene terephthalate

Pyrolysis of polymers is often used in literature to study their characteristic decomposition products. The investigation of the evolved gas mixture of PET evaporated during TG-MS enabled the detection of pyrolysis products and the identification of possible decomposition pathways as well as gas phase reactions. The combination of different ionisation techniques as well as mass spectrometric analysers, comparable to the approach described above for asphaltenes [82], allowed the comprehensive chemical description of the pyrolysis effluent in real time. With TG-APCI-FT-ICR MS data, I could contribute elemental compositions for higher molecular weight pyrolysis products, which helped to construct the PET degradation mechanism [163].

Degradation products investigated by TG-APCI-FT-ICR MS covered mainly the O4- and O3-class, but also compounds of the CH-, O1-, and O2-class, as well as highly oxidised compounds of the O7- and O8-class were detected. The highest abundance was observed for *m/z* 193.0495 and 149.0233, which correspond to $C_{10}H_9O_4^+$ and $C_8H_5O_3^+$, respectively. $C_{10}H_9O_4^+$ could most likely be attributed to vinyl-terephthalic acid, which also was observed in the literature [164] as pyrolysis product. Moreover, *m/z* 219.0652 ($C_{12}H_{11}O_4^+$) and *m/z* 167.0339 ($C_8H_7O_4^+$) could be attributed to divinyl terephthalate and terephthalic acid, respectively. Highly oxidised compounds, such as $C_{20}H_{17}O_8^+$ and $C_{18}H_{13}O_7^+$, most likely corresponded to attributed to ester-bridged cyclic or linear dimers [164, 165]. Dimers were found to appear later than smaller pyrolysis products. Their delayed detection may indicate that these compounds are formed in condensed solid or liquid phase and are then transferred to the gas phase at higher temperatures. In a prior study by Dhahak et al. [23] applying direct infusion ESI-FT-ICR MS, oligomers up to *m/z* 550 were observed. The absence of those compounds in TG-APCI-FT-ICR MS indicate their formation by repolymerisation during condensation of the pyrolysis products. This finding emphasises the strength of applying TG-FT-ICR MS as real-time measurement technique. The results obtained by TG-FT-ICR MS were further combined with the

information obtained by TG-SPI-TOF MS and TG-REMPI-TOF MS. With the first mentioned technique, mostly acetaldehyde (*m/z* 44), benzoic acid (*m/z* 122) and a fragment of the PET monomer (*m/z* 149) were detected. The latter selectively ionised aromatic compounds, with *m/z* 230, 178, and 254 as most prominent signals. The data integration of all techniques enabled to propose degradation mechanisms for the major PET pyrolysis products as depicted in Figure 24 [163].

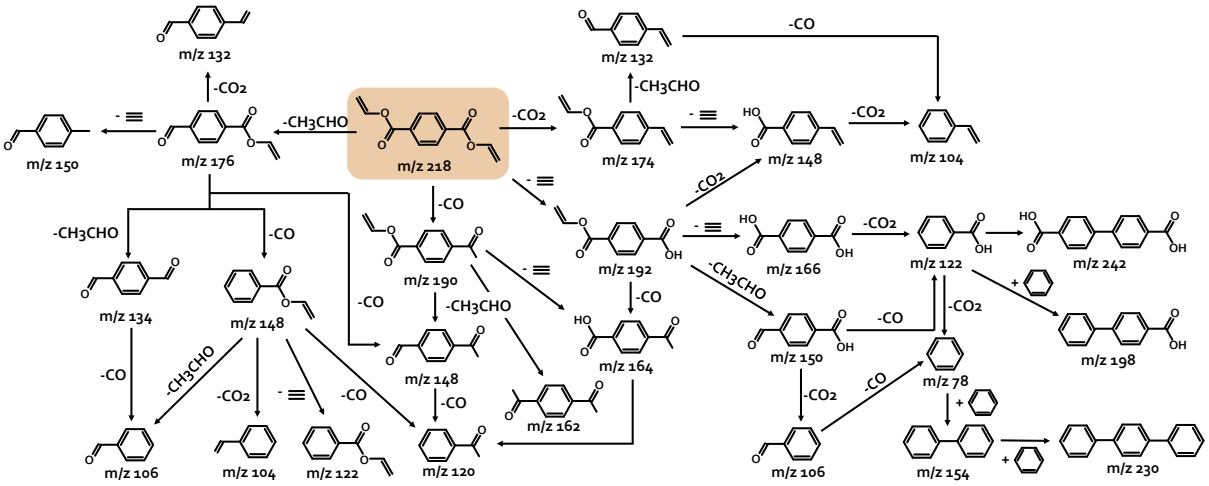

Figure 24: Proposed degradation reaction pathways for the major products of PET degradation [161].

4.2.2 Understanding the aging effects in bitumen at the molecular level

The investigation of aging effects in bitumen is one of the main applicative examples for the analytical value of the TG-FT-ICR MS hyphenation applied in this PhD work. Especially in publication 4, the sum formula assignments of the high-resolution data were supported, validated, and extended in chemical space by structural information obtained by GC×GC-HR-TOF MS. The data integration strategy for both methods is already presented in section 4.1. However, as bitumen is derived from vacuum distillation residues, its share in volatile and semi-volatile compounds is rather low. Typical bitumen is therefore hardly accessible by any gas chromatographic technique. To circumvent this limitation, a model bitumen was generated from a heavy crude oil by removing volatile compounds evaporating below 200 °C. The model bitumen was then subjected to prolonged short-term aging conditions (modified RFT-test) and was aged for 7 days. Each day, a sample was taken and the complete aging series was measured by both techniques in triplicates. Due to the continuum model of petroleum, sum formula assignments as well as structural information can be extrapolated to higher boiling point species, which are mainly represented in "real" bitumen.

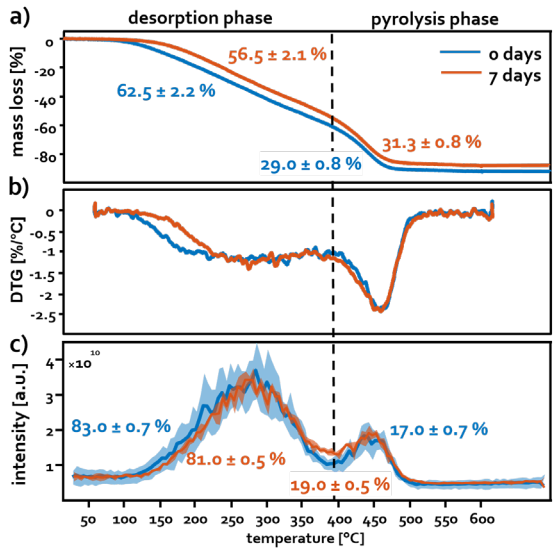

Figure 25: a) Mass loss diagram of the non-aged and 7 days-aged model bitumen (average of the triplicates). b) The corresponding mass loss rates. c) TIC signal of the FT-ICR MS data.

Already on the level of thermogravimetric data, I could reveal alterations between non-aged and 7 days-aged model bitumen. In Figure 25 a), the mass loss and in b), the mass loss rate is depicted. The phase of intact desorption and the pyrolysis phase are

separated at approximately 400 °C. Aging shifted the beginning of the mass loss during the desorption phase to higher temperatures and yielded slightly higher TGA residues. These observations may be caused by the evaporation of semivolatile compounds during the aging procedure or by an increased polarity of the molecules due to oxidation reactions. The total ion count (TIC) detected by FT-ICR MS in Figure 25 c) confirmed these results obtained by thermogravimetry. Non-aged model bitumen revealed a slightly higher abundant desorption phase, whereas the 7 days-aged samples were slightly more abundant in the pyrolysis phase.

Table 1: Compilation of aging related trends observed for different compound classes revealed by TG-APCI-FT-ICR MS for desorption (des) and pyrolysis (pyr) phase.

			CH	O1	O2	S1	S1O1	S1O2	S2	S2O1	N1	N1O1	N1S1	N1S2	N2
number of formulae	(des)	MS	-	(↗)	(↗)	-	(↗)	**↗**	(↘)	-	**↘**	-	(↘)	-	-
		MS/MS	-	**↗**	**↗**	-	-	**↗**	-	**↗**	**↘**	**↗**	(↘)	-	**↘**
	(pyr)	MS	-	**↗**	(↗)	-	**↗**	-	(↘)	-	(↘)	-	(↘)	-	-
		MS/MS	-	**↗**	**↗**	-	**↗**	**↗**	-	(↗)	(↘)	**↗**	(↘)	-	(↘)
summed intensity	(des)	MS	-	**↗**	-	-	-	**↗**	-	-	**↘**	-	(↘)	-	-
		MS/MS	-	**↗**	**↗**	-	**↗**	**↗**	-	**↗**	(↘)	(↗)	(↘)	-	-
	(pyr)	MS	-	**↗**	-	-	**↗**	-	-	-	-	-	(↘)	-	-
		MS/MS	-	**↗**	**↗**	-	**↗**	**↗**	-	**↗**	(↘)	**↗**	(↘)	-	-
intensity-weighed m/z	(des)	MS	-	(↗)	**↗**	-	-	-	**↘**	-	(↘)	-	(↘)	-	-
		MS/MS	-	**↗**	(↗)	-	(↗)	(↘)	-	-	-	**↗**	**↘**	-	(↘)
	(pyr)	MS	(↘)	(↗)	**↗**	(↘)	-	-	**↘**	-	(↘)	-	**↘**	-	-
		MS/MS	-	**↗**	-	-	(↗)	-	-	-	(↘)	**↗**	(↘)	(↘)	(↘)
intensity-weighed DBE	(des)	MS	(↘)	(↗)	**↗**	-	(↗)	**↘**	**↗**	-	(↘)	-	(↘)	(↘)	-
		MS/MS	(↘)	-	(↗)	-	**↗**	**↘**	-	-	(↘)	**↗**	(↘)	-	-
	(pyr)	MS	(↘)	(↗)	-	-	(↗)	-	-	-	(↘)	-	(↘)	-	-
		MS/MS	-	(↗)	-	-	-	-	-	-	(↘)	-	-	-	-

↗ significant increasing trend during aging
(↗) non-significant increasing trend during aging

↘ significant decreasing trend during aging
(↘) non-significant decreasing trend during aging

High resolution FT-ICR MS data enabled the assignment of hundreds of sum formulae during the TG measurements. Due to the application of APCI, especially semi-polar to polar species could be detected. To obtain a general overview on the results, sum formulae are grouped into compound classes and average values, such as summed intensity, abundance-weighted *m/z* or abundance-weighted DBE, are calculated. Table 1 summarizes average values obtained for the desorption and pyrolysis phase of intact FT-ICR MS spectra (MS-mode) and CID-fragmented spectra (MS/MS-mode). Significant aging trends, which were evaluated by the Weir t-test, are highlighted in bold, red (increase) or blue (decrease) colour. Short-term aging caused an increase in number of sum formulae and summed abundance of oxygen-containing compounds of the O1-, O2-, S1O1-, S1O2-, S2O1-, and N1O1-class. Additionally, especially the O1- and O2-class revealed an increase of the mean *m/z* value in MS/MS-mode, which indicates the preferential oxidation of aromatic cores. These findings were in congruence with results provided by other analytical techniques in literature [26, 27]. At this depth of chemical characterization, the CH-class and the S1-class revealed no significant, aging related alterations. However, for nitrogen-containing compound classes, such as the N1-, N1S1-, and N2-class, a decreasing trend was observed. This finding was, to my knowledge, first described by me in publication 4.

Group-type analysis of 2D GC×GC-EI-HR-TOF MS data provided information on structural moieties as well as distinct chemical functionalities influenced by short-term aging. The main classified chemical groups are summarized for the whole aging series in Figure 26. TG-FT-ICR MS data visualized as DBE versus #C diagrams in Figure 27, however, showed distinct aging-related alteration at the molecular level

with respect to changes in DBE or carbon number of the molecules. In contrast to the gas chromatographic technique, TG-FT-ICR MS provided information on high boiling point compounds, occurring during the pyrolysis phase, as well. The DBE versus #C diagrams in Figure 27 represent the compositional space obtained for the desorption phase as well as the corresponding CID data of selected compound classes, whereas in publication 4 also the pyrolysis phase is visualized in detail.

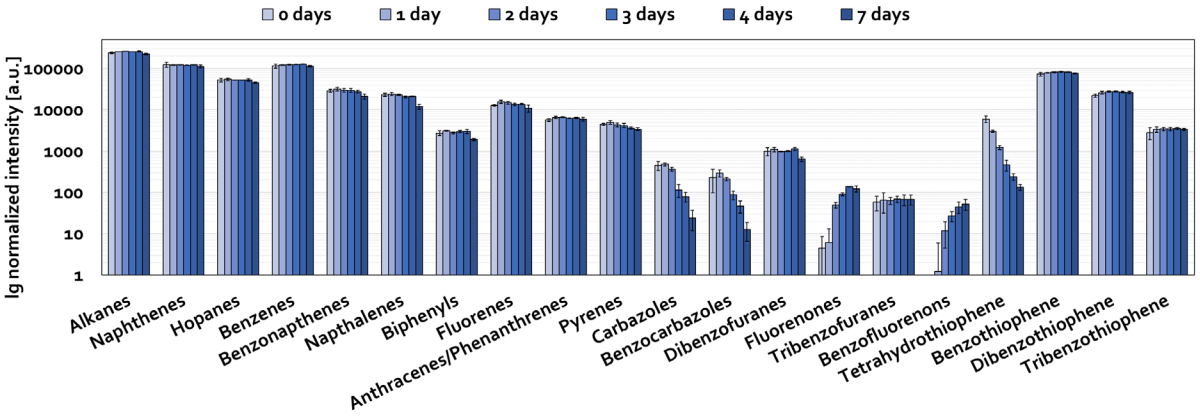

Figure 26: Group-type analysis of 2D GC×GC-EI-HR-TOF MS data of the complete aging series. Carbazoles, benzocarbazoles and tetrahydrothiophenes revealed a distinct decrease over the aging time. Fluorenones and benzofluorenones strongly increased during aging.

GC×GC-HR-TOF MS revealed that 80-82 % of the classified peak area in the model bitumen accounts for hydrocarbons, which can be subdivided into n- and iso-alkanes, cycloalkanes, and aromatics. As Figure 26 shows, all these chemical classes revealed no significant alterations during aging. Similar was observed for the desorption phase of the FT-ICR MS data, whereas the pyrolysis phase revealed a slight increase of low alkylated aromatic compounds as well as highly aromatic core structures. Far more pronounced, the O1-class and O2-class revealed a steady increase during aging in the desorption and pyrolysis phase. In MS-mode, especially compounds with low carbon numbers increased, indicating an influence of steric hindrance of longer alkyl chains. O1-class species with DBE 10, tentatively attributed to fluorenones, revealed the strongest increase. Moreover, it was observed that oxidised compounds survive the fragmentation process, which suggests an oxidation at the aromatic core rather than at side chains, which would be cleaved of during the CID process. GC×GC-HR-TOF MS are in good accordance with structural suggestion made for the FT-ICR MS information. Fluorenones and benzofluorenones revealed a distinct increase during aging, whereas furans exhibited no changes. The formation of carbonylic functions, especially on aromatic compounds with activated carbon, was shown to be preferred in contrast to the formation of cyclic bonded oxygen and is in congruence with the literature [27, 166–169].

Sulphur-containing compounds dominated the FT-ICR MS spectra as a consequence of the applied ionisation technique APCI. With respect to the average values, S-classes hardly revealed any changes. Nonetheless, on the molecular level, I could show a significant decrease for S1-class compounds with DBE values below 4. Similar was observed for tetrahydrothiophenes in the GC×GC-HR-TOF MS data, whereas benzothiophenes (DBE 6), dibenzothiophenes (DBE 9) and benzonaphthothiophenes (DBE 12) revealed no changes during aging. This led to the assumption, that especially non-aromatic sulphur-components are affected by aging [170, 171]. The formation of sulfoxides is one of the main short-term aging effects of bitumen described in literature [27, 34]. TG-FT-ICR MS data revealed an increase in S1O1-class compounds with DBE values between 4 and 15, whereas low DBE compounds decreased. The increasing effect could be attributed to the oxidation of thiophenic structures. The decrease of low DBE compounds was most probably caused by further oxidation of the S1O1-species to S1O2-class compounds.

The alterations of N-containing compounds in bitumen during aging are poorly described in the literature [172]. In this publication, I could reveal a significant decrease of aromatic nitrogen compounds in the TG-FT-ICR MS data. Both, desorption and pyrolysis phase, as well as CID spectra, revealed a reduced abundance after aging. These findings were supported by GC×GC-HR-TOF MS information, which showed a distinct reduction of carbazoles and benzocarbazoles over aging time. Two possible aging reactions were suggested to explain the decrease. The first reaction is the oxidation of highly aromatic N-species, which was indicated by an increase of the N1O1-class in the MS/MS-spectra. The second possible reaction was indicated by a slight increase of low alkylated aromatic thermal fragments during the pyrolysis phase, which gave evidence for possible condensation reactions [173].

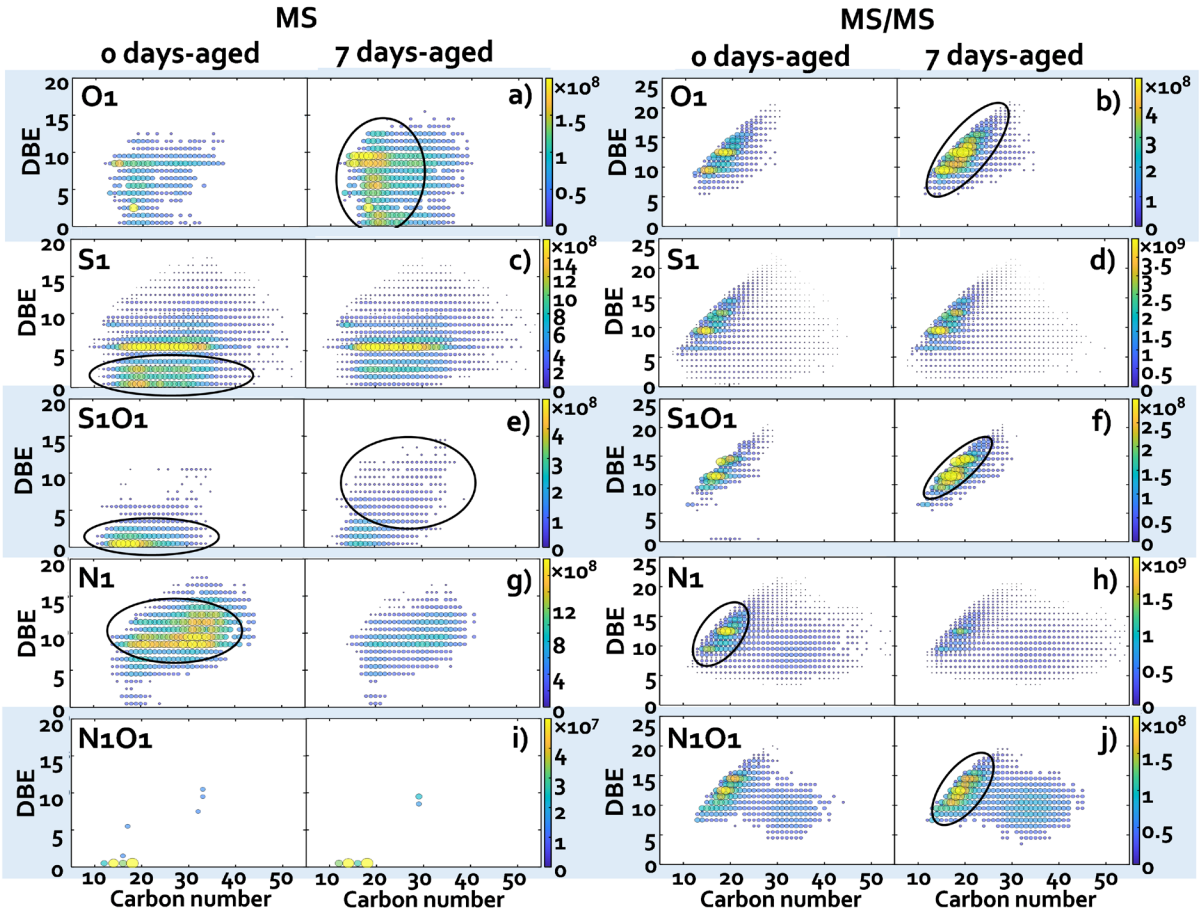

Figure 27: Selected DBE versus #C plots for MS-mode and MS/MS-mode of the desorption phase of non-aged and 7 days-aged model bitumen.

To conclude, in publication 4, I could show that the data integration of TG-APCI-FT-ICR MS with CID fragmentation and GC×GC-EI-HR-TOF MS is suitable to investigate aging effects in bitumen. Furthermore, I could reveal distinct aging effects. Oxygen-containing compounds, such as the O1-, O2-, S1O1-, and N1O1-class as well as distinct chemical functionalities, such as fluorenones and sulfoxides, were found to increase. Non-aromatic sulphur-containing compounds, including thiolanes, as well as aromatic nitrogen-containing compounds, such as acridines, were found to strongly decrease during aging.

4.2.3 Chemical characterization of occluded material and pyrolysis products of asphaltenes

Asphaltenes are known as the petroleum fraction with the highest compositional and structural complexity associated with one of the biggest analytical challenges. However, in this PhD work, I could show that evolved gas analysis of thermally degraded asphaltenes in combination with high resolution mass spectrometry is a versatile and valuable tool to head for the elucidation of the chemical und structural composition of asphaltenes. Publication 1, 2 and 5 occupy different aspects of asphaltene characterization. Nonetheless, since all publications include the thermal degradation of asphaltenes, the three main pathways asphaltenes undergo during heating are presented in more detail in the following and are illustrated in Figure 28.

(1) Asphaltenes are known to aggregate already at very low concentrations [174, 175]. Compounds of the maltene fraction can be occluded by asphaltenes in pores or by polar interactions [83, 176, 177]. During heating, occluded compounds are (partially) released from the aggregates and are observed as intact evaporated compounds during the desorption phase at temperatures up to approximately 300 °C. [45, 78]

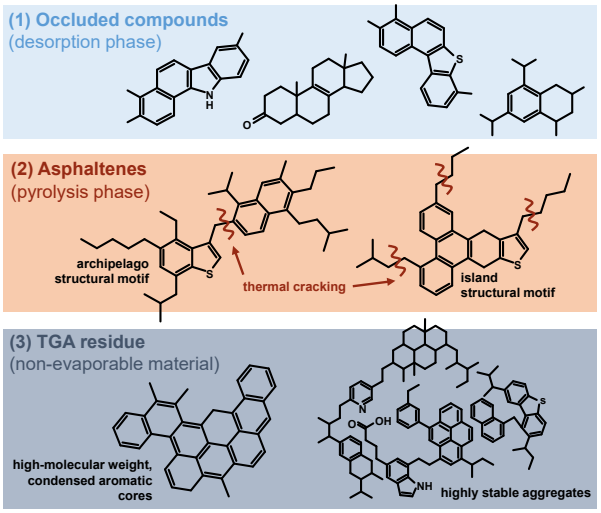

Figure 28: Evaporation and thermal decomposition behaviour of asphaltenes.

(2) During the pyrolysis phase, which starts between 300 to 350 °C, asphaltenes decompose by cleavage of C-C or C-S bonds [104]. Depending on the molecular structure, different pyrolysis pathways can be observed. Archipelago-type (multicore) asphaltenes tend to decompose at aliphatic linkers bridging smaller aromatic cores preserving alkyl side chains [61, 63, 79]. Island-type (single core) asphaltenes likely decompose by the cleavage of side chains, while a low alkylated, highly aromatic core remains [79, 105–107].

(3) High molecular weight aromatic core structures, which cannot be evaporated, form coke during pyrolysis and remain as residue [78, 79, 105, 107]. Besides that, highly stable asphaltene aggregates may survive the heating process and form coke instead of thermally degrading into smaller, evaporable fragments [178].

During the precipitation of asphaltenes from crude oil/ toluene mixture with paraffinic solvents, species of the maltene fraction can be co-precipitated with the asphaltenes. The occluded compounds can be trapped inside pores of asphaltene aggregates, entangled with asphaltenes or bound by polar interactions [83, 177, 179–181]. In publication 1 we showed by TG-APCI-FT-ICR MS that poorly washed asphaltenes contained a variety of occluded material, which chemically differs and in abundance between n-pentane (C5), n-hexane (C6) and n-heptane (C7) as precipitation solvent. Figure 29 illustrates the differences between the precipitation effects for one exemplary heavy oil asphaltene. In Figure 29 a), the total ion chromatogram (TIC) of the mass spectrometric measurements for the C5-, C6-, and C7-precipitated asphaltenes are presented, while the dashed line indicates the separation into desorption and pyrolysis

phase. For C5-precipitation, the highest amount of intactly evaporable material was observed during the desorption phase. With larger paraffins as solvent, the abundance of the desorption phase decreases. Figure 29 b) emphasizes the differences between C5- and C7-precipitated asphaltenes. Temperature-resolved mass spectra of C5-asphaltenes clearly revealed a higher abundant desorption phase as C7-asphaltenes precipitated from the same heavy oil. Species occurring in the desorption phase exhibited lower mean DBE values between 5-7 in comparison to a mean DBE of 8-10 during the pyrolysis phase. CID-fragmentation revealed in mean three to four-ring aromatic core structures for occluded material and four to five fused aromatic rings for asphaltene pyrolysis decomposition products. Publication 1 further revealed that occluded material differed in compound class distribution from the asphaltene pyrolysis phase, which is depicted in Figure 29 c). C5-precipitated asphaltenes were enriched in heteroatom-containing classes, such as the O1-, S1-, S1O1- and O2-class. Co-precipitated maltenes were shown to vary in their chemical composition to a larger extent among the precipitant than the asphaltene pyrolysis products.

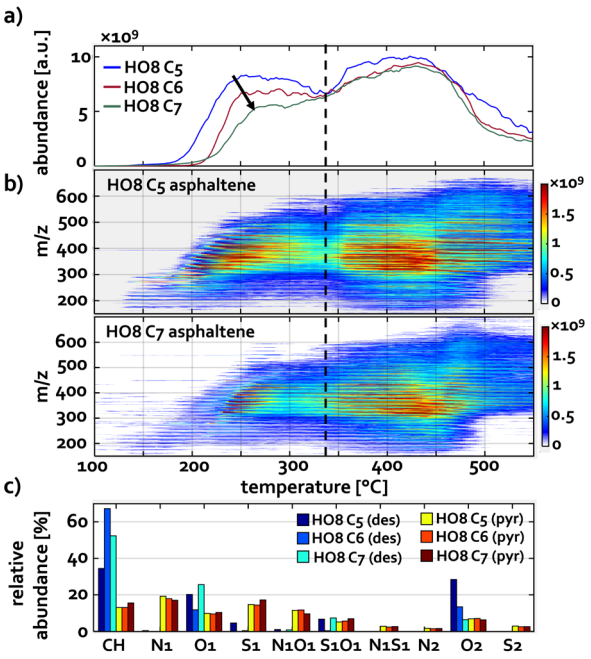

Figure 29: Heavy oil petroleum asphaltenes precipitated with different paraffinic solvents. a) TIC signal of C5-, C6- and C7-precipitated asphaltenes. b) Temperature-resolved mass spectra of C5- and C7-precipitated asphaltenes. c) Compound class distribution of the desorption and pyrolysis phase, exemplarily shown for one heavy oil asphaltene.

Since occluded compounds cause matrix effects and distort the chemical characterization of asphaltenes, increased efforts were made to clean asphaltenes from occluded material [181, 182]. The asphaltene provided during the interlaboratory study for the PetroPhase 2017 conference was highly purified through intensive Soxhlet extraction of occluded material with n-heptane [83, 88] and was subject of publication 2. In contrast to the poorly washed asphaltenes in publication 1, we revealed no occluded material evaporating below approximately 300 °C during the desorption phase with several analytical techniques. Neither TG-FT-ICR MS, nor TG-TOF MS, nor pyrolysis GC as well as the application of five different ionisation techniques revealed any considerable signal for temperatures associated with intact desorption.

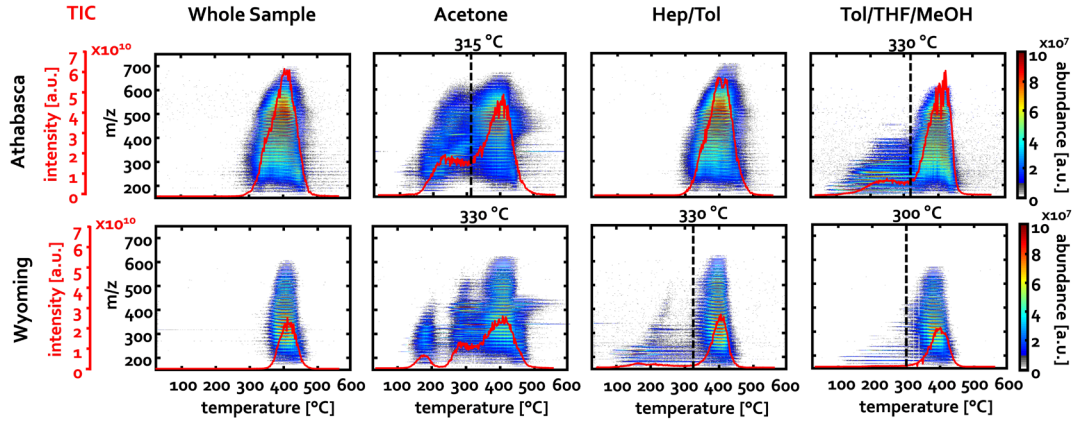

Figure 30: Temperature-resolved mass spectra of highly purified Athabasca and Wyoming asphaltenes and their different solubility fractions. The TIC is overlaid in red. Whole asphaltene revealed no desorbable material, whereas extrography fractions exhibited occluded material released during the desorption phase.

Similar was observed in Publication 5 for Athabasca bitumen asphaltenes and Wyoming deposit asphaltenes purified with the same protocol as the Petro-Phase 2017 asphaltene. Nonetheless, after extrography fractionation on silica with acetone, heptane /toluene (Hep/Tol 1:1 v/v), and toluene/ tetrahydrofuran/ methanol (Tol/THF/MeOH 10:10:1) [86, 87, 89], additional occluded material could be released and detected with TG-APCI-FT-ICR MS. Figure 30 shows the time resolved mass spectra obtained for both asphaltene samples and their solubility fractions. Especially the acetone fraction revealed high abundant signal during the desorption phase, followed by the Tol/THF/MeOH fraction and the Hep/Tol fraction. In this publication, I could indicate that highly occluded material is potentially bonded by polar interactions into cooperative aggregates formed by asphaltene molecules of different solubility fractions. During the fractionation process, these aggregates seem to partially be dispersed, which enables the release of smaller, occluded compounds during the desorption phase of the TG-FT-ICR MS measurements. Asphaltenes enriched in archipelago structural motifs (Athabasca) exhibited higher abundant occluded material than asphaltenes enriched in island structural motifs (Wyoming). Publication 5 further reveals, that the released occluded material differs in chemical composition as well as structure among the solubility fractions depending on the geological origin of the asphaltenes. The extraction with acetone was shown to yield the broadest chemical diversity, whereas the Tol/THF fraction was enriched in occluded oxygen-containing asphaltenes. Figure 31 presents DBE versus #C plots of selected compound classes of Athabasca asphaltenes. The diagrams clearly reveal that occluded material covers two different compositional spaces: The first region contains species with high aromaticity and short alkylation (island-like), while the other region is composed of compounds with lower DBE and higher carbon numbers (archipelago-like). It depends on the compound class and the solubility fraction as well as the asphaltene origin, how pronounced the different regions are.

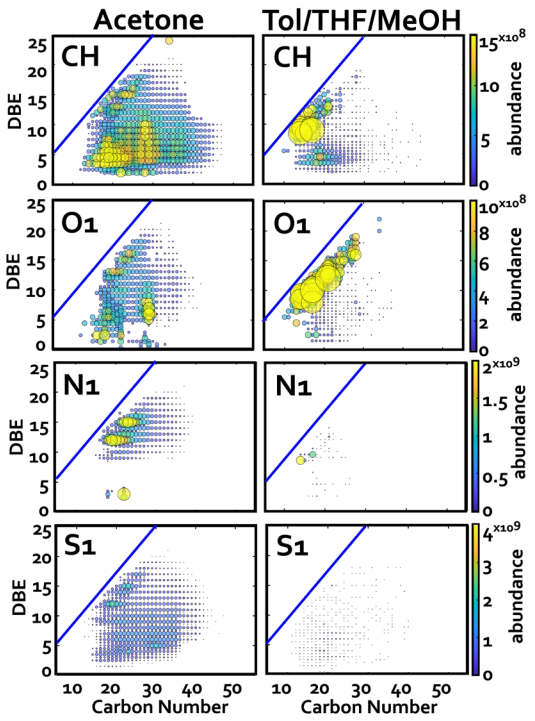

Figure 31: Selected DBE versus #C diagrams of occluded material of Athabasca asphaltenes released during the desorption phase of TG-APCI-FT-ICR MS. The blue line indicates the planar aromatic limit.

This PhD work not only contributes to the chemical characterization of occluded compounds in asphaltenes, it also aimed to add information to the debate of the asphaltenes' structure by employing thermal gravimetry hyphenated to high resolution mass spectrometry. In publication 2, we combined TG-FT-ICR MS, using APCI and APPI as ionisation techniques, with data from TG-SPI/REMPI-TOF MS as well as pyrolysis GC-MS to propose an average molecular structure for the PetroPhase 2017 asphaltene. The evolved gas analysis of the pyrolysis products of the highly purified asphaltene revealed information on smaller building blocks. Each ionisation technique, however, covers a specific chemical space and only the integration of the data from all techniques provides a comprehensive information. Pyrolysis GC-MS, with universal electron ionisation, showed a dominant alkene and alkane pattern, which provided information likely on alkyl side chains cleaved off during the pyrolysis process. Comparable information was revealed by TG-SPI-TOF MS. The spectra exhibited an intense C3-C35 alkene pattern, which peaks at propene and decreases exponentially in intensity towards higher carbon numbers. Furthermore, H_2S was detected with high abundance indicating the decomposition of sulphur bridges linking aromatic cores. TG-REMPI-TOF

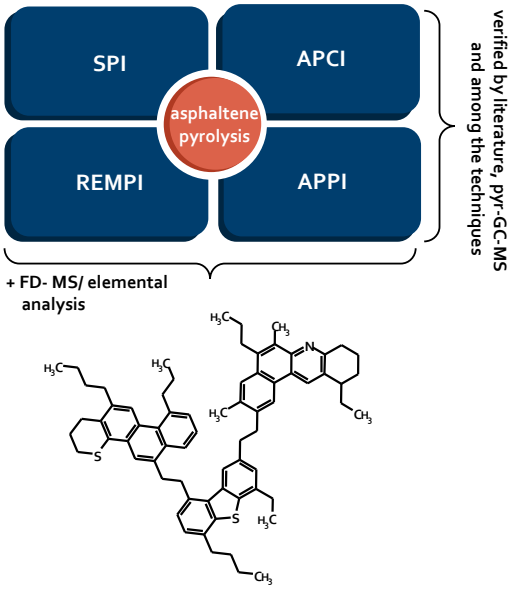

Figure 32: The integration of different ionisation methods for the investigation of thermal decomposition products of the Petrophase 2017 asphaltene enabled the suggestion of an average recomposed molecular structure.

MS accesses, due to the resonance-enhanced multi-photon ionisation process, selectively aromatic thermal decomposition products. The PetroPhase 2017 asphaltene revealed 1-5 ring aromatic core structures and their alkylated homologues series up to *m/z* 500, with a mean m/z value around 225 and 2-3 aromatic rings with 3-10 alkyl units on average. TG-APCI-FT-ICR MS and TG-APPI-FT-ICR MS revealed remarkably similar results. The high resolving power as well as the selectivity to semi-polar to polar compounds of these techniques enabled the identification of an intense homologous series of benzothiophenes and dibenzothiophenes and their alkylated derivatives, while APCI additionally highlighted oxygen-containing compounds. By data integration of the obtained results in combination with additional information from field desorption /ionisation MS (molecular weight distribution) and elemental analysis, an average molecular structure for the PetroPhase 2017 asphaltene could be recomposed. The proposed structure is depicted in Figure 32, showing an archipelago-type asphaltene composed of three core structures linked by alkyl bridges.

The tendency of asphaltenes to form aggregates drastically complicates their analytical investigation [14, 85–87]. In direct infusion mass spectrometry, asphaltenes were shown to strongly differ in monomer ion yield with respect to their structure [85]. Island-type asphaltenes revealed high monomer ion yield, whereas archipelago-type asphaltenes tend to form non-ionisable aggregates [85]. Nonetheless, the application of infrared multiphoton dissociation (IRMPD) on direct infusion FT-ICR MS spectra contributed valuable information to the structural debate [84–87]. In Publication 5, which is one of the main contributions in my PhD work, I could show that also TG-FT-ICR MS is a valuable technique to participate in the structural discussion on asphaltenes. In this study, I investigated two different asphaltenes, one of which is enriched in the island structural motif (Wyoming Deposit asphaltenes) and one is enriched in the archipelago structural motif (Athabasca bitumen asphaltenes). To deepen the chemical and structural investigation, both asphaltenes were fractionated by extrography into an acetone, heptane/ toluene (Hep/Tol 1:1 v/v), and toluene/ tetrahydrofuran/ methanol (Tol/THF/MeOH 10:10:1) fraction [86, 87, 89]. Already the thermal gravimetric data, which are depicted in Figure 33, revealed noticeable differences between both asphaltenes. Archipelago-enriched asphaltenes were shown to considerably form less TGA residue (37-50 wt.-%) than island enriched asphaltenes (57-78 wt.-%). Furthermore, it was revealed that whole asphaltenes yield higher TGA residues than their solubility fractions. This result indicated effects caused by cooperative aggregation between asphaltene molecules of different fractions. The aggregates were suggested to be highly thermally stable, which likely led to coke formation instead

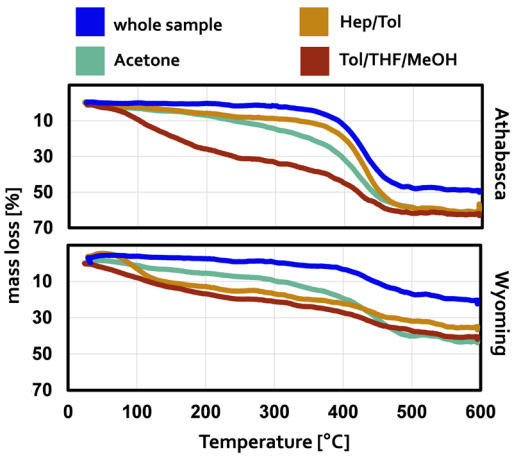

Figure 33: Mass loss diagram of archipelago-enriched asphaltenes (Athabasca) and island-enriched asphaltenes (Wyoming). Athabasca asphaltenes revealed noticeably higher mass loss for all fractions than Wyoming asphaltenes.

of thermal decomposition into smaller, evaporable pyrolysis products. The mass spectrometric signal I revealed by TG-APCI-FT-ICR MS is presented in Figure 30. Desorption and pyrolysis phase were separated at the minimum TIC signal (overlaid in red) between both phases indicated by the dashed line. Although both phases partially overlap, the desorption phase is mostly represented by occluded compounds discussed in detail above, whereas the pyrolysis phase is mostly represented by thermal decomposition products of "real" asphaltenes. The investigation of fractionated asphaltenes in publication 5 increased the number of assigned sum formulae 1.5 to twice the amount in comparison to the whole asphaltene samples, likely because of reducing matric effects and aggregation. The acetone fraction revealed the highest amount of assigned elemental compositions for both asphaltenes which is presumably an effect caused by aggregation effects, because acetone is known to extract asphaltene compounds with high monomer ion yield [85, 86, 180, 183]. For the asphaltene pyrolysis phase, eleven compound classes were detected, consisting of the CH-, S1-, S2-, S3-, O1-, O2-, N1-, S1O1-, S1O2-, N1O1-, and N1S1-class. In comparison to direct infusion FT-ICR MS spectra, asphaltene species detected with TG-FT-ICR MS exhibit at first glance unusual low complexity as a result of pyrolytic cracking [11, 79]. In Figure 34, exemplary structures of mono-heteroatom- as well as poly-heteroatom-containing asphaltenes of both structural motifs are presented. If multicore asphaltenes containing heteroatoms in different cores are thermally cracked into smaller building blocks, the complexity of the compound classes is reduced. Single core, multi-heteroatom asphaltenes likely form coke due to their high polarity and the large size of their aromatic moiety instead of being evaporated.

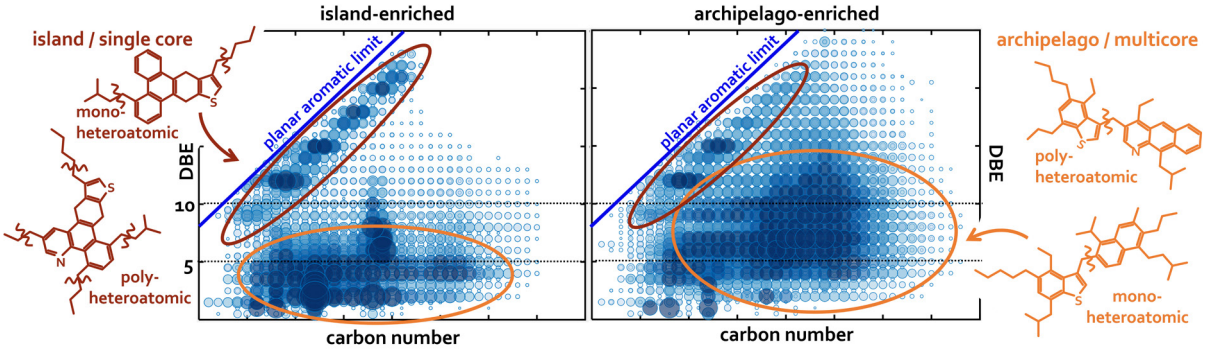

Figure 34: DBE vs. #C diagrams of the acetone fraction pyrolysis phase of island-enriched and archipelago-enriched asphaltenes measured by TG-APCI-FT-ICR MS. All compound classes are overlaid. Island-type asphaltenes decompose into highly aromatic core structures with short alkylation and thermal fragments with DBE values below 5 and comparatively high alkylation. Archipelago-type asphaltenes revealed high abundant thermal fragments with DBEs of less than 15 and high carbon numbers /alkylation.

The DBE vs. #C diagrams in Figure 34 present one of the main findings I revealed in publication 5. Thermal decomposition products of island-type and archipelago-type asphaltenes cover different compositional spaces. Pyrolysis fragments of island-type asphaltenes are characterised by abundant, highly aromatic compounds with low alkylation (carbon numbers) clustering at the planar aromatic limit, which are formed by the cleavage of alkyl side chains from the single, highly aromatic core. Island-enriched asphaltenes further revealed high abundant thermal fragments with DBE values of less than 5, most probably formed by cleaved small pendant groups or side chains, which formed alkenes or naphthenes due to the thermal decomposition process. Archipelago-type asphaltenes are characterized by abundant pyrolysis products with DBE values below 15 and comparatively high carbon numbers/ alkylation, which are caused by the thermal decomposition of alkyl linkers bridging several aromatic cores. Highly aromatic core structures are less abundant in archipelago enriched asphaltenes compared to island-enriched asphaltenes.

To conclude, I could reveal in this PhD work, that TG-FT-ICR MS provides valuable information for the chemical characterization of occluded material coprecipitated with asphaltenes as well as valuable contributions concerning the critical debate on the asphaltene structural motifs. Those insights are of interest from petroleum processing, upgrading through to petroleum transportation and storing. As fossil fuels, even bio crude oils contain asphaltenes, which emphasizes the importance of asphaltene characterization with regard to future fuels.

4.3 Development of new analysis techniques for the investigation of complex mixtures

Thus far, I could show in this PhD work, that reducing the complexity of crude oil-derived material by fractionation or by applying selective ionisation techniques, drastically improves the comprehensive chemical characterization of those complex mixtures. By applying selective ionisation techniques, matrix effects can be reduced even without additional sample pre-treatment. Therefore, the development of selective and sensitive ionisation methods is of high analytical interest. In this section, I present the further development of APPI by applying this techniques with other wavelength than commonly available. Furthermore, in publication 6, I aimed to combine the advantages of APPI, which covers a broad chemical space, and APLI, which achieves very low detection limits, by introducing a new ionisation technique: atmospheric pressure single photon laser ionisation (APSPLI).

4.3.1 Xe/Kr-atmospheric pressure photo ionisation

Each ionisation technique covers a specific compositional space. By applying a certain technique, particular compound classes can be highlighted, reduced, or even completely disregarded. Reducing the chemical space also helps to decrease matrix effects and enables improved detection of less abundant species. The further development of ionisation techniques is therefore essential to obtain comprehensive chemical characterization of complex organic mixtures in mass spectrometry. In this section, I aimed to further develop atmospheric pressure photo ionisation by applying a Xenon discharge lamp for ionisation instead of the commonly applied Krypton discharge lamps. The data presented is still unpublished. In Figure 35, ionisation energies of different, commercially available noble gases discharge lamps are presented. With commonly applied Krypton discharge lamps, species with an ionisation energy below 10.6 (117 nm) or 10.0 eV (124 nm) can be ionised. Xenon

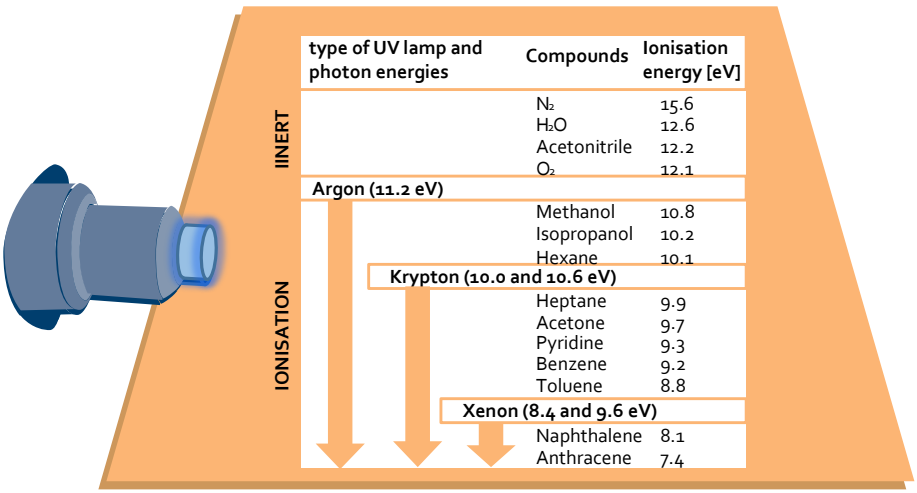

Figure 35: Ionisation energies of different, commercially available discharge lamps.

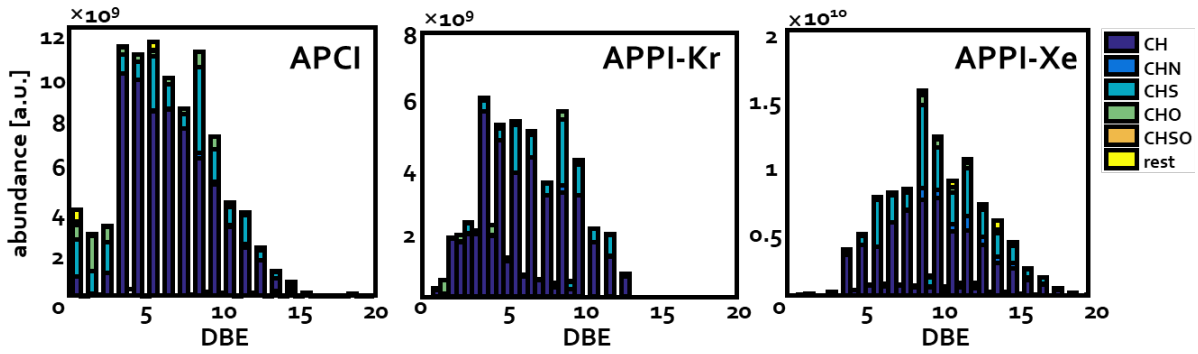

Figure 36: Stacked bar plots of for different compound classes showing the radical cation and protonated ion distribution for a light crude oil measured by APCI-, Kr-APPI- and Xe-APPI-TG-FT-ICR MS. APCI revealed mostly protonated ions for all compound classes. Kr-APPI showed protonated as well as radical cations, especially for low-DBE CH-class compounds. Xe-APPI mostly revealed radical cations for all compound classes.

discharge lamps provide photons with 8.4 (148 nm) and 9.6 eV (129 nm). Predominantly polyaromatic hydrocarbons lie below this ionisation energy.

In this PhD work, I investigated Xe-APPI as potential ionisation technique for gas phase ionisation in combination with TG-FT-ICR MS. To define the accessible chemical space of Xe-APPI, the technique was compared to the established ionisation techniques Kr-APPI and APCI. As exemplary sample, a light crude oil (CPC-blend) was applied and measured with all techniques under the same conditions. All ionisation techniques mainly revealed compounds of the CH-, O1-, S1- and N1-class. Nonetheless, small differences in the relative abundancies between the ionisation techniques were observed. APCI revealed approximately 66 % for the CH-class, 23 % for the S1-class, 8.7 for the O1-class and 1.1 % for the N1-class. In comparison, Kr-APPI revealed a higher percentage for the CH-class, which can be mostly attributed to the fact that Kr-APPI produces both radical molecular cations and protonated quasi-molecular ions [125]. S1-class, O1-class, and N1-class contributed approximately 17 %, 6.1 %, and 0.7 %, respectively. Interestingly, Xe-APPI provides a lower relative abundance for the CH-class of approximately 57 % compared to the afore-mentioned ionisation techniques. S1-, O1-, and N1-class account for 31 %, 4.7 % and 5.3 %, respectively. Figure 36 presents the abundance distribution as stacked bar plot for the main compound classes for each DBE value. Protonated species occur on half-integer DBE values (even electron configuration), whereas radical cations have integer DBE (odd electron configuration). APCI predominantly produced protonated ions for all compound classes as well as DBE values. Kr-APPI, however, revealed especially for low-DBE compounds both ion types. Mostly non-aromatic compounds with DBE-values below 4 re-

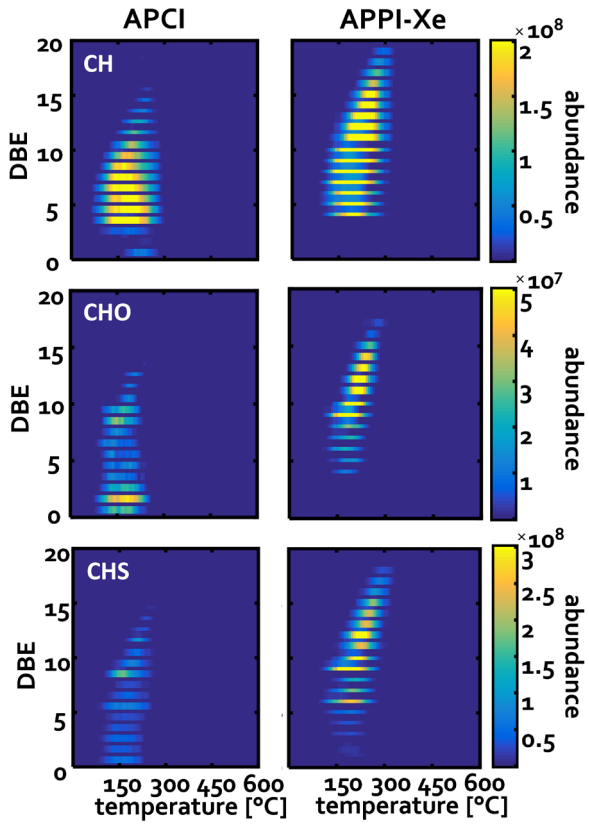

Figure 37: Temperature-resolved DBE plots colour-coded with the absolute abundance for different compound classes of a light crude oil measured by APCI- and Xe-APPI-TG-FT-ICR MS.

vealed both ion types, whereas aromatic compounds reveal higher abundancies for radical cations. The higher the DBE value, the more the ratio between odd and even ions is shifted to the radical cations. Xe-APPI is predominantly able to ionise aromatic compounds with DBE values greater or equal to 4. Radical cations are strongly pronounced, and protonated species occurred only in minor amounts. Furthermore, the DBE distribution is shifted to higher DBE values compared to the other ionisation techniques.

In Figure 37, temperature-resolved DBE plots for a light crude oil measured by APCI- and Xe-APPI-TG-FT-ICR MS are presented for the CH-, O1-, and S1-class. Although both techniques revealed signal between 100 to 300 °C, the covered DBE range differs. APCI more efficiently ionises low-DBE compounds than Xe-APPI. The Xe-APPI data clearly revealed a distinct cut-off at DBE 4, especially for the CH- and O1-class. This result indicated that only aromatic compounds are ionised by Xe-APPI. Furthermore, highly aromatic compounds with DBE values up to 20 were pronounced in Xe-APPI. The detection of compounds with higher DBE values compared to APCI could be an effect of the low ionisation potential of highly aromatic compounds as well as the reduced complexity of the mass spectrometric data by Xe-APPI.

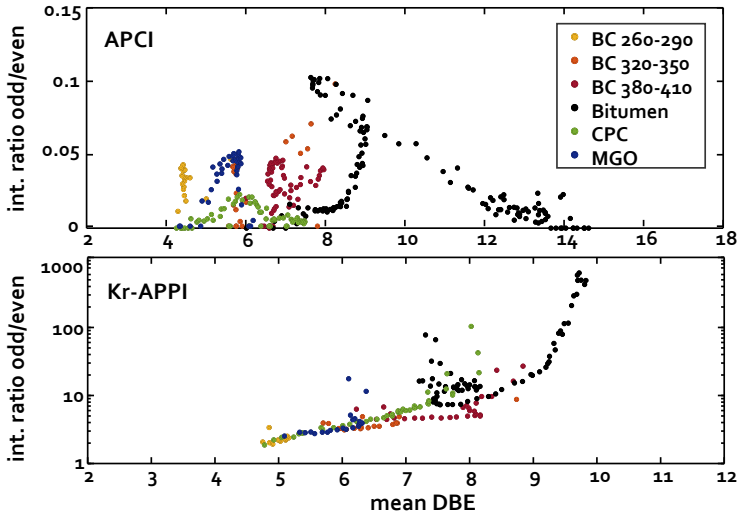

Figure 38: intensity ratio of radical cations (odd) and protonated ions (even) for temperature-resolved TG-FT-ICR MS measurements. The odd/even ratio is plotted over the mean DBE of each spectrum. APCI revealed no trend, whereas APPI revealed an increase of the odd/even ratio for higher mean DBE values.

As already indicated for APPI above, the higher the DBE, the higher is the number of radical cations in comparison to protonated species. To investigate this correlation, I measured different petroleum boiling cuts (BC), marine gas oil (MGO), CPC-Blend, and a bitumen. Each of these samples covered a distinct chemical space. The boiling range of the samples and therefore, their average molecular mass as well as DBE can be sorted in the following order: BC 260-290 °C, MGO, BC 320-350 °C, BC 380-410 °C, and bitumen. Since CPC-blend is a light crude oil, it covers a broader chemical space. All samples were measured temperature resolved by TG-FT-ICR MS. For each spectrum, the intensity ratio of cations (odd) and protonated ions (even) was calculated. In Figure 38, the odd/even ratio is plotted over the mean DBE for each spectrum. APCI and Kr-APPI showed distinct differences. APCI revealed no trend correlating with molecular weight or DBE, whereas Kr-APPI revealed an increasing trend. Comparable results were obtained for Xe-APPI, but the increasing trend for the bitumen sample was less pronounced than in Kr-APPI. In APCI, other aspects, such as chemical functionalities, are more important for the ion-type formation than aromaticity.

4.3.2 Atmospheric pressure single photon laser ionisation

In the last two decades, a variety of atmospheric pressure ionisation techniques were developed enormously increasing the application field of mass spectrometry. In 1999, atmospheric pressure laser ionisation was introduced by Schmidt et al. [126] as additional ionisation approach to the existing ESI, APCI, and APPI techniques. While ESI and APCI are able to ionise polar to semi-polar compounds, APPI and APLI are

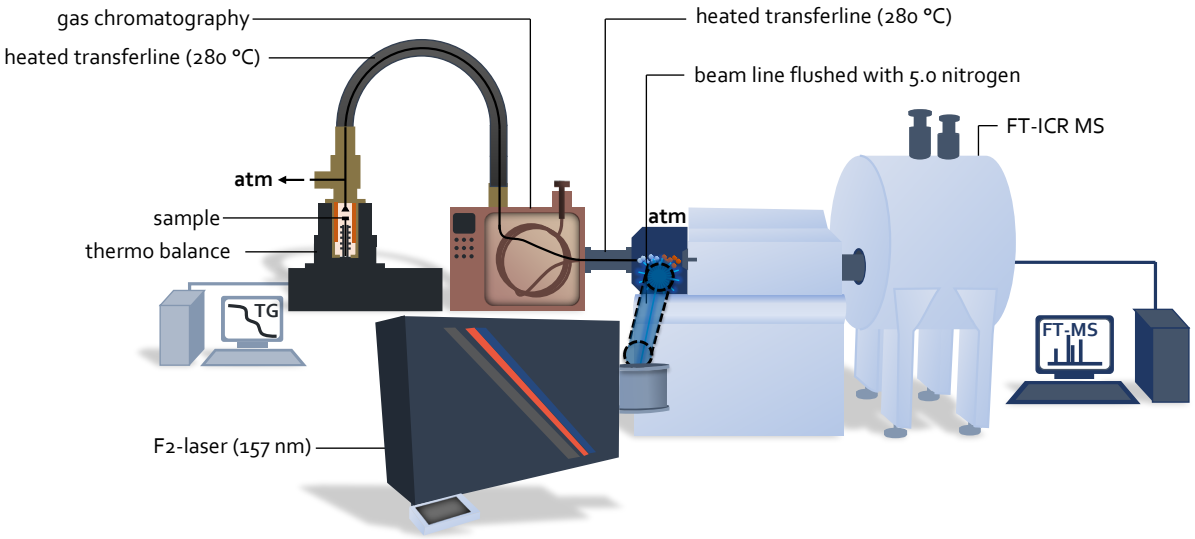

Figure 39: Schematic setup of the TG-FT-ICR MS as well as GC-FT-ICR MS hyphenations with APSPLI as ionisation technique. APSPLI is carried out by applying a fluorine laser emitting photons of 157 nm (7.9 eV).

more suitable for the ionisation of semi-polar to non-polar compounds [119]. Since APLI is based on a multiphoton ionisation mechanism, it selectively ionises mostly aromatic compounds [127]. Due to the high photon density of the emitted laser light, efficient ionisation was achieved, which led to very low detection limits of poly aromatic hydrocarbons (PAH) of approximately one order of magnitude lower than reported for APPI [184]. Nonetheless, despite higher detection limits for PAHs, APPI covers a broader chemical space due to its single photon ionisation mechanism. As explained in more detail in section 4.3.1, single photon ionisation is able to ionise compounds by direct photoionization, which have an ionisation potential below the energy of the emitted photons. In publication 6, I aimed to combine both advantages of APLI and APPI by introducing atmospheric pressure single photon laser ionisation, further referred to as APSPLI. APSPLI combines the high photon flux of APLI as well as the ability to ionise a broad chemical space. In publication 6, I evaluated APSPLI for gas phase ionisation in thermal analysis and gas chromatographic coupling. In Figure 39, a schematic overview of the applied setup is given. The TG-FT-ICR MS hyphenation is equal to the setup used in the other publications presented within this PhD thesis [45, 78, 82, 163] and was mainly used for pretests by constantly introducing a standard substance, but also for the proof-of-concept of complex mixture analysis. The GC-FT-ICR MS setup [185] was applied to investigate different ionisation parameters with PAH standard mixtures, but complex materials were introduced to GC as well. Both separation techniques were hyphenated via a heated transferline (280 °C) to the ion source and used as gas phase sample introduction systems. APSPLI was carried out applying a fluorine excimer laser emitting photons of 7.9 eV (157 nm). The laser beam was guided through a beam line flushed with 5.0 nitrogen avoiding the

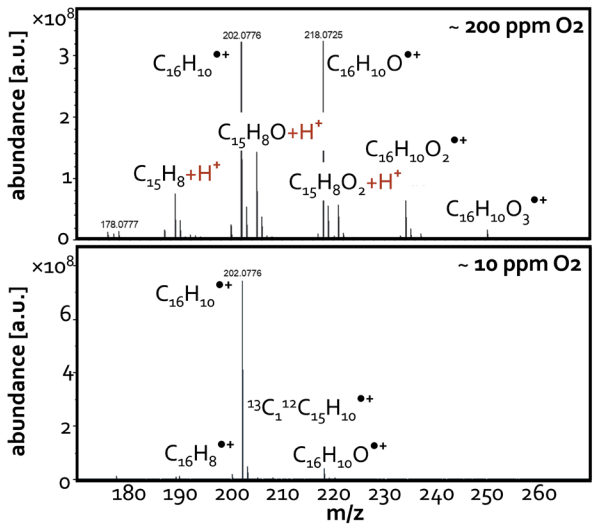

Figure 40: Influence of oxygen in the ionisation atmosphere. (top) APSPLI-FT-ICR MS spectrum of pyrene with massive oxidation artefacts due to approximately 200 ppm oxygen in the ion source atmosphere. (bottom) Pyrene spectrum ionised in a source atmosphere containing approximately 10 ppm oxygen.

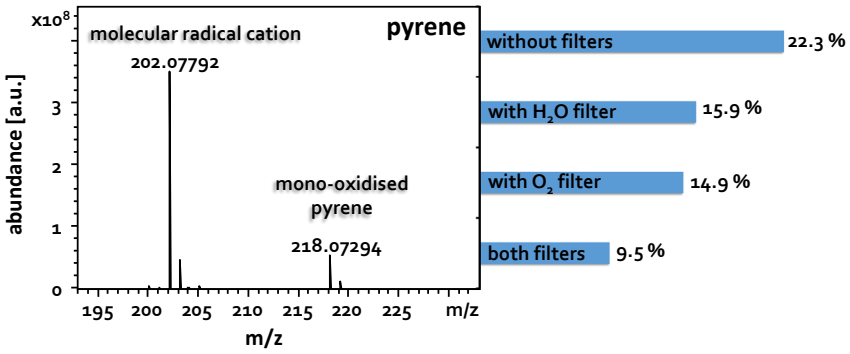

Figure 41: Exemplary spectrum of pyrene measured by gas phase APSPLI-FT-ICR MS. The mono-oxidised ionisation artefact is highest, when no additional filter cartridges are applied, and lowest, when both H2O- and O2-filter cartridges are applied.

absorption of the VUV-light by atmospheric oxygen and enters the ion source through a magnesium fluoride window. The ion source is constantly flushed with pure nitrogen.

The amount of oxygen is a critical parameter, when using VUV-light for ionisation under atmospheric pressure conditions. The nitrogen-flushed beamline is necessary to guide the light from the laser source to the ionisation chamber entrance without being absorbed by oxygen of the surrounding air. However, oxygen inside the ionisation chamber also has large influence on the ionisation process. UV radiation with wavelengths below 240 nm causes photodissociation of oxygen into radicals [186]. Further reaction pathways lead to the formation of reactive ozone or hydroxyl radicals [187]. In Figure 40, the influence of oxygen on the ionisation of pyrene is shown. Pyrene was introduced via the thermogravimetry coupling with a constant concentration of approximately 300 ppb. The upper spectrum was recorded in a source atmosphere containing approximately 200 ppm oxygen. Pyrene was highly oxidised, while the mono-oxidised radical cation ($C_{16}H_{10}O^{\bullet+}$) was as high as the molecular radical cation ($C_{16}H_{10}^{\bullet+}$), but also oxidation products with up to three oxygen atoms were observed. Both, radical cations and protonated species, were found suggesting a complex reaction cascade. By reducing the amount of oxygen in the source atmosphere to approximately 10 ppm, also ionisation artefacts could be drastically reduced. Figure 40 (bottom) shows the corresponding pyrene spectrum with reduced oxygen concentration. The radical cation of the molecular ion clearly dominates the spectrum, whereas oxidation products and other ionisation artefacts occurred only in minor amounts.

I further investigated the influence of oxygen and water by installing filter cartridges used for purification of the nitrogen gas supply, which flushes the ionization chamber. Figure 41 presents an exemplary spectrum of pyrene ionised by APSPLI as well as the percentage of the mono-oxidised species after the application of no filters, a H2O-filter cartridge, an O2-filter cartridge, and both filter cartridges. Without additional filter cartridges, the signal of the mono-oxidised artefact accounts for over 22 % of the molecular radical cation signal. By the application of both O2- and H2O-filter cartridges, the oxidation artefacts could be reduced by a factor of 2-3 below 10 %. Similar was observed for a wide range of PAHs introduced by gas chromatography. The standard mixture contained two-ring aromatics, such as naphthalene, and up to seven-ring aromatics (coronene). The oxidation artefacts of the ionisable PAHs could be mostly reduced from 18-26 % to 10-15 % by the application of both filter cartridges. Naphthalene, however, was not observed due to its higher ionisation energy of 8.14 eV [188], which is greater than the photon energy of

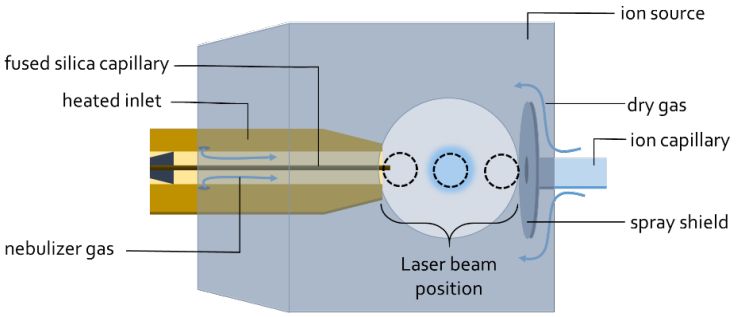

Figure 42: Schematic of the ion source. Nebulizer gas flow and the laser beam position were found to have the highest influence on the signal intensity of the molecular radical cation as well as of the oxidation artefacts.

7.9 eV provided by the applied fluorine excimer laser. This result suggests, that the ionisation process is solely induced by direct photoionisation and is not carried out by a reaction cascade of several sub-reactions with other molecules present in the ion source atmosphere, such as water.

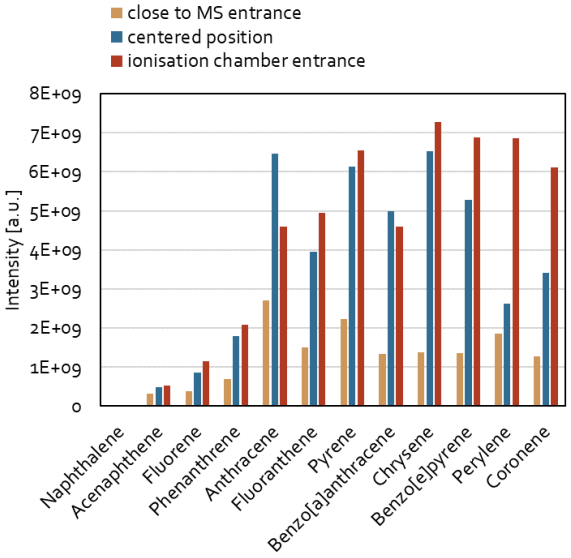

Figure 43: PAH standard ionised by APSPLI at different positions in the ion source. The intensity of the radical cations depended on the ionisation location.

Besides the implementation of oxygen and water cartridges, other parameters showed an influence on signal intensity and the amount of oxidation products as well. In Figure 42, a schematic of the ion source is presented. Especially the nebulizer gas flow as well as the position of the laser beam showed the highest influence on the ionisation efficiency investigated with PAH standard substances introduced by gas chromatography. The nebulizer gas flow showed comparatively low influence on the overall intensity of the formation of the molecular radical cations. Flow rates of 1.5 l/min, 4.5 l/min and 6.0 l/min were investigated. The highest nebulizer gas flow rate showed the lowest signal intensities, whereas the lowest flow rate showed the highest signal intensities. The high nebulizer gas flow rate suggests a rapid dilution with nitrogen of the sample entering the ion source. Therefore, less of the sample material can be ionised by APSPLI and a lower signal intensity was observed. Conversely, the highest nebulizer gas flow yielded in the lowest percentage of oxidation artefacts. This finding indicated, that the high flow of clean nitrogen is able to supress reactions with remaining oxygen in the ion source. The position of the laser beam in the ion source were found to have a high influence on the signal intensity of the molecular radical cation. Three different positions of the laser beam were investigated: 1) close to the mass spectrometer entrance, 2) a centred position, and 3) close to the ion chamber entrance. The results are depicted in Figure 43. The highest intensities for radical cations was found by ionising near the ionisation chamber entrance, whereas the lowest intensity was found closely to the MS entrance. This finding indicated that the flow conditions in the ion source led to a distribution of the neutral molecules in the chamber volume. Therefore, the concentration of analyte is highest at the ionisation chamber entrance and lowest at the MS entrance. Furthermore, the percentage of oxidation was also found to be lowest, when ionising directly after the ionisation chamber entrance, which may be an effect of the highly pure nebulizer gas stream introducing the sample to the ion source.

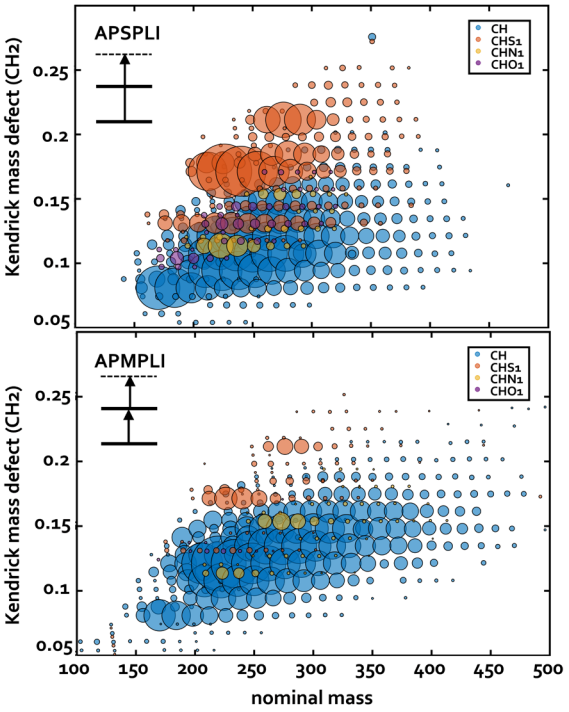

Figure 44: Kendrick diagrams of a light crude oil ionised by APSPLI (top) and APMPLI (bottom) subjected to the ionisation source by TG-FT-ICR MS.

In the context of this PhD thesis, I applied the newly developed ionisation method APSPLI to complex organic mixtures introduced via thermogravimetry or gas chromatography. To define the differences to

the closely related APLI, both techniques were applied to the same complex sample. To easier distinguish between the single photon and multi photon ionisation approach, APLI is further referred to as atmospheric pressure multiphoton laser ionisation (APMPLI). In Figure 44, the average Kendrick diagrams of a light crude oil measured by both techniques are presented. The Kendrick mass is defined by setting a certain repeating unit (mostly CH_2) to an integer value. This conversion of the mass scale enables to easily visualize and identify homologous series in a complex mass spectrum. In a Kendrick diagram, the Kendrick mass defect, which is defined as the difference between the nominal mass and the Kendrick exact mass, is plotted against the nominal mass. The arising horizontal lines differ by CH_2 units. Each homologous series correspond to a distinct Kendrick mass defect causing a vertical separation by e.g. the degree of unsaturation or heteroatom content. [189–192] In Figure 44, the compound classes are highlighted in different colours. The comparison of both ionisation techniques revealed, that APMPLI is able to ionise aromatic hydrocarbons without any heteroatoms more efficiently than APSPLI. However, for N-, O- or S-containing species, the ionisation with APSPLI is advantageous. Especially sulphur-containing compounds are highlighted by APSPLI. In Figure 45, an exemplary measurement of a light crude oil with GC-APSPLI-FT-ICR MS is presented. As the crude oil was diluted 1:100 and only 1 µL was injected for this measurement, the high sensitivity of this approach could be demonstrated. The summed mass spectrum in Figure 45 b) revealed species with *m/z* up to 450, covering mostly the CH-, S_1-, O_1-, N_1-, and S_1O_1-classes. Compounds with the highest summed intensity corresponded to the S_1-class emphasizing the high sensitivity of APSPLI towards sulphur-containing compounds. Furthermore, the preceding GC separation enabled the identification of oxidised ionisation artefacts [185]. Artefacts will have the same chromatographic elution profile as the their corresponding molecular cation and can be removed by automatized processing routines [185].

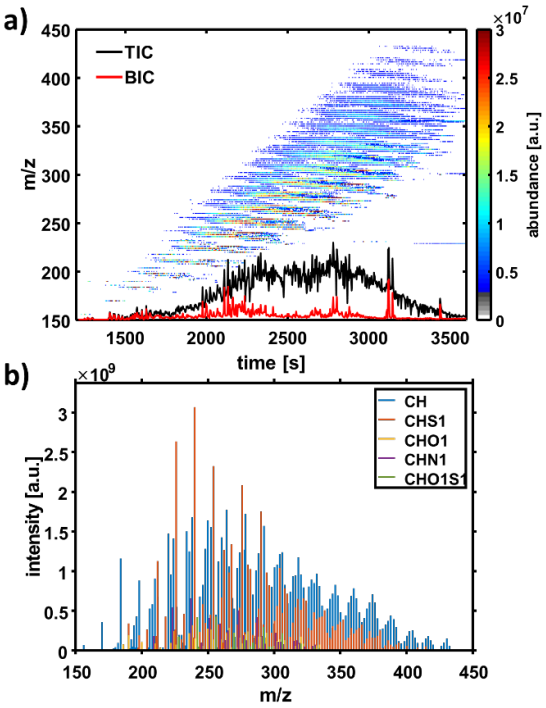

Figure 45: GC-APSPLI-FT-ICR MS spectrum. a) time-resolved mass spectrum with total ion chromatogram (black) and biggest ion chromatogram (red) overlaid

To conclude, in this PhD thesis, I developed a new ionisation technique by using single photon laser ionisation under atmospheric pressure (APSPLI) conditions. The concentration of oxygen is a crucial parameter in APSPLI with respect to side reaction induced by UV-dissociation of O_2 molecules, which lead to oxidised ionisation artefacts. Nonetheless, those artefacts could be reduced by applying O_2/H_2O filter cartridges to further purify the nitrogen supply, high nitrogen flow rates, and the ionisation of the analytes immediately after being introduced to the ionisation chamber. Furthermore, APSPLI was successfully applied to complex petroleum-derived mixtures introduced by thermogravimetry or gas chromatography. Due to the single photon-based ionisation approach, APSPLI is able to overcome the limitations of classical APLI/ APMPLI, which is limited by the lifetime of the excited state after the absorption of the first photon. Especially sulphur-containing compounds revealed relatively high detection limits in APLI [193]. APSPLI, however, specifically highlights sulphur-containing compounds and covers in general a broader compositional space. Furthermore, the large differences in ionisation cross section associated with REMPI or APLI are negotiated by single photon ionisation.

5 Conclusion and Outlook

This PhD work revealed the high value of thermogravimetry (TG) coupled to Fourier transform ion cyclotron resonance mass spectrometry (FT-ICR MS) for the investigation of current research questions related to heavy petroleum-derived materials. The application of this technique enables the detailed, online description of the pyrolysis products of polyethylene terephthalate (PET). For the most complex constituents of petroleum, the asphaltenes, TG-FT-ICR MS revealed valuable information on the molecular architecture regarding the prevalent structural motifs. The combination of TG-FT-ICR MS with different ionisation techniques, several mass spectrometric analysers, as well as the fractionation of the complex asphaltene matrix further deepened their chemical characterization. For the investigation of aging effects in bitumen, the integration of TG-FT-ICR MS data and two-dimensional gas chromatography high-resolution time-of-flight mass spectrometry (GC×GC-HR-TOF MS) information enabled the elucidation of several short-term aging effects. This PhD thesis has further shown that reducing matrix effects by using selective ionisation techniques is advantageous for the chemical description of heavy petroleum samples. Consequently, the extension of existing or the development of new ionisation techniques may help to address specific analytical challenges. In this PhD work, I showed the further development of atmospheric pressure photoionisation (APPI) by applying a Xenon discharge lamp instead of the commonly used Krypton discharge lamps, leading to a simplification of the complex FT-ICR MS spectra by ionising species mainly as radical cations. Furthermore, a new ionisation technique was introduced, which is based on single photon laser ionisation under atmospheric pressure conditions (APSPLI). Although oxidation is a critical aspect in APSPLI, the new ionisation method could successfully be applied to complex petroleum-derived materials measured by thermal analysis or gas chromatographic hyphenation.

The results of my PhD thesis will be the starting point for several future studies. As TG-FT-ICR MS showed high value for the chemical description of heavy petroleum-derived materials, a detailed comparison study between direct infusion FT-ICR MS and TG-FT-ICR MS will help for an improved data integration of both techniques and will be an important step towards predictive petroleomics. With respect to the investigated heavy petroleum samples, further studies may focus on the highest polar fraction of asphaltenes, which was irreversibly absorbed on silica during extrography fractionation. TG-FT-ICR MS may be a valuable tool to investigate those species by directly evaporating the compounds from the adsorption material. The understand of the absorption of those compounds on LC columns might lead to new developments making direct LC analysis of asphaltenes feasible. Moreover, as molecular level characterization is poorly applied for the investigation of aging effects in bitumen, a variety of analytical issues can be addressed in further studies. For example, long-term aging effects of bitumen binders, the differences between laboratory aging methods and real conditions, or the effect of the addition of additives should be addressed at molecular level as well. Aside from the planned applicative studies, the further development and characterization of the newly introduced ionisation techniques is of high interest for the analytical community. Xe-APPI needs to be properly characterized by standard mixtures as well as complex mixtures. To define the accessible compositional space, Xe-APPI will be compared to other atmospheric pressure ionisation techniques. APSPLI revealed great potential for selective and sensitive ionisation of low-polar and semi-polar hydrocarbons. Further studies will focus on optimising the ionisation process by further reduction of the oxidation artefacts abundance. Due to the high sensitivity, APSPLI may help in the characterisation of low concentrated ultra-complex mixtures, such as ambient aerosols or may address chlorine- or bromine-containing analytes. The chemical space addressed by APSPLI can further be widened by deploying lasers emitting photons with higher energy, which enables to ionise also compounds with higher ionisation potentials than 7.9 eV as provided by the presented fluorine excimer laser.

6 References

[1] J. G. Speight. *The Chemistry and Technology of Petroleum*. CRC Press.

[2] O. C. Mullins (Ed.). *Asphaltenes, heavy oils and petroleomics*. Springer, New York, NY.

[3] M. N. Dunkle, W. L. Winniford. *Analytical techniques in the oil and gas industry for environmental monitoring*. Wiley, Hoboken.

[4] N. J. Hyne. *Nontechnical guide to petroleum geology, exploration, drilling, and production*, 3rd ed. ed. PennWell Corporation, Tulsa, Okla.

[5] S. Matar, L. F. Hatch. *Chemistry of petrochemical processes*, 2nd ed. ed. Gulf Professional Pub, Boston.

[6] N. Berkowitz. *Fossil hydrocarbons. Chemistry and technology*. Academic Press, San Diego.

[7] J. G. Speight. *The desulfurization of heavy oils and residua*, 2. ed., rev. and expanded. ed. Dekker, New York.

[8] M. M. Boduszynski. Composition of heavy petroleums. 1. Molecular weight, hydrogen deficiency, and heteroatom concentration as a function of atmospheric equivalent boiling point up to 1400.degree.F (760.degree.C), *Energy Fuels*. **1987**, *1*, 2–11.

[9] M. M. Boduszynski, J. F. McKay, D. R. Latham. Asphaltenes, where are you?, *Asphalt Paving Technology*. **1980**, *49*, 123–143.

[10] M. M. Boduszynski. Composition of heavy petroleums. 2. Molecular characterization, *Energy Fuels*. **1988**, *2*, 597–613.

[11] M. L. Chacón-Patiño, S. M. Rowland, R. P. Rodgers in *ACS symposium series, Vol. 1282* (Eds.: C. Ovalles, M. E. Moir). American Chemical Society, Washington DC, **2018**.

[12] A. M. McKenna, J. M. Purcell, R. P. Rodgers, A. G. Marshall. Heavy Petroleum Composition. 1. Exhaustive Compositional Analysis of Athabasca Bitumen HVGO Distillates by Fourier Transform Ion Cyclotron Resonance Mass Spectrometry: A Definitive Test of the Boduszynski Model, *Energy Fuels*. **2010**, *24*, 2929–2938.

[13] A. M. McKenna, A. G. Marshall, R. P. Rodgers. Heavy Petroleum Composition. 4. Asphaltene Compositional Space, *Energy Fuels*. **2013**, *27*, 1257–1267.

[14] A. M. McKenna, L. J. Donald, J. E. Fitzsimmons, P. Juyal, V. Spicer, K. G. Standing, A. G. Marshall, R. P. Rodgers. Heavy Petroleum Composition. 3. Asphaltene Aggregation, *Energy Fuels*. **2013**, *27*, 1246–1256.

[15] R. Geyer, J. R. Jambeck, K. L. Law. Production, use, and fate of all plastics ever made, *Science Advances*. **2017**, *3*, e1700782.

[16] T. D. Nielsen, J. Hasselbalch, K. Holmberg, J. Stripple. Politics and the plastic crisis: A review throughout the plastic life cycle, *WIREs Energy Environ.* **2020**, *9*.

[17] D. Kawecki, P. R. W. Scheeder, B. Nowack. Probabilistic Material Flow Analysis of Seven Commodity Plastics in Europe, *Environmental Science & Technology*. **2018**, *52*, 9874–9888.

[18] N. E. Zander, M. Gillan, R. H. Lambeth. Recycled polyethylene terephthalate as a new FFF feedstock material, *Additive Manufacturing*. **2018**, *21*, 174–182.

[19] S. D. Anuar Sharuddin, F. Abnisa, Wan Daud, Wan Mohd Ashri, M. K. Aroua. A review on pyrolysis of plastic wastes, *Energy Conversion and Management*. **2016**, *115*, 308–326.

[20] S. M. FakhrHoseini, M. Dastanian. Predicting Pyrolysis Products of PE, PP, and PET Using NRTL Activity Coefficient Model, *Journal of Chemistry*. **2013**, *2013*, 1–5.

[21] İ. Çit, A. Sınağ, T. Yumak, S. Uçar, Z. Mısırlıoğlu, M. Canel. Comparative pyrolysis of polyolefins (PP and LDPE) and PET, *Polym. Bull.* **2010**, *64*, 817–834.

[22] A. Dhahak, G. Hild, M. Rouaud, G. Mauviel, V. Burkle-Vitzthum. Slow pyrolysis of polyethylene terephthalate: Online monitoring of gas production and quantitative analysis of waxy products, *Journal of Analytical and Applied Pyrolysis*. **2019**, *142*, 104664.

[23] A. Dhahak, V. Carre, F. Aubriet, G. Mauviel, V. Burkle-Vitzthum. Analysis of Products Obtained from Slow Pyrolysis of Poly(ethylene terephthalate) by Fourier Transform Ion Cyclotron Resonance Mass Spectrometry Coupled to Electrospray Ionization (ESI) and Laser Desorption Ionization (LDI), *Ind. Eng. Chem. Res.* **2020**, *59*, 1495–1504.

[24] M. Saraji-Bozorgzad, R. Geissler, T. Streibel, F. Mühlberger, M. Sklorz, E. Kaisersberger, T. Denner, R. Zimmermann. Thermogravimetry coupled to single photon ionization quadrupole mass spectrometry: a tool to investigate the chemical signature of thermal decomposition of polymeric materials, *Anal. Chem.* **2008**, *80*, 3393–3403.

[25] J. D. Badia, A. Martinez-Felipe, L. Santonja-Blasco, A. Ribes-Greus. Thermal and thermo-oxidative stability of reprocessed poly(ethylene terephthalate), *Journal of Analytical and Applied Pyrolysis*. **2013**, *99*, 191–202.

[26] D. Lesueur. The colloidal structure of bitumen: consequences on the rheology and on the mechanisms of bitumen modification, *Adv. Colloid Interface Sci.* **2009**, *145*, 42–82.

[27] J. C. Petersen. *A Review of the Fundamentals of Asphalt Oxidation: Chemical, Physicochemical, Physical Property, and Durability Relationships*. Transportation Research Board, Washington, D.C.

[28] J. F. Chipps, R. R. Davison, C. J. Glover. A Model for Oxidative Aging of Rubber-Modified Asphalts and Implications to Performance Analysis, *Energy Fuels*. **2001**, *15*, 637–647.

[29] L. M. Rebelo, J. S. de Sousa, A. S. Abreu, M.P.M.A. Baroni, A.E.V. Alencar, S. A. Soares, J. Mendes Filho, J. B. Soares. Aging of asphaltic binders investigated with atomic force microscopy, *Fuel*. **2014**, *117*, 15–25.

[30] A. Themeli, E. Chailleux, F. Farcas, C. Chazallon, B. Migault, N. Buisson. Molecular structure evolution of asphaltite-modified bitumens during ageing; Comparisons with equivalent petroleum bitumens, *Int. J. Pavement Res. Technol.* **2017**, *10*, 75–83.

[31] J. F. Branthaver, J. C. Petersen, R. E. Robertson, J. J. Duvall, S. S. Kim, P. M. Harnsberger, T. Mill, E. K. Ensly, F. A. Barbour, J. F. Scharbron. *Binder Characterization and Evaluation. Volume 2: Chemistry*. Strategic Highway Research Program. National Research Council. National Academy of Sciences.

[32] B. Hofko, A. Cannone Falchetto, J. Grenfell, L. Huber, X. Lu, L. Porot, L. D. Poulikakos, Z. You. Effect of short-term ageing temperature on bitumen properties, *Road Mater. Pavement Des.* **2017**, *18*, 108–117.

[33] B. Hofko, M. Hospodka. Rolling Thin Film Oven Test and Pressure Aging Vessel Conditioning Parameters: Effect on Viscoelastic Behavior and Binder Performance Grade, *Transp. Res. Rec.* **2016**, *2574*, 111–116.

[34] G. Tarsi, A. Varveri, C. Lantieri, A. Scarpas, C. Sangiorgi. Effects of Different Aging Methods on Chemical and Rheological Properties of Bitumen, *J. Mater. Civ. Eng.* **2018**, *30*, 4018009.

[35] R. Bonaquist, D. A. Anderson. *Investigation of Short-Term Laboratory Aging of Neat and Modified Asphalt Binders*. National Academies Press, Washington, D.C.

[36] O. A. Ehinola, O. A. Falode, G. Jonathan. Softening point and Penetration Index of bitumen from parts of Southwestern Nigeria, *NAFTA*. **2012**, *63*, 319–323.

[37] B. Hofko, L. Eberhardsteiner, J. Füssl, H. Grothe, F. Handle, M. Hospodka, D. Grossegger, S. N. Nahar, A. J. M. Schmets, A. Scarpas. Impact of maltene and asphaltene fraction on mechanical behavior and microstructure of bitumen, *Mater. Struct.* **2016**, *49*, 829–841.

[38] A. Grilli, M. I. Gnisci, M. Bocci. Effect of ageing process on bitumen and rejuvenated bitumen, *Constr. Build. Mater.* **2017**, *136*, 474–481.

[39] L. Eberhardsteiner, J. Füssl, B. Hofko, F. Handle, M. Hospodka, R. Blab, H. Grothe. Towards a microstructural model of bitumen ageing behaviour, *Int. J. Pavement Eng.* **2015**, *16*, 939–949.
[40] L. Eberhardsteiner, J. Füssl, B. Hofko, F. Handle, M. Hospodka, R. Blab, H. Grothe. Influence of asphaltene content on mechanical bitumen behavior: experimental investigation and micromechanical modeling, *Mater. Struct.* **2015**, *48*, 3099–3112.
[41] L. W. Corbett. Composition of asphalt based on generic fractionation, using solvent deasphaltening, elution-adsorption chromatography, and densimetric characterization, *Anal. Chem.* **1969**, *41*, 576–579.
[42] M. Le Guern, E. Chailleux, F. Farcas, S. Dreessen, I. Mabille. Physico-chemical analysis of five hard bitumens: Identification of chemical species and molecular organization before and after artificial aging, *Fuel*. **2010**, *89*, 3330–3339.
[43] P. Mikhailenko, A. Bertron, E. Ringot. Methods for Analyzing the Chemical Mechanisms of Bitumen Aging and Rejuvenation with FTIR Spectrometry, *International Symposium on Testing and Characterization of Sustainable and Innovative Bituminous Materials*. **2016**, *11*, 203–214.
[44] M. R. Nivitha, E. Prasad, J. M. Krishnan. Ageing in modified bitumen using FTIR spectroscopy, *Int. J. Pavement Eng.* **2016**, *17*, 565–577.
[45] A. Neumann, U. Käfer, T. Gröger, T. Wilharm, R. Zimmermann, C. P. Rüger. Investigation of Aging Processes in Bitumen at the Molecular Level with High-Resolution Fourier-Transform Ion Cyclotron Mass Spectrometry and Two-Dimensional Gas Chromatography Mass Spectrometry, *Energy Fuels*. **2020**, *34*, 10641–10654.
[46] T. Fan, J. S. Buckley. Rapid and Accurate SARA Analysis of Medium Gravity Crude Oils, *Energy Fuels*. **2002**, *16*, 1571–1575.
[47] Y. Cho, J.-G. Na, N.-S. Nho, S. Kim, S. Kim. Application of Saturates, Aromatics, Resins, and Asphaltenes Crude Oil Fractionation for Detailed Chemical Characterization of Heavy Crude Oils by Fourier Transform Ion Cyclotron Resonance Mass Spectrometry Equipped with Atmospheric Pressure Photoionization, *Energy Fuels*. **2012**, *26*, 2558–2565.
[48] N. Aske, H. Kallevik, J. Sjöblom. Determination of Saturate, Aromatic, Resin, and Asphaltenic (SARA) Components in Crude Oils by Means of Infrared and Near-Infrared Spectroscopy, *Energy Fuels*. **2001**, *15*, 1304–1312.
[49] K. K. Bissada, J. Tan, E. Szymczyk, M. Darnell, M. Mei. Group-type characterization of crude oil and bitumen. Part I: Enhanced separation and quantification of saturates, aromatics, resins and asphaltenes (SARA), *Organic Geochemistry*. **2016**, *95*, 21–28.
[50] A. M. Kharrat, J. Zacharia, V. J. Cherian, A. Anyatonwu. Issues with Comparing SARA Methodologies, *Energy Fuels*. **2007**, *21*, 3618–3621.
[51] J. J. Adams. Asphaltene Adsorption, a Literature Review, *Energy Fuels*. **2014**, *28*, 2831–2856.
[52] K. Akbarzadeh et al. Asphaltenes—Problematic but Rich in Potential, *Oilfield Review*. **2007**, 22–43.
[53] J. S. Buckley. Asphaltene Deposition, *Energy Fuels*. **2012**, *26*, 4086–4090.
[54] A. Hammami, J. Ratulowski in *Asphaltenes, heavy oils and petroleomics* (Ed.: O. C. Mullins). Springer, New York, NY, **2007**.
[55] J.A. Moulijn, A.E. van Diepen, F. Kapteijn. Catalyst deactivation: is it predictable?, *Applied Catalysis A: General*. **2001**, *212*, 3–16.
[56] D. S. Pinkston, P. Duan, V. A. Gallardo, S. C. Habicht, X. Tan, K. Qian, M. Gray, K. Müllen, H. I. Kenttämaa. Analysis of Asphaltenes and Asphaltene Model Compounds by Laser-Induced Acoustic Desorption/Fourier Transform Ion Cyclotron Resonance Mass Spectrometry, *Energy Fuels*. **2009**, *23*, 5564–5570.
[57] A. E. Pomerantz, M. R. Hammond, A. L. Morrow, O. C. Mullins, R. N. Zare. Two-step laser mass spectrometry of asphaltenes, *Journal of the American Chemical Society*. **2008**, *130*, 7216–7217.

[58] A. E. Pomerantz, M. R. Hammond, A. L. Morrow, O. C. Mullins, R. N. Zare. Asphaltene Molecular-Mass Distribution Determined by Two-Step Laser Mass Spectrometry †, *Energy Fuels*. **2009**, *23*, 1162–1168.

[59] H. Groenzin, O. C. Mullins. Molecular Size and Structure of Asphaltenes from Various Sources, *Energy Fuels*. **2000**, *14*, 677–684.

[60] M. R. Hurt, D. J. Borton, H. J. Choi, H. I. Kenttämaa. Comparison of the Structures of Molecules in Coal and Petroleum Asphaltenes by Using Mass Spectrometry, *Energy Fuels*. **2013**, *27*, 3653–3658.

[61] J. D. Payzant, E. M. Lown, O. P. Strausz. Structural units of Athabasca asphaltene: the aromatics with a linear carbon framework, *Energy Fuels*. **1991**, *5*, 445–453.

[62] V. Calemma, R. Rausa, P. D'Anton, L. Montanari. Characterization of Asphaltenes Molecular Structure, *Energy Fuels*. **1998**, *12*, 422–428.

[63] A. M. McKenna, M. L. Chacón-Patiño, C. R. Weisbrod, G. T. Blakney, R. P. Rodgers. Molecular-Level Characterization of Asphaltenes Isolated from Distillation Cuts, *Energy Fuels*. **2019**, *33*, 2018–2029.

[64] T. F. Yen, J. G. Erdman, S. S. Pollack. Investigation of the Structure of Petroleum Asphaltenes by X-Ray Diffraction, *Anal. Chem.* **1961**, *33*, 1587–1594.

[65] O. C. Mullins. The Modified Yen Model †, *Energy Fuels*. **2010**, *24*, 2179–2207.

[66] B. Schuler et al. Heavy Oil Based Mixtures of Different Origins and Treatments Studied by Atomic Force Microscopy, *Energy Fuels*. **2017**, *31*, 6856–6861.

[67] B. Schuler, G. Meyer, D. Peña, O. C. Mullins, L. Gross. Unraveling the Molecular Structures of Asphaltenes by Atomic Force Microscopy, *Journal of the American Chemical Society*. **2015**, *137*, 9870–9876.

[68] B. Schuler et al. Characterizing aliphatic moieties in hydrocarbons with atomic force microscopy, *Chemical science*. **2017**, *8*, 2315–2320.

[69] Y. Zhang, B. Schuler, S. Fatayer, L. Gross, M. R. Harper, J. D. Kushnerick. Understanding the Effects of Sample Preparation on the Chemical Structures of Petroleum Imaged with Noncontact Atomic Force Microscopy, *Ind. Eng. Chem. Res.* **2018**, *57*, 15935–15941.

[70] L. Artok, Y. Su, Y. Hirose, M. Hosokawa, S. Murata, M. Nomura. Structure and Reactivity of Petroleum-Derived Asphaltene, *Energy Fuels*. **1999**, *13*, 287–296.

[71] P. T. H. Nascimento, A. F. Santos, C. I. Yamamoto, L. V. Tose, E. V. Barros, G. R. Gonçalves, J. C. C. Freitas, B. G. Vaz, W. Romão, A. P. Scheer. Fractionation of Asphaltene by Adsorption onto Silica and Chemical Characterization by Atmospheric Pressure Photoionization Fourier Transform Ion Cyclotron Resonance Mass Spectrometry, Fourier Transform Infrared Spectroscopy Coupled to Attenuated Total Reflectance, and Proton Nuclear Magnetic Resonance, *Energy Fuels*. **2016**, *30*, 5439–5448.

[72] H. Sabbah, A. L. Morrow, A. E. Pomerantz, O. C. Mullins, X. Tan, M. R. Gray, K. Azyat, R. R. Tykwinski, R. N. Zare. Comparing Laser Desorption/Laser Ionization Mass Spectra of Asphaltenes and Model Compounds, *Energy Fuels*. **2010**, *24*, 3589–3594.

[73] H. Sabbah, A. L. Morrow, A. E. Pomerantz, R. N. Zare. Evidence for Island Structures as the Dominant Architecture of Asphaltenes, *Energy Fuels*. **2011**, *25*, 1597–1604.

[74] A. Karimi, K. Qian, W. N. Olmstead, H. Freund, C. Yung, M. R. Gray. Quantitative Evidence for Bridged Structures in Asphaltenes by Thin Film Pyrolysis, *Energy Fuels*. **2011**, *25*, 3581–3589.

[75] M. R. Gray. Consistency of Asphaltene Chemical Structures with Pyrolysis and Coking Behavior, *Energy Fuels*. **2003**, *17*, 1566–1569.

[76] R. I. Rueda-Velásquez, H. Freund, K. Qian, W. N. Olmstead, M. R. Gray. Characterization of Asphaltene Building Blocks by Cracking under Favorable Hydrogenation Conditions, *Energy Fuels*. **2013**, *27*, 1817–1829.

[77] O. P. Strausz, T. W. Mojelsky, F. Faraji, E. M. Lown, P.'a. Peng. Additional Structural Details on Athabasca Asphaltene and Their Ramifications, *Energy Fuels*. **1999**, *13*, 207–227.

[78] C. P. Rüger, A. Neumann, M. Sklorz, T. Schwemer, R. Zimmermann. Thermal Analysis Coupled to Ultrahigh Resolution Mass Spectrometry with Collision Induced Dissociation for Complex Petroleum Samples: Heavy Oil Composition and Asphaltene Precipitation Effects, *Energy Fuels*. **2017**, *31*, 13144–13158.

[79] M. L. Chacón-Patiño, C. Blanco-Tirado, J. A. Orrego-Ruiz, A. Gómez-Escudero, M. Y. Combariza. Tracing the Compositional Changes of Asphaltenes after Hydroconversion and Thermal Cracking Processes by High-Resolution Mass Spectrometry, *Energy Fuels*. **2015**, *29*, 6330–6341.

[80] P. E. Savage, M. T. Klein, S. G. Kukes. Asphaltene reaction pathways. 3. Effect of reaction environment, *Energy Fuels*. **1988**, *2*, 619–628.

[81] O. P. Strausz, T. W. Mojelsky, E. M. Lown. The molecular structure of asphaltene: an unfolding story, *Fuel*. **1992**, *71*, 1355–1363.

[82] C. P. Rüger, C. Grimmer, M. Sklorz, A. Neumann, T. Streibel, R. Zimmermann. Combination of Different Thermal Analysis Methods Coupled to Mass Spectrometry for the Analysis of Asphaltenes and Their Parent Crude Oils: Comprehensive Characterization of the Molecular Pyrolysis Pattern, *Energy Fuels*. **2018**, *32*, 2699–2711.

[83] M. L. Chacón-Patiño, S. J. Vesga-Martínez, C. Blanco-Tirado, J. A. Orrego-Ruiz, A. Gómez-Escudero, M. Y. Combariza. Exploring Occluded Compounds and Their Interactions with Asphaltene Networks Using High-Resolution Mass Spectrometry, *Energy Fuels*. **2016**, *30*, 4550–4561.

[84] D. C. Podgorski, Y. E. Corilo, L. Nyadong, V. V. Lobodin, B. J. Bythell, W. K. Robbins, A. M. McKenna, A. G. Marshall, R. P. Rodgers. Heavy Petroleum Composition. 5. Compositional and Structural Continuum of Petroleum Revealed, *Energy Fuels*. **2013**, *27*, 1268–1276.

[85] M. L. Chacón-Patiño, S. M. Rowland, R. P. Rodgers. Advances in Asphaltene Petroleomics. Part 1: Asphaltenes Are Composed of Abundant Island and Archipelago Structural Motifs, *Energy Fuels*. **2017**, *31*, 13509–13518.

[86] M. L. Chacón-Patiño, S. M. Rowland, R. P. Rodgers. Advances in Asphaltene Petroleomics. Part 2: Selective Separation Method That Reveals Fractions Enriched in Island and Archipelago Structural Motifs by Mass Spectrometry, *Energy Fuels*. **2018**, *32*, 314–328.

[87] M. L. Chacón-Patiño, S. M. Rowland, R. P. Rodgers. Advances in Asphaltene Petroleomics. Part 3. Dominance of Island or Archipelago Structural Motif Is Sample Dependent, *Energy Fuels*. **2018**, *32*, 9106–9120.

[88] D. Giraldo-Dávila, M. L. Chacón-Patiño, A. M. McKenna, C. Blanco-Tirado, M. Y. Combariza. Correlations between Molecular Composition and Adsorption, Aggregation, and Emulsifying Behaviors of PetroPhase 2017 Asphaltenes and Their Thin-Layer Chromatography Fractions, *Energy Fuels*. **2018**, *32*, 2769–2780.

[89] D. Giraldo-Dávila, M. L. Chacón-Patiño, J. A. Orrego-Ruiz, C. Blanco-Tirado, M. Y. Combariza. Improving compositional space accessibility in (+) APPI FT-ICR mass spectrometric analysis of crude oils by extrography and column chromatography fractionation, *Fuel*. **2016**, *185*, 45–58.

[90] J. C. Putman et al. Probing Aggregation Tendencies in Asphaltenes by Gel Permeation Chromatography. Part 2: Online Detection by Fourier Transform Ion Cyclotron Resonance Mass Spectrometry and Inductively Coupled Plasma Mass Spectrometry, *Energy Fuels*. **2020**.

[91] R. P. Rodgers, M. M. Mapolelo, W. K. Robbins, M. L. Chacón-Patiño, J. C. Putman, S. F. Niles, S. M. Rowland, A. G. Marshall. Combating selective ionization in the high resolution mass spectral characterization of complex mixtures, *Faraday discussions*. **2019**, *218*, 29–51.

[92] A. W. Coats, J. P. Redfern. Thermogravimetric analysis. A review, *Analyst*. **1963**, *88*, 906.

[93] O. Karacan, M. V. Kok. Pyrolysis Analysis of Crude Oils and Their Fractions, *Energy Fuels*. **1997**, 385–391.

[94] J. Douda, M.E. Llanos, R. Alvarez, C. L. Franco, J.A. M. de La Fuente. Pyrolysis applied to the study of a Maya asphaltene, *Journal of Analytical and Applied Pyrolysis*. **2004**, *71*, 601–612.
[95] M. E. Brown (Ed.). *Introduction to Thermal Analysis*. Kluwer Academic Publishers, Dordrecht.
[96] Y. Kitahara, S. Takahashi, T. Fujii. Thermal analysis of polyethylene glycol: evolved gas analysis with ion attachment mass spectrometry, *Chemosphere*. **2012**, *88*, 663–669.
[97] M. Saraji-Bozorgzad, R. Geissler, T. Streibel, F. Mühlberger, M. Sklorz, E. Kaisersberger, T. Denner, R. Zimmermann. Thermogravimetry coupled to single photon ionization quadrupole mass spectrometry: a tool to investigate the chemical signature of thermal decomposition of polymeric materials, *Anal. Chem.* **2008**, *80*, 3393–3403.
[98] M. R. Saraji-Bozorgzad, T. Streibel, M. Eschner, T. M. Groeger, R. Geissler, E. Kaisersberger, T. Denner, R. Zimmermann. Investigation of polymers by a novel analytical approach for evolved gas analysis in thermogravimetry, *J Therm Anal Calorim*. **2011**, *105*, 859–866.
[99] K. Jayaraman, I. Gokalp. Thermogravimetric and evolved gas analyses of high ash Indian and Turkish coal pyrolysis and gasification, *J Therm Anal Calorim*. **2015**, *121*, 919–927.
[100] R. Geißler, M. Saraji-Bozorgzad, T. Streibel, E. Kaisersberger, T. Denner, R. Zimmermann. Investigation of different crude oils applying thermal analysis/mass spectrometry with soft photoionisation, *J Therm Anal Calorim*. **2009**, *96*, 813–820.
[101] R. Geissler et al. Single Photon Ionization Orthogonal Acceleration Time-of-Flight Mass Spectrometry and Resonance Enhanced Multiphoton Ionization Time-of-Flight Mass Spectrometry for Evolved Gas Analysis in Thermogravimetry: Comparative Analysis of Crude Oils, *Anal. Chem.* **2009**, *81*, 6038–6048.
[102] T. Streibel, A. Fendt, R. Geißler, E. Kaisersberger, T. Denner, R. Zimmermann. Thermal analysis/mass spectrometry using soft photo-ionisation for the investigation of biomass and mineral oils, *J Therm Anal Calorim*. **2009**, *97*, 615–619.
[103] C. P. Rüger, T. Miersch, T. Schwemer, M. Sklorz, R. Zimmermann. Hyphenation of Thermal Analysis to Ultrahigh-Resolution Mass Spectrometry (Fourier Transform Ion Cyclotron Resonance Mass Spectrometry) Using Atmospheric Pressure Chemical Ionization For Studying Composition and Thermal Degradation of Complex Materials, *Anal. Chem.* **2015**, *87*, 6493–6499.
[104] Y. Zhao, M. R. Gray, K. H. Chung. Molar Kinetics and Selectivity in Cracking of Athabasca Asphaltenes, *Energy Fuels*. **2001**, *15*, 751–755.
[105] A. Hauser, F. AlHumaidan, H. Al-Rabiah, M. A. Halabi. Study on Thermal Cracking of Kuwaiti Heavy Oil (Vacuum Residue) and Its SARA Fractions by NMR Spectroscopy, *Energy Fuels*. **2014**, *28*, 4321–4332.
[106] J. Douda, R. Alvarez, J. Navarrete Bolaños. Characterization of Maya Asphaltene and Maltene by Means of Pyrolysis Application, *Energy Fuels*. **2008**, *22*, 2619–2628.
[107] S. Chiaberge, G. Guglielmetti, L. Montanari, M. Salvalaggio, L. Santolini, S. Spera, P. Cesti. Investigation of Asphaltene Chemical Structural Modification Induced by Thermal Treatments, *Energy Fuels*. **2009**, *23*, 4486–4495.
[108] D. A. Skoog. *Fundamentals of analytical chemistry*, 9. ed., [internat. ed.] ed.
[109] J. R. Gilbert et al. in *Comprehensive Analytical Chemistry : Advanced Techniques in Gas Chromatography–Mass Spectrometry (GC–MS–MS and GC–TOF–MS) for Environmental Chemistry* (Eds.: I. Ferrer, E. M. Thurman). Elsevier, **2013**.
[110] T. Górecki, J. Harynuk, O. Panić. The evolution of comprehensive two-dimensional gas chromatography (GC x GC), *J. Sep. Science*. **2004**, *27*, 359–379.
[111] H. J. Cortes, B. Winniford, J. Luong, M. Pursch. Comprehensive two dimensional gas chromatography review, *Journal of Separation Science*. **2009**, *32*, 883–904.

[112] C. Meinert, U. J. Meierhenrich. A new dimension in separation science: comprehensive two-dimensional gas chromatography, *Angewandte Chemie (International ed. in English)*. **2012**, *51*, 10460–10470.
[113] J. Dallüge, R. J. J. Vreuls, J. Beens, U. A. T. Brinkman. Optimization and characterization of comprehensive two-dimensional gas chromatography with time-of-flight mass spectrometric detection (GC×GC-TOF MS), *J. Sep. Science*. **2002**, *25*, 201–214.
[114] J. Dallüge, L. L.P. van Stee, X. Xu, J. Williams, J. Beens, R. J.J. Vreuls, U. A.T. Brinkman. Unravelling the composition of very complex samples by comprehensive gas chromatography coupled to time-of-flight mass spectrometry, *Journal of Chromatography A*. **2002**, *974*, 169–184.
[115] J. H. Gross. *Mass Spectrometry. A Textbook*, 2. ed. ed. Springer-Verlag Berlin Heidelberg, Berlin, Heidelberg.
[116] E. C. Horning, M. G. Horning, D. I. Carroll, I. Dzidic, R. N. Stillwell. New picogram detection system based on a mass spectrometer with an external ionization source at atmospheric pressure, *Anal. Chem.* **1973**, *45*, 936–943.
[117] J. B. FENN, M. MANN, C. K. MENG, S. F. WONG, C. M. WHITEHOUSE. ChemInform Abstract: Electrospray Ionization for Mass Spectrometry of Large Biomolecules, *ChemInform*. **1990**, *21*.
[118] J. B. Fenn, M. Mann, C. K. Meng, S. F. Wong, C. M. Whitehouse. Electrospray ionization-principles and practice, *Mass Spectrometry Reviews*. **1990**, *9*, 37–70.
[119] D.-X. Li, L. Gan, A. Bronja, O. J. Schmitz. Gas chromatography coupled to atmospheric pressure ionization mass spectrometry (GC-API-MS): review, *Analytica chimica acta*. **2015**, *891*, 43–61.
[120] I. Dzidic, D. I. Carroll, R. N. Stillwell, E. C. Horning. Comparison of positive ions formed in nickel-63 and corona discharge ion sources using nitrogen, argon, isobutane, ammonia and nitric oxide as reagents in atmospheric pressure ionization mass spectrometry, *Anal. Chem.* **1976**, *48*, 1763–1768.
[121] A. K. Huba, K. Huba, P. R. Gardinali. Understanding the atmospheric pressure ionization of petroleum components: The effects of size, structure, and presence of heteroatoms, *The Science of the total environment*. **2016**, *568*, 1018–1025.
[122] J. A. Syage, K. A. Hanold, T. C. Lynn, J. A. Horner, R. A. Thakur. Atmospheric pressure photoionization, *Journal of Chromatography A*. **2004**, *1050*, 137–149.
[123] Robb, Covey, Bruins. Atmospheric pressure photoionization: an ionization method for liquid chromatography-mass spectrometry, *Anal. Chem.* **2000**, *72*, 3653–3659.
[124] T. J. Kauppila, T. Kuuranne, E. C. Meurer, M. N. Eberlin, T. Kotiaho, R. Kostiainen. Atmospheric pressure photoionization mass spectrometry. Ionization mechanism and the effect of solvent on the ionization of naphthalenes, *Anal. Chem.* **2002**, *74*, 5470–5479.
[125] T. J. Kauppila, H. Kersten, T. Benter. The ionization mechanisms in direct and dopant-assisted atmospheric pressure photoionization and atmospheric pressure laser ionization, *Journal of the American Society for Mass Spectrometry*. **2014**, *25*, 1870–1881.
[126] S. Schmidt, M. F. Appel, R. M. Garnica, R. N. Schindler, T. Benter. Atmospheric pressure laser ionization. An analytical technique for highly selective detection of ultralow concentrations in the gas phase, *Anal. Chem.* **1999**, *71*, 3721–3729.
[127] M. Constapel, M. Schellenträger, O. J. Schmitz, S. Gäb, K. J. Brockmann, R. Giese, T. Benter. Atmospheric-pressure laser ionization: a novel ionization method for liquid chromatography/mass spectrometry, *Rapid communications in mass spectrometry : RCM*. **2005**, *19*, 326–336.
[128] H. Kersten, M. Lorenz, K. J. Brockmann, T. Benter. Evaluation of the performance of small diode pumped UV solid state (DPSS) Nd:YAG lasers as new radiation sources for atmospheric pressure laser ionization mass spectrometry (APLI-MS), *Journal of the American Society for Mass Spectrometry*. **2011**, *22*, 1063–1069.

[129] R. Schiewek, M. Schellenträger, R. Mönnikes, M. Lorenz, R. Giese, K. J. Brockmann, S. Gäb, T. Benter, O. J. Schmitz. Ultrasensitive determination of polycyclic aromatic compounds with atmospheric-pressure laser ionization as an interface for GC/MS, *Anal. Chem.* **2007**, *79*, 4135–4140.
[130] C. Stader, F. T. Beer, C. Achten. Environmental PAH analysis by gas chromatography-atmospheric pressure laser ionization-time-of-flight-mass spectrometry (GC-APLI-MS), *Analytical and bioanalytical chemistry*. **2013**, *405*, 7041–7052.
[131] B. Kanawati, P. Schmitt-Kopplin (Eds.). *Fundamentals and applications of Fourier transform mass spectrometry*. Elsevier, Amsterdam, Netherlands, Cambridge, MA, United States.
[132] J. I. Amster. Fourier Transform Mass Spectrometry, *J. Mass Spectrom.* **1996**, *31*, 1325–1337.
[133] E. O. Lawrence, M. S. Livingston. The Production of High Speed Protons Without the Use of High Voltages, *Phys. Rev.* **1931**, *38*, 834.
[134] E. O. Lawrence, N. E. Edlefsen. The National Academy of Science, *Science (New York, N.Y.)*. **1930**, *72*, 372–378.
[135] H. Sommer, H. A. Thomas, J. A. Hipple. The Measurement of eM by Cyclotron Resonance, *Phys. Rev.* **1951**, *82*, 697–702.
[136] M. B. Comisarow, A. G. Marshall. Fourier transform ion cyclotron resonance spectroscopy, *Chemical Physics Letters*. **1974**, *25*, 282–283.
[137] A. G. Marshall, T. Chen. 40 years of Fourier transform ion cyclotron resonance mass spectrometry, *International Journal of Mass Spectrometry*. **2015**, *377*, 410–420.
[138] P. Caravatti, M. Allemann. The 'infinity cell': A new trapped-ion cell with radiofrequency covered trapping electrodes for fourier transform ion cyclotron resonance mass spectrometry, *Journal of Mass Spectrometry*. **1991**, *26*, 514–518.
[139] E. N. Nikolaev, I. A. Boldin, R. Jertz, G. Baykut. Initial experimental characterization of a new ultra-high resolution FTICR cell with dynamic harmonization, *Journal of the American Society for Mass Spectrometry*. **2011**, *22*, 1125–1133.
[140] Y. Qi, M. Witt, R. Jertz, G. Baykut, M. P. Barrow, E. N. Nikolaev, P. B. O'Connor. Absorption-mode spectra on the dynamically harmonized Fourier transform ion cyclotron resonance cell, *Rapid Commun. Mass Spectrom.* **2012**, *26*, 2021–2026.
[141] Y. I. Kostyukevich, G. N. Vladimirov, E. N. Nikolaev. Dynamically harmonized FT-ICR cell with specially shaped electrodes for compensation of inhomogeneity of the magnetic field. Computer simulations of the electric field and ion motion dynamics, *Journal of the American Society for Mass Spectrometry*. **2012**, *23*, 2198–2207.
[142] D. F. Smith, D. C. Podgorski, R. P. Rodgers, G. T. Blakney, C. L. Hendrickson. 21 Tesla FT-ICR Mass Spectrometer for Ultrahigh-Resolution Analysis of Complex Organic Mixtures, *Anal. Chem.* **2018**, *90*, 2041–2047.
[143] C. L. Hendrickson, J. P. Quinn, N. K. Kaiser, D. F. Smith, G. T. Blakney, T. Chen, A. G. Marshall, C. R. Weisbrod, S. C. Beu. 21 Tesla Fourier Transform Ion Cyclotron Resonance Mass Spectrometer: A National Resource for Ultrahigh Resolution Mass Analysis, *Journal of the American Society for Mass Spectrometry*. **2015**, *26*, 1626–1632.
[144] A. G. Marshall, C. L. Hendrickson, G. S. Jackson. Fourier transform ion cyclotron resonance mass spectrometry: A primer, *Mass Spectrom. Rev.* **1998**, *17*, 1–35.
[145] A. G. Marshall. Ion Cyclotron Resonance and Nuclear Magnetic Resonance Spectroscopies: Magnetic Partners for Elucidation of Molecular Structure and Reactivity, *Acc. Chem. Res.* **1996**, *29*, 307–316.
[146] J. T. Adamson, K. Hakansson in *Lectins*. *Analytical technologies* (Ed.: C. L. Nilsson). Elsevier, Amsterdam, **2007**.

[147] S. Guan, A. G. Marshall, S. E. Scheppele. Resolution and chemical formula identification of aromatic hydrocarbons and aromatic compounds containing sulfur, nitrogen, or oxygen in petroleum distillates and refinery streams, *Anal. Chem.* **1996**, *68*, 46–71.
[148] A. G. Marshall, M. B. Comisarow, G. Parisod. Relaxation and spectral line shape in Fourier transform ion resonance spectroscopy, *The Journal of Chemical Physics*. **1979**, *71*, 4434–4444.
[149] A. G. Marshall, S. Guan. Advantages of High Magnetic Field for Fourier Transform Ion Cyclotron Resonance Mass Spectrometry, *Rapid Commun. Mass Spectrom.* **1996**, *10*, 1819–1823.
[150] Z. Wu, S. Jernström, C. A. Hughey, R. P. Rodgers, A. G. Marshall. Resolution of 10 000 Compositionally Distinct Components in Polar Coal Extracts by Negative-Ion Electrospray Ionization Fourier Transform Ion Cyclotron Resonance Mass Spectrometry, *Energy Fuels*. **2003**, *17*, 946–953.
[151] C. A. Hughey, R. P. Rodgers, A. G. Marshall. Resolution of 11,000 compositionally distinct components in a single electrospray ionization Fourier transform ion cyclotron resonance mass spectrum of crude oil, *Anal. Chem.* **2002**, *74*, 4145–4149.
[152] *IUPAC Compendium of Chemical Terminology*.
[153] A. G. Marshall, R. P. Rodgers. Petroleomics: chemistry of the underworld, *PNAS*. **2008**, *105*, 18090–18095.
[154] E. N. Nikolaev, R. Jertz, A. Grigoryev, G. Baykut. Fine structure in isotopic peak distributions measured using a dynamically harmonized Fourier transform ion cyclotron resonance cell at 7 T, *Anal. Chem.* **2012**, *84*, 2275–2283.
[155] A. G. Marshall, R. P. Rodgers. Petroleomics: the next grand challenge for chemical analysis, *Acc. Chem. Res.* **2004**, *37*, 53–59.
[156] D. W. van Krevelen. *Coal science*. *Aspects of coal constitution*. Elsevier Pub. Co., Amsterdam.
[157] A. K. Burnham in *Techniques in Dentistry and Oral & Maxillofacial Surgery* (Ed.: K. Thankappan). Springer, [New York, New York], **2019**.
[158] D. C. Palacio Lozano, M. J. Thomas, H. E. Jones, M. P. Barrow. Petroleomics: Tools, Challenges, and Developments, *Annual review of analytical chemistry (Palo Alto, Calif.)*. **2020**, *13*, 405–430.
[159] M. Guilhaus in *Encyclopedia of analytical science* (Eds.: P. J. Worsfold, A. Townshend, C. F. Poole). Elsevier, [S.l.], **2010?**
[160] M. Yavor, A. Verentchikov, J. Hasin, B. Kozlov, M. Gavrik, A. Trufanov. Planar multi-reflecting time-of-flight mass analyzer with a jig-saw ion path, *Physics Procedia*. **2008**, *1*, 391–400.
[161] W. R. Plaß, T. Dickel, C. Scheidenberger. Multiple-reflection time-of-flight mass spectrometry, *International Journal of Mass Spectrometry*. **2013**, *349-350*, 134–144.
[162] M. R. Djokic, H. Muller, N. D. Ristic, A. R. Akhras, S. H. Symoens, G. B. Marin, K. M. van Geem. Combined characterization using HT-GC × GC-FID and FT-ICR MS: A pyrolysis fuel oil case study, *Fuel Processing Technology*. **2018**, *182*, 15–25.
[163] A. Dhahak, C. Grimmer, A. Neumann, C. Rüger, M. Sklorz, T. Streibel, R. Zimmermann, G. Mauviel, V. Burkle-Vitzthum. Real time monitoring of slow pyrolysis of polyethylene terephthalate (PET) by different mass spectrometric techniques, *Waste management (New York, N.Y.)*. **2020**, *106*, 226–239.
[164] S. Ubeda, M. Aznar, C. Nerín. Determination of oligomers in virgin and recycled polyethylene terephthalate (PET) samples by UPLC-MS-QTOF, *Analytical and bioanalytical chemistry*. **2018**, *410*, 2377–2384.
[165] A. L. M. Nasser, L. M. X. Lopes, M. N. Eberlin, M. Monteiro. Identification of oligomers in polyethyleneterephthalate bottles for mineral water and fruit juice. Development and validation of a high-performance liquid chromatographic method for the determination of first series cyclic trimer, *Journal of Chromatography A*. **2005**, *1097*, 130–137.
[166] J. C. Petersen. *Binder characterization and evaluation*. Strategic Highway Research Program, National Research Council, Washington, D.C.

[167] S. M. Dorrence, F. A. Barbour, J. C. Petersen. Direct evidence of ketones in oxidized asphalts, *Anal. Chem.* **1974**, *46*, 2242–2244.
[168] J. C. Petersen. A dual, sequential mechanism for the oxidation of petroleum asphalts, *Pet. Sci. Technol.* **1998**, *16*, 1023–1059.
[169] J. C. Petersen, R. Glaser. Asphalt Oxidation Mechanisms and the Role of Oxidation Products on Age Hardening Revisited, *Road Mater. Pavement Des.* **2011**, *12*, 795–819.
[170] V. V. Lobodin, W. K. Robbins, J. Lu, R. P. Rodgers. Separation and Characterization of Reactive and Non-Reactive Sulfur in Petroleum and Its Fractions, *Energy Fuels*. **2015**, *29*, 6177–6186.
[171] C. F.C. Porto et al. Characterization of organosulfur compounds in asphalt cement samples by ESI(+)FT-ICR MS and 13C NMR spectroscopy, *Fuel*. **2019**, *256*, 115923.
[172] F. Handle et al. Tracking Aging of Bitumen and Its Saturate, Aromatic, Resin, and Asphaltene Fractions Using High-Field Fourier Transform Ion Cyclotron Resonance Mass Spectrometry, *Energy Fuels*. **2017**, *31*, 4771–4779.
[173] J. Chiron, J.-P. Galy. Reactivity of the Acridine Ring: A Review, *Synthesis*. **2004**, 313–325.
[174] Z. Hosseini-Dastgerdi, S.A.R. Tabatabaei-Nejad, E. Khodapanah, E. Sahraei. A comprehensive study on mechanism of formation and techniques to diagnose asphaltene structure; molecular and aggregates: a review, *Asia-Pac. J. Chem. Eng.* **2015**, *10*, 1–14.
[175] Y. Zhang, M. Siskin, M. R. Gray, C. C. Walters, R. P. Rodgers. Mechanisms of Asphaltene Aggregation: Puzzles and a New Hypothesis, *Energy Fuels*. **2020**.
[176] T. V. Cheshkova, V. P. Sergun, E. Y. Kovalenko, N. N. Gerasimova, T. A. Sagachenko, R. S. Min. Resins and Asphaltenes of Light and Heavy Oils: Their Composition and Structure, *Energy Fuels*. **2019**, *33*, 7971–7982.
[177] J. Douda, M. E. Llanos, R. Alvarez, J. Navarrete Bolaños. Structure of Maya Asphaltene–Resin Complexes through the Analysis of Soxhlet Extracted Fractions, *Energy Fuels*. **2004**, *18*, 736–742.
[178] M. R. Gray, R. R. Tykwinski, J. M. Stryker, X. Tan. Supramolecular Assembly Model for Aggregation of Petroleum Asphaltenes, *Energy Fuels*. **2011**, *25*, 3125–3134.
[179] S. Acevedo, J. M. Cordero T., H. Carrier, B. Bouyssiere, R. Lobinski. Trapping of Paraffin and Other Compounds by Asphaltenes Detected by Laser Desorption Ionization–Time of Flight Mass Spectrometry (LDI–TOF MS): Role of A1 and A2 Asphaltene Fractions in This Trapping, *Energy Fuels*. **2009**, *23*, 842–848.
[180] P.'a. Peng, A. Morales-Izquierdo, A. Hogg, O. P. Strausz. Molecular Structure of Athabasca Asphaltene: Sulfide, Ether, and Ester Linkages, *Energy Fuels*. **1997**, *11*, 1171–1187.
[181] O. P. Strausz, M. Torres, E. M. Lown, I. Safarik, J. Murgich. Equipartitioning of Precipitant Solubles between the Solution Phase and Precipitated Asphaltene in the Precipitation of Asphaltene, *Energy Fuels*. **2006**, *20*, 2013–2021.
[182] H. Alboudwarej, J. Beck, W. Y. Svrcek, H. W. Yarranton, K. Akbarzadeh. Sensitivity of Asphaltene Properties to Separation Techniques, *Energy Fuels*. **2002**, *16*, 462–469.
[183] Z. Frakman, T. M. Ignasiak, E. M. Lown, O. P. Strausz. Oxygen compounds in Athabasca asphaltene, *Energy Fuels*. **1990**, *4*, 263–270.
[184] H. Moriwaki, M. Ishitake, S. Yoshikawa, H. Miyakoda, J.-F. Alary. Determination of polycyclic aromatic hydrocarbons in sediment by liquid chromatography-atmospheric pressure photoionization-mass spectrometry, *Analytical sciences : the international journal of the Japan Society for Analytical Chemistry*. **2004**, *20*, 375–377.
[185] T. Schwemer, C. P. Rüger, M. Sklorz, R. Zimmermann. Gas Chromatography Coupled to Atmospheric Pressure Chemical Ionization FT-ICR Mass Spectrometry for Improvement of Data Reliability, *Anal. Chem.* **2015**, *87*, 11957–11961.
[186] B. Eliasson, U. Kogelschatz. Ozone Generation with Narrow–Band UV Radiation, *Ozone: Science & Engineering*. **1991**, *13*, 365–373.

[187] H. Huang, H. Lu, H. Huang, L. Wang, J. Zhang, D. Y. C. Leung. Recent Development of VUV-Based Processes for Air Pollutant Degradation, *Front. Environ. Sci.* **2016**, *4*, 17.

[188] J. C. Poveda, A. Guerrero, I. Álvarez, C. Cisneros. Multiphoton ionization and dissociation of naphthalene at 266, 355, and 532nm, *Journal of Photochemistry and Photobiology A: Chemistry*. **2010**, *215*, 140–146.

[189] E. Kendrick. A Mass Scale Based on CH 2 = 14.0000 for High Resolution Mass Spectrometry of Organic Compounds, *Anal. Chem.* **1963**, *35*, 2146–2154.

[190] A. G. Marshall, R. P. Rodgers. Petroleomics: the next grand challenge for chemical analysis, *Acc. Chem. Res.* **2004**, *37*, 53–59.

[191] S. Pourshahian. Mass Defect from Nuclear Physics to Mass Spectral Analysis, *J. Am. Soc. Mass Spectrom.* **2017**, *28*, 1836–1843.

[192] C. A. Hughey, C. L. Hendrickson, R. P. Rodgers, A. G. Marshall, K. Qian. Kendrick mass defect spectrum: a compact visual analysis for ultrahigh-resolution broadband mass spectra, *Anal. Chem.* **2001**, *73*, 4676–4681.

[193] W. Schrader, S. K. Panda, K. J. Brockmann, T. Benter. Characterization of non-polar aromatic hydrocarbons in crude oil using atmospheric pressure laser ionization and Fourier transform ion cyclotron resonance mass spectrometry (APLI FT-ICR MS), *The Analyst*. **2008**, *133*, 867–869.

Appendix

Curriculum Vitae

20.-23.08.2018	Participation in the end user school 1 of the EU FT-ICR MS project in Joensuu, Finland *Winner of the presenter price of the school*
since 01.01.2018	PhD student on EU FT-ICR MS project at University of Rostock *Working on the development of ionisation schemes for complex mixtures, especially photoionisation for the chemical characterisation of petroleum-derived materials*
since 10.2016	PhD student, Chair of Analytical Chemistry, University of Rostock *Working on FT-ICR MS for complex petroleum-derived samples*
10. 2014 - 09.2016	Master of Science, University of Rostock, final grade: 1,4
10. 2011 - 09. 2014	Bachelor of Science, University of Rostock
08.2004 - 06.2011	Secondary school, Gymnasium Raabeschule, Braunschweig graduation: Abitur

Conference Contribution

- Anika Neumann, Christopher P. Rüger, Martin Sklorz, Ralf Zimmermann, "**Thermal and laser desorption atmospheric pressure photo ionisation ultra-high resolution mass spectrometry – Concept and application towards complex samples**", 50th annual conference of the German Society for Mass Spectrometry (DGMS), 05.-08.03.2017, Kiel, Germany, (Poster)

- Anika Neumann, Christopher Paul Rüger, Theo Schwemer, Martin Sklorz, Ralf Zimmermann, "**Investigation of volatile and semi-volatile species from primary combustion aerosol via thermo desorption atmospheric pressure photo ionisation ultra-high resolution mass spectrometry**" ANAKON, 03.-06.04.2017, Tübingen, Germany, (Poster)

- Anika Neumann, Christopher P. Rüger, Martin Sklorz, Ralf Zimmermann, "**Comparison of atmospheric pressure photo ionisation with 8.6/9.4 and 10/10.6 eV to atmospheric pressure chemical ionisation for the analysis of complex mixtures**", 13th EFTMS Workshop, 24.-27.4.2018, Freising, (Poster)

- Anika Neumann, Christopher P. Rüger, Martin Sklorz, Ralf Zimmermann, „**Comparison of Xe/Kr atmospheric pressure photo ionisation (APPI) to atmospheric pressure chemical ionisation for the analysis of complex mixtures**", 51st European Mass Spectrometry Conference, 11.-15.3.2018, Saarbrücken, Germany, (Poster)

- Anika Neumann, Christopher P. Rüger, Martin Sklorz, Ralf Zimmermann, "**Comparison of atmospheric pressure chemical and photo ionization for evolved gas analysis high resolution FT-ICR MS for petroleum-derived material**", 1st EU-FT-ICR MS End-User school, Joensuu, Finland, 20.-24.8.2018, (Talk)

Declaration on the contribution to the manuscripts for cumulative thesis

Title: Thermal analysis coupled to ultra-high resolution mass spectrometry with collision induced dissociation for complex petroleum samples – heavy oil composition and asphaltene precipitation effects

Authors: Christopher P. Rüger, Anika Neumann, Martin Sklorz, Theo Schwemer, and Ralf Zimmermann

Journal: Energy Fuels, 31, 12, 13144–13158

Year: 2017

Anika Neumann contributed to the conception of the study, data visualisation and interpretation, literature research and improved the manuscript.

Title: Combination of Different Thermal Analysis Methods Coupled to Mass Spectrometry for the Analysis of Asphaltenes and Their Parent Crude Oils: Comprehensive Characterization of the Molecular Pyrolysis Pattern

Authors: Christopher P. Rüger, Christoph Grimmer, Martin Sklorz, Anika Neumann, Thorsten Streibel, and Ralf Zimmermann

Journal: Energy Fuels, 32, 3, 2699–2711

Year: 2018

Anika Neumann carried out the TG-APPI-FT-ICR MS measurements, contributed to the data interpretation, data visualization and approved the manuscript.

Title: Real time monitoring of slow pyrolysis of polyethylene terephthalate (PET) by different mass spectrometric techniques

Authors: Asma Dhahak, Christoph Grimmer, Anika Neumann, Christopher P. Rüger, Martin Sklorz, Thorsten Streibel, Ralf Zimmermann, Guillain Mauviel, and Valérie Burkle-Vitzthum

Journal: Waste Management, 106, 226–239

Year: 2020

Anika Neumann mentored and completed the TG-APCI-FT-ICR MS measurements, processed the data and approved the manuscript.

Title: Investigation of Aging Processes in Bitumen at the Molecular Level with High-Resolution Fourier-Transform Ion Cyclotron Mass Spectrometry and Two-Dimensional Gas Chromatography Mass Spectrometry

Authors: Anika Neumann, Uwe Käfer, Thomas Gröger, Thomas Wilharm, Ralf Zimmermann, and Christopher P. Rüger

Journal: Energy Fuels, 34, 9, 10641–10654

Year: 2020

Anika Neumann carried out the TG-APCI-FT-ICR MS measurements, their processing as well as data interpretation. Anika Neumann further carried out the data visualisation, the main data interpretation and integration. The manuscript was written by Anika Neumann. Uwe Käfer carried out the GC×GC-HR-TOF MS measurements and their processing; he also assisted in data interpretation of the GC×GC-HR-TOF MS measurements. Co-authors further improved and approved the manuscript.

Title: Investigation of island/ single-core and archipelago/ multi-core enriched asphaltenes and their solubility fractions by thermal analysis coupled to high resolution Fourier transform ion cyclotron resonance mass spectrometry

Authors: Anika Neumann, Martha Liliana Chacón-Patiño, Ryan P. Rodgers, Christopher P. Rüger, and Ralf Zimmermann

Journal: Energy Fuels, submitted

Year: 2020

Anika Neumann carried out the TG-APCI-FT-ICR MS measurements, their processing as well as data interpretation. Anika Neumann further carried out the data visualisation and the data interpretation. The manuscript was written by Anika Neumann. The extrography fractionation was carried out by Martha Chacón-Patiño. Co-authors contributed to the discussion of the data and improved the manuscript.

Title: Atmospheric pressure single photon laser ionization (APSPLI) mass spectrometry using a 157 nm Fluorine excimer laser for sensitive and selective detection of non-polar to semi-polar hydrocarbons

Authors: Christopher P. Rüger, Anika Neumann, Martin Sklorz, and Ralf Zimmermann

Journal: Analytical Chemistry, submitted

Year: 2020

Anika Neumann assisted in the setting up of GC/TG-APSPLI-FT-ICR MS. Anika Neumann carried out the measurements, most of their processing as well as data interpretation. Anika Neumann contributed to the writing of the manuscript. Martin Sklorz was strongly involved in the setting up of the APSPLI system. Christopher P. Rüger mainly wrote the manuscript. All co-authors approved the manuscript.

Publications for the cumulative thesis

Publication 1

Thermal analysis coupled to ultra-high resolution mass spectrometry with collision induced dissociation for complex petroleum samples – heavy oil composition and asphaltene precipitation effects

by

Christopher P. Rüger, Anika Neumann, Martin Sklorz, Theo Schwemer, Ralf Zimmermann

Energy and Fuels, 31 (12), S. 13144-13158

DOI: 10.1021/acs.energyfuels.7b01778

Publication 2

Combination of Different Thermal Analysis Methods Coupled to Mass Spectrometry for the Analysis of Asphaltenes and Their Parent Crude Oils: Comprehensive Characterization of the Molecular Pyrolysis Pattern

by

Rüger, Christopher P.; Grimmer, Christoph; Sklorz, Martin; Neumann, Anika; Streibel, Thorsten; Zimmermann, Ralf

Energy and Fuels, 32 (3), S. 2699-2711

DOI: 10.1021/acs.energyfuels.7b02762

Publication 3

Real time monitoring of slow pyrolysis of polyethylene terephthalate (PET) by different mass spectrometric techniques

by

Dhahak, Asma; Grimmer, Christoph; Neumann, Anika; Rüger, Christopher; Sklorz, Martin; Streibel, Thorsten; Zimmermann, Ralf; Mauviel, Guillain; Burkle-Vitzthum, Valérie

Waste management (NewYork, N. Y.), 106, S. 226-239

DOI: 10.1016/j.wasman.2020.03.028

Publication 4

Investigation of Aging Processes in Bitumen at the Molecular Level with High-Resolution Fourier-Transform Ion Cyclotron Mass Spectrometry and Two-Dimensional Gas Chromatography Mass Spectrometry

by

Neumann, Anika; Käfer, Uwe; Gröger, Thomas; Wilharm, Thomas; Zimmermann, Ralf; Rüger, Christopher P.

Energy and Fuels, 34 (9), S. 10641-10654

DOI: 10.1021/ACS.ENERGYFUELS.0C01242

energy&fuels
SEPTEMBER 2020 VOLUME 34
pubs.acs.org/EF

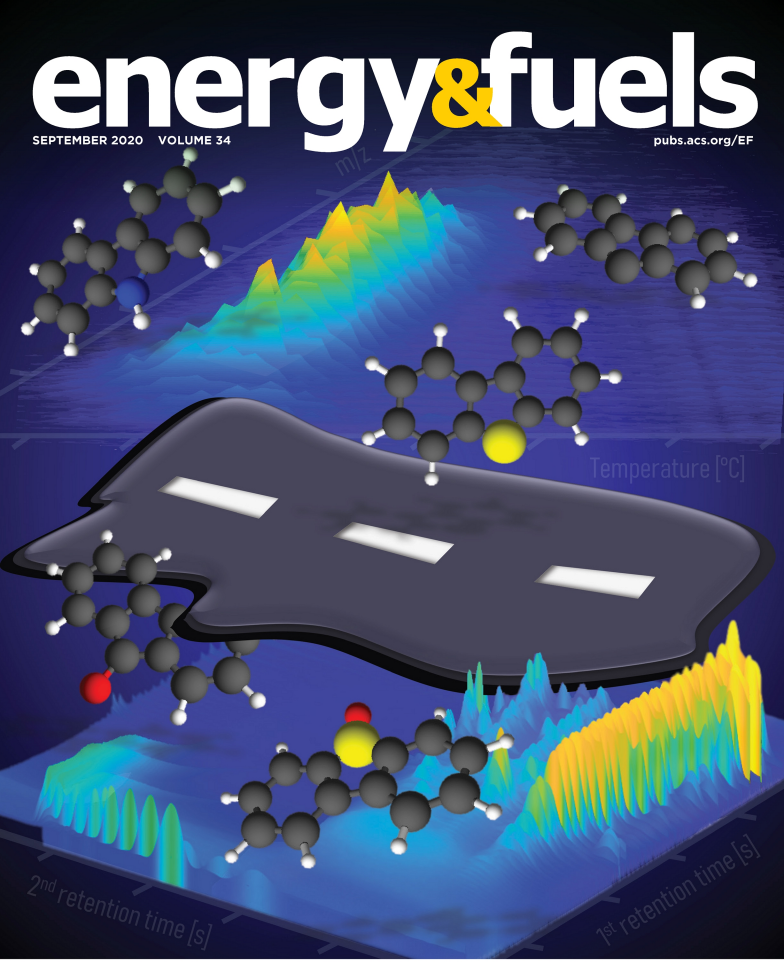

ACS Publications
Most Trusted. Most Cited. Most Read.
www.acs.org

energy&fuels

pubs.acs.org/EF

Article

Investigation of Aging Processes in Bitumen at the Molecular Level with High-Resolution Fourier-Transform Ion Cyclotron Mass Spectrometry and Two-Dimensional Gas Chromatography Mass Spectrometry

Anika Neumann, Uwe Käfer, Thomas Gröger, Thomas Wilharm, Ralf Zimmermann, and Christopher P. Rüger*

Cite This: *Energy Fuels* 2020, 34, 10641−10654

Read Online

ACCESS | Metrics & More | Article Recommendations | Supporting Information

ABSTRACT: Bitumen is a highly viscous and chemically complex petroleum-derived material, which is applied as a binder in road construction. However, the asphalt undergoes hardening, cracking, and embrittlement not only due to oxidative short-term aging during the mixing and paving process but also due to long-term aging during the service time of the pavement. In this study, chemical changes occurring during short-term aging, mimicked by a prolonged rotating flask procedure, are investigated for an artificial bitumen model at the molecular level. The model bitumen enables the application of two complementary analytical techniques for obtaining a comprehensive insight into the aging effects: high-resolution Fourier-transform ion cyclotron mass spectrometry (FT-ICR MS) coupled to thermogravimetry was applied to investigate the aging effects on polar to semipolar high-molecular-weight compounds ionized by atmospheric pressure chemical ionization. Aromatic core structures were analyzed by alternating collision-induced dissociation. In order to support structural assignments from FT-ICR MS data in the semivolatile region, comprehensive two-dimensional gas chromatography mass spectrometry (GC × GC−HRTOFMS) with electron ionization at 70 eV was applied for the group-type analysis and the investigation of particular chemical functionalities. Oxidation processes were revealed to be the prevalent reactions caused by short-term aging of the hydrocarbons (CH-class) and sulfur-containing classes. Aromatic species with low steric hindrance or activated carbon positions as well as high aromatic core structures are favorably oxidized, forming carbonyl functionalities. For molecules with one sulfur atom (S1-class), nonaromatic species such as tetrahydrothiophenes decrease, whereas aromatic S1-compounds remain constant. Nonaromatic S1O1-species tend to further oxidize, while higher aromatic species are formed with ongoing aging time. Moreover, this study highlights the aging behavior of nitrogen-containing compounds, such as carbazoles. A significant reduction of the N-classes was observed during aging, indicating thermal-induced condensation reactions as well as favored oxidation of highly aromatic core structures.

INTRODUCTION

Bitumen is a viscous, involatile, and highly complex mixture derived from petroleum vacuum residues or naturally occurring asphalt. It is composed of high-boiling molecules with high aromaticity as well as a high content of nitrogen, sulfur, and oxygen, which are present as functional groups such as sulfides, pyridinic- or pyrrolic-type structures, phenolic compounds, or carboxylic acids.[1,2] In road construction, bitumen is used as a binder for mineral aggregates to create asphalt concrete. Several modifiers, such as elastomers, plastomers, or crumb rubber, can be added to design and improve the viscosity, elasticity, hardness, and the lifetime of the pavement.[3−5] During service time, the asphalt becomes more viscous, harder, brittle, and eventually cracked, which can be caused by the aging of the material.[6] The aging process can be divided into two different time ranges. First, short-term aging occurs during the mixing of the binder with the aggregates as well as the paving process and is characterized by high temperatures (150−160 °C) and a high specific surface of the bitumen mixture. Second, long-term aging appears during the service time of the bitumen and is induced by climatic conditions, void content of the material, and oxidation. In laboratory studies, short-term aging is simulated by the rolling thin film oven test (RTFOT) or rotating flask test, while long-term aging is performed in a pressure-aging vessel and usually carried out after RTFOT-conditioning.[7−12] Different mechanisms lead to altered characteristics of the bitumen caused by the aging process. Besides the evaporation of low volatile species, the phase separation of bitumen compounds, and the physical hardening due to molecular organization, the mechanism considered as most important is oxidative aging.[13,14] Oxidation causes hardening and embrittlement of the binder because of the formation of polar functional groups, such as sulfoxides, anhydrides, carboxylic acids, and carbonyls.[1,2]

Received: April 16, 2020
Revised: June 18, 2020
Published: June 25, 2020

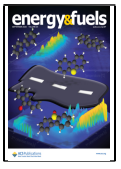

https://dx.doi.org/10.1021/acs.energyfuels.0c01242
Energy Fuels 2020, 34, 10641−10654

The effects of aging on bitumen are routinely investigated by the determination of physical properties, such as the penetration index[15,16] or rheological properties measured by dynamic shear rheometry,[9,17−21] which provide insights into mechanical characteristics. Aging typically results in hardening, a decrease in elasticity, and an increased viscosity. Because of the extreme complexity of bitumen, detailed chemical characterization of aging effects is still an analytical challenge, and therefore, chemical analyses are mostly limited to functional group analysis or fractionation in saturates, aromatics, resins, and asphaltenes (SARA fractionation).[22] With infrared spectroscopy, the formation of carbonyl as well as sulfoxide functions during oxidative aging has been frequently reported in the literature.[4,23−25] It was shown that sulfoxides are formed with higher reaction rates than carbonyls, and moreover, a temperature dependence of the oxidation reaction was revealed.[9,26−28] SARA fractionation has been used since the 1960s for the chemical description of bitumen.[29] Saturates are considered as almost inert with respect to oxidation,[18,25] while resins and asphaltenes show stronger changes.[4,25] Petersen et al. (2009) ranked the reactivity of the SARA fractions with oxygen in the following order: saturates < aromatics < resins < asphaltenes, while the asphaltene fraction is the most reactive one.[1] Hofko et al. (2016) showed that the asphaltene content is strongly related to the rheological properties of bitumen.[20] Atomic force microscopy reveals a micelle-like structure of asphaltenes surrounded by resin and polar aromatic molecules, and different aging studies showed an increase in resin and asphaltene structures over aging time.[3,30,31] Recently, Weigel and Stephan (2017) showed a modeling approach with which physical, rheological, and aging behavior could be derived from the SARA distribution.[32] Nonetheless, the molecular level of bitumen aging is still poorly understood. In 2017, Handle et al. demonstrated the potential of Fourier-transform ion cyclotron resonance mass spectrometry (FT-ICR MS) to investigate the aging behavior of highly polar species in the bituminous material.[33] In the last few decades, FT-ICR MS provided, because of its high mass accuracy and ultrahigh resolution, valuable insights into the field of petroleomics, and particularly in highly complex fractions such as asphaltenes or vacuum residues.[34−39] Besides the typical spray-based sample introduction, the hyphenation of thermogravimetry (TG) has already shown in different studies its value for the investigation of high-boiling petroleum fractions.[40,41] For more volatile as well as less polar fractions, two-dimensional (2D) gas chromatography (GC) coupled to MS (GC × GC−MS) is extensively used in the field of petroleomics to cope with the enormous complexity of petroleum-derived sample materials.[38,42−45] Chromatographic separation in two orthogonal dimensions with subsequent MS detection enables the separation of complex mixtures, identification of resolved analytes, and classification into chemical groups. However, because of the volatility limit of GC techniques, GC × GC−MS is only applicable for the analysis of volatile to semivolatile fractions. Combining the advantages of FT-ICR MS and GC × GC−MS was already shown to allow for a comprehensive description of several crude oils,[46] petroleum cuts,[47] and bio-oils.[48,49]

The aim of this study is to investigate oxidative short-term aging of bitumen at the molecular level in an attempt to achieve a detailed understanding of the complex chemical processes. Identifying compounds, which are highly affected by aging, will help design durable and long-living pavements. To focus on the aging effects in neat bitumen, an artificial bitumen model was generated without adding any modifiers and specifically designed to contain components in the boiling range of GC application offering the opportunity for structural elucidation. The model bitumen was treated under prolonged short-term aging conditions to enhance chemical reactions triggered by high temperatures in the presence of oxygen and to allow for their detection. Multiple sampling during the aging procedure enables the tracing of aging-related chemical changes. The occurring effects were analyzed by atmospheric pressure chemical ionization (APCI) TG-FT-ICR MS and confirmed as well as partially complemented by electron ionization (EI) GC × GC−HRTOFMS. The application of TG-FT-ICR MS enables the attribution of sum formulae up to the highly complex heavy end of the model bitumen. Additionally, aromatic core structures were addressed by alternating collision-induced dissociation (CID). Heteroatom-containing minorities were highlighted by APCI, which selectively ionized semipolar to polar species.[50,51] The additional chromatographic analytical dimension of GC × GC−HRTOFMS is able to contribute structural information, which supports and confirms structural estimations of FT-ICR MS data, especially in the semivolatile region. Because of the compositional continuum (Boduszynski model) known for crude oil-derived materials,[52−56] the results can, to a certain extent, be expanded to high-boiling regions. The universal ionization technique EI applied for GC × GC−HRTOFMS allows for a broad chemical description of the sample material including nonpolar hydrocarbons, which complements the smaller chemical space obtained by APCI for FT-ICR MS data. In this study, a detailed description of short-term aging effects in the bitumen model was envisioned by the combination of both techniques. Aging-related alterations are presented at the molecular level for different hydrocarbon classes, oxidized hydrocarbons, sulfur- and nitrogen-containing species, and their corresponding oxidized representatives.

MATERIALS AND METHODS

Sample Preparation. For the preparation of the model bitumen, a heavy crude oil (Mittelplate crude oil) with an API gravity of 21° was used. The volatile compounds (up to 200 °C) of the crude oil were removed by distillation in accordance with ASTM D2892[57] using a 15-theoretical plate batch distillation system (Pilodist 100, Pilodist, Meckenheim, Germany) to generate a controlled sample matrix without any chemical modifiers. Detailed information on the distillation procedure can be found elsewhere.[43] The remaining residue was aged with a modified rotating flask test for 168 h at 150 °C under an air atmosphere. In this setup, skin formation of the viscous sample is prevented by the constant rotation of the flask, and continuous renewal of the sample surface is ensured. Moreover, in order to prevent depletion of oxygen in the atmosphere, a constant air flow of 2 L/min was maintained. The model bitumen was sampled after 1 day (24 h), 2 days (48 h), 3 days (72 h), 4 days (96 h), and 7 days (168 h). Including the nonaged sample (0 days), a sample set containing six different aging stages was obtained, which enables a continuous, multistage description of chemical changes in the matrix.

TG FT-ICR MS with APCI (TG-APCI-FT-ICR MS). Each of the bitumen samples representing different aging stages was measured by TG coupled to APCI FT-ICR MS in triplicates. The detailed description of the setup can be found elsewhere.[58] The method was previously shown to reveal valuable information on highly complex petroleum samples.[40,41] In short, approximately 1 mg of the samples was directly introduced into a single-use aluminum crucible of the thermobalance (TG 209 cell thermobalance, Netzsch, Selb, Germany). Under a constant flow of nitrogen of 200 mL/min, the

https://dx.doi.org/10.1021/acs.energyfuels.0c01242
Energy Fuels 2020, 34, 10641−10654

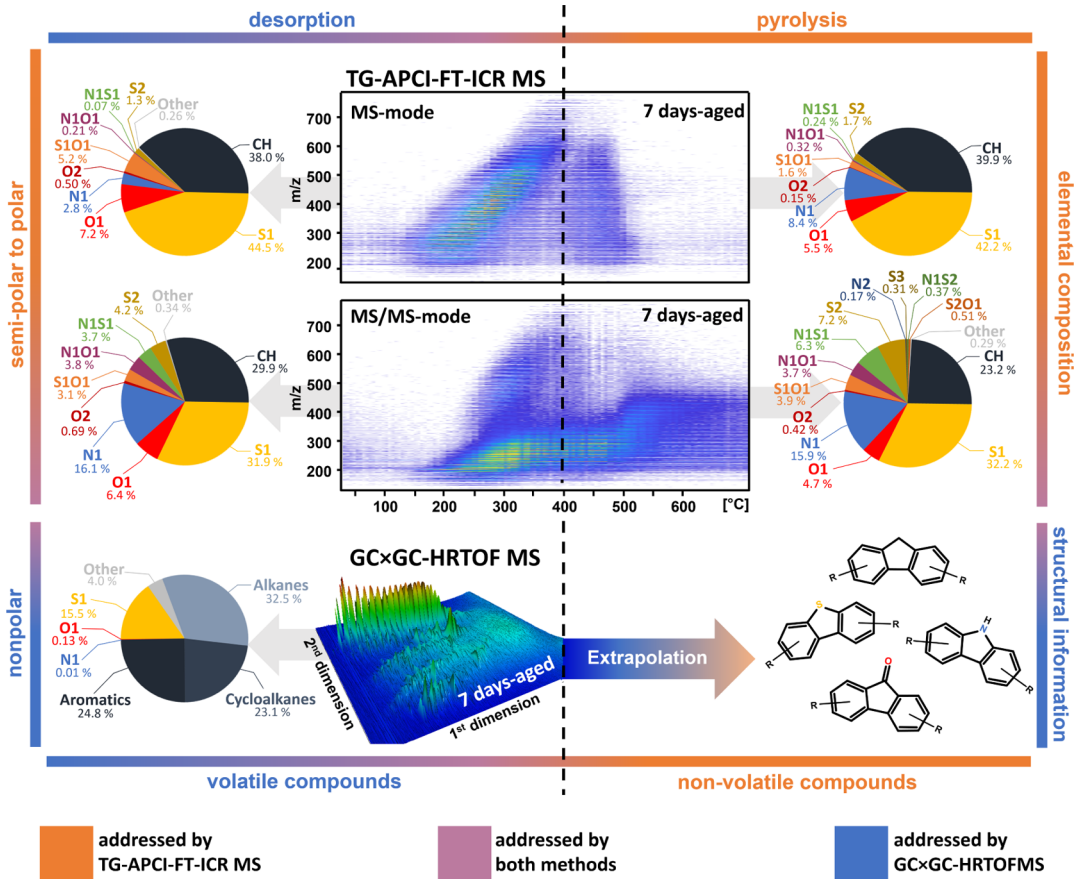

Figure 1. Method integration of TG-APCI-FT-ICR MS and GC × GC−HRTOFMS exemplarily depicted for the 7 days aged model bitumen. Desorbable and pyrolyzable species are separated at the dashed line. Pie charts on the left side correspond to the class distribution found for desorption, while pie charts on the right side give the class distribution for the pyrolysis phase. TG-APCI-FT-ICR MS is able to attribute sum formulae to semivolatile to pyrolyzable compounds. Because of APCI, semipolar to polar minorities are highlighted. The 2D survey view of the temperature-resolved mass spectra for the MS-mode and the MS/MS-mode color-coded with intensity shows the characteristic increase of the m/z with the increase of temperature in the desorption phase, while an enlarged m/z range is simultaneously covered in the pyrolysis phase. GC × GC−HRTOFMS enables the structural elucidation of volatile compounds. With EI, nonpolar compounds are covered as well. 2D GC allows for group-type analysis of volatile compounds up to roughly m/z 600.

sample was heated from 20 °C (held for 2 min) up to 600 °C (held for 10 min) with a heating rate of 10 K/min. The evolved gas mixture (2 mL/min) was transferred to the ionization chamber via a slight overpressure of 8 mbar over a heated transfer-line (deactivated fused silica capillary, 0.53 mm ID, 300 °C). The filled TG crucibles were weighed before and after the measurements to determine the residual masses, which are summarized in Table S1 for each measurement. APCI was carried out in a GC-APCI II ion source (Bruker Daltonics, Bremen, Germany) using a current of 3000 nA for corona discharge. Temperature-resolved mass spectra were recorded on a 7 T FT-ICR MS equipped with an infinity cell (APEX Qe, Bruker Daltonics, Bremen, Germany) with a resolving power of 260,000 at m/z 400 resulting from 2 s transient. Every 10 s, a broadband spectrum for m/z 100−1000 was recorded in the MS-mode consisting of five microscans for enhancing the signal-to-noise ratio of low-abundant signals. An alternating MS/MS-mode was applied, that is, five microscans of the intact molecules were registered in turns with five microscans of fragmented molecules. This procedure allows investigating the aromatic core structures of alkylated constituents.[59,60] For fragmentation, CID was applied using a collision voltage of 30 V and a higher accumulation time of 1 s.

Comprehensive time-resolved processing was carried out using Bruker DataAnalysis 5.1 for m/z precalibration of the summed mass spectra and a self-written tool CERES based on in-house MATLAB scripting (R2018b, 64-bit) for further processing (feature detection) and sum formula calculation (including evaluation and validation). Every measurement was internally linearly calibrated on homologue rows in DataAnalysis, and again every single spectrum during processing in CERES to correct for frequency shifts resulting from varying ion loads in the FT-ICR MS cell. The elemental composition attribution was carried out for MS spectra with the following restrictions: #C 6−70, #H 4−200, #N 0−1, #O 0−4, #S 0−2, H/C ratio 0−3, ring and double bond equivalent (DBE) 0−40, and a sum formula error of 1 ppm. For MS/MS spectra, the following restrictions were applied: #C 6−70, #H 4−200, #N 0−2, #O 0−2, #S 0−3, H/C ratio 0−3, DBE 0−40, and a sum formula error of 1 ppm. In Figure S1, the sum formula error distribution is given for a nonaged model bitumen. In general, sum formulae could be obtained with a root-mean-square error below 0.28 ppm for the MS-mode and below 0.31 ppm for the MS/MS-mode.

2D GC Coupled to High-Resolution Time-of-Flight MS (GC × GC−HRTOFMS). Samples were dissolved in dichloromethane[61] (20% wt), and 1 μL of the solution was injected using a programmable temperature vaporizing unit (Optic 4, GL Sciences, Eindhoven, Netherlands). GC × GC experiments were conducted on a Leco Pegasus HRT 4D (Leco, St. Joseph, MI, USA) with an Agilent Technologies 7890A gas chromatograph (Palo Alto, CA, USA). The system was equipped with a dual-stage liquid nitrogen thermal modulator and a secondary oven, placed inside the main GC oven. The GC method used for analyzing the model bitumen samples was already evaluated and applied for heavy fractions in earlier studies.[42,43,62,63] In brief, a high-temperature column combination consisting of a Phenomenex Zebron ZB-35HT Inferno (30 m × 0.25 mm; film: 0.1 μm) as the first dimension and a SGE BPX1 (1.5 m ×

https://dx.doi.org/10.1021/acs.energyfuels.0c01242
Energy Fuels 2020, 34, 10641−10654

0.1 mm; film: 0.1 μm) as the second dimension were used. The complete overview of instrumental parameters is presented in the Supporting Information in Table S2. Each sample was measured in triplicates to determine the methodological variance.

GC × GC data were postprocessed with ChromaTOF HRT (version 5.10, Leco, St. Joseph, MI, USA). Chromatograms were manually checked for the presence of chemical classes, and the subsequently detected peaks were classified by retention time regions and mass spectral filters to compound classes. Details about the classification procedure can be found in the literature.[62,63] Peak areas were normalized to the total ion current and summarized to compound classes to obtain the relative abundance of respective chemical groups.

RESULTS AND DISCUSSION

In the following, the aging effects observed by TG-FT-ICR MS supported by GC × GC−HRTOFMS are discussed shortly on a macroscopic level for generally observed alterations and in detail for three groups of compound classes at the molecular level. The components were divided into the hydrocarbon class (CH-class), sulfur-containing classes (S_x-class), nitrogen-containing classes (N_x-class), and their corresponding oxidation products (O_x-class, S_xO_y-class, and N_xO_y-class). Aging-related trends were statistically validated at 95% statistical certainty applying the Weir *t*-test,[64] which is specially designed for a limited number of replicates.

Before discussing the observed aging effects, the capabilities of the applied techniques are introduced in more detail. Figure 1 illustrates the integration of the methodologies using the example of the 7 days aged model bitumen. Additional temperature-resolved FT-ICR MS mass spectra, as well as GC × GC−HRTOFMS chromatograms, for the nonaged sample and the 7-day aged sample are given in Figures S2 and S3 of the Supporting Information, respectively. Because of the thermogravimetric sample introduction under a nitrogen atmosphere, TG-FT-ICR MS data can be divided into two phases attributable to temperature, which is visualized by the dashed line in Figure 1. From 100 to 400 °C, a desorption phase is observed, in which intact species up to m/z 750 are evaporated. In the second phase from 400 to 600 °C, pyrolysis occurs, leading to a decomposition of high-molecular-weight species into smaller thermal fragments. In addition to the differentiation into desorption and pyrolysis phases of the FT-ICR MS data, CID was applied in the MS/MS-mode alternating with the recording of normal MS spectra. Typically, when using CID under moderate conditions, aromatic compounds are partially dealkylated and the charge remains on the aromatic core.[59,60] Because of the mass loss due to dealkylation and enhanced ion storage time, smaller molecules and/or compounds with a low DBE shift under the detectable mass limit of the FT-ICR MS, and therefore MS/MS data give a slightly shifted view concerning m/z or DBE. On the other hand, valuable information is obtained on the high-molecular species because of two mutual enhancing effects. First, because of longer accumulation times, low abundant or only weakly ionized species could also be detected, and second, a variety of compounds with different degrees of alkylation are fragmented to the same core structure also enhancing the intensity. FT-ICR MS was equipped with the soft ionization technique APCI, resulting in the detection of preserved molecular ions and highlighting semipolar to polar minorities. Figure 1 illustrates the class distributions as pie charts for desorption and pyrolysis phases to reveal the differences in relative intensity of the attributed classes between the different phases. In general, the pyrolysis phase exhibits a higher chemical diversity than the desorption phase, which can be explained by the Boduszynski model.[55] In petroleum-derived materials, high-boiling fractions exhibit a higher amount of heteroatoms and chemical complexity than lighter fractions. On this macroscopic scale, aging effects are hardly noticeable and are discussed at the molecular level below.

In order to support the findings from TG-FT-ICR MS experiments, GC × GC−HRTOFMS was complementarily applied, enabling the separation of isomers and a more detailed identification of molecular structures. The application of EI with 70 eV, as a universal ionization technique, further enables the detection of nonpolar hydrocarbons, such as alkanes or cycloalkanes. The class distribution of the GC data is depicted in Figure 1 (bottom), revealing the predominance of nonpolar to semipolar species. As a chromatographic-based technique, only volatile compounds could be targeted, which excludes high-molecular species in the model bitumen. However, with the applied high-temperature method, species with m/z up to 600 could be detected. The desorption phase observed during TG-FT-ICR MS is to a great extent congruent with the boiling range covered by GC × GC−HRTOFMS allowing the confirmation of structural assessments derived from elemental compositions as well as the calculated DBE.[65] Because of the compositional continuum of the crude oil-derived material,[55] structural motifs, obtained by GC × GC−HRTOFMS for desorbable species, can be extrapolated to nonvolatile compounds observed during the pyrolysis phase with TG-FT-ICR MS.

General Alterations. The first information on the aging process can be obtained from the mass loss curves of the TG measurements and its derivative (DTG) in Figure 2a,b, respectively. The comparison of the averaged mass loss curves of the nonaged and the 7 days aged model bitumen reveals a decrease of the mass loss in the desorption phase from 62.5 ± 2.2 to 56.5 ± 2.1% during aging and an increase of the pyrolysis phase from 29 ± 0.8 to 31.3 ± 0.8%. In addition, the averaged nonevaporable residue increases from 8.5 ± 1.9 to 12.2 ± 1.4%, which leads to the assumption that low-boiling compounds are evaporated or transformed into higher boiling point species during the aging at elevated temperatures. This conjecture is supported by the DTG curves showing a shift in the beginning of the desorption phase of about 50 °C from 100 to 150 °C after 7 days of aging, while the pyrolysis phase starts in both cases at approximately 400 °C. Besides the TG information, average MS data, such as the averaged total ion count (TIC) depicted in Figure 2c, also reveal a shift to a higher proportion of the pyrolysis phase. In the nonaged model bitumen, 83.0 ± 0.7% of the TIC accounts for the desorption phase and 17.0 ± 0.7% for the pyrolysis phase. After 7 days of aging, the desorption phase is reduced to 81.0 ± 0.5%, while the pyrolysis phase is increased to 19.0 ± 0.5%. Furthermore, GC × GC−HRTOFMS data gave evidence that this shift is partially caused by evaporation due to the decrease of low-boiling semivolatiles after intensive aging, which is more specifically discussed for the CH-class later. A magnified view of the affected region for different aging stages is given in Figure S4, showing that the evaporation effect is most severe after 7 days of aging. Generally, the loss of volatiles is known as an aging effect in the literature, causing hardening and embrittlement due to the compositional changes of the bituminous material. Lerfald (2000) stated that molecular alterations in the presence of air can occur because of the

https://dx.doi.org/10.1021/acs.energyfuels.0c01242
Energy Fuels 2020, 34, 10641−10654

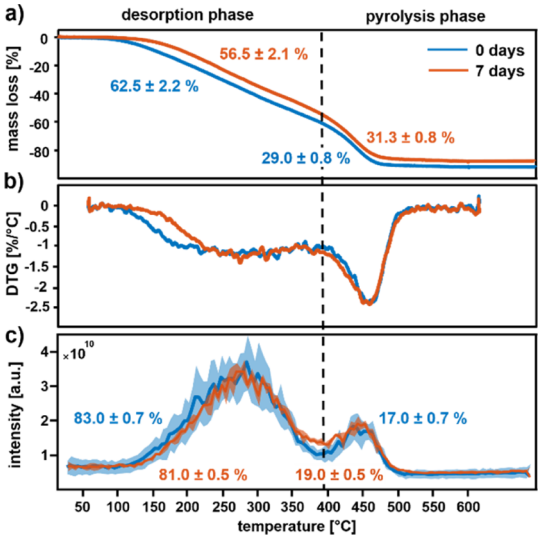

Figure 2. Depiction of the desorption and pyrolysis phases of the model bitumen obtained by TG-APCI-FT-ICR MS. The desorption and pyrolysis phases were separated manually for each spectrum at the dashed line. (a) Comparison of the TG curves (three replicates averaged) of nonaged (blue) and 7 days aged (orange) model bitumen. Aging shows a shift in the beginning of the desorption phase of about 50 °C up to higher temperatures. Additionally, the nonevaporable residue increases from 10 to 16%. (b) DTG curves clarifying the different starting points of the desorption phase of nonaged and 7 days aged model bitumen. (c) Temperature profile of the total ion count (TIC) of nonaged and 7 days aged model bitumen. The shaded area accounts for the average of three replicates plus/minus the standard deviation.

evaporation of the existing molecules or the reaction of oxygen with bitumen compounds leading to less volatile species.[14] This effect is most severe at high temperatures or when the material is present in thin films, both of which are characteristic of short-term aging during the mixing process of bitumen and aggregates.[2,14]

CH-Class and Oxidized O_x-Classes. The CH-class is the most prevalent chemical class in the model bitumen, as revealed by GC × GC−HRTOFMS data. A total of 80−82% of the classified peak area accounts for hydrocarbons, which can be subdivided into 32−33% *n*- and *iso*-alkanes, 22−24% cycloalkanes, and 25−26% aromatics, respectively. Figure 1 illustrates the compound class distribution for the 7 days aged model bitumen for both measurement techniques. The corresponding diagrams for the nonaged sample are given in Figure S5. The FT-ICR MS data show a noticeably lower proportion of the CH-class, which is accounted for by the applied ionization method APCI. Under atmospheric pressure conditions, nonpolar hydrocarbons, such as alkanes and cycloalkanes, cannot be ionized by the chemical ionization process initiated by a corona discharge. Consequently, approximately 55% of the matrix is disregarded, enabling the focus on heteroatom-containing minorities. Nonetheless, unsaturated CH-species, especially aromatic compounds, are considered by APCI as well. A total of 35−38% of the intact species in the desorption phase account for the CH-class, while 37−40% amount to thermal fragments in the pyrolysis phase.

For FT-ICR MS data, different average parameters, such as the number of assigned sum formulae, summed intensity, intensity weighed *m*/*z*, and DBE, are investigated concerning the complete aging row of six samples. General trends are summarized in Table 1 and exemplarily depicted as bar graphs for the intact species of the desorption phase in Figure 3. The corresponding information on the pyrolysis phase and MS/MS spectra is given in Figure S6. The CH-class of the model bitumen shows no significant changes during aging. Nonetheless, while the intensity and the number of assigned sum formulae stay consistent over the aging time, a slight decrease

Table 1. Effects of Aging on the Model Bitumen: Compilation of Different Parameters Obtained from Average MS and MS/MS Data of the Desorption and Pyrolysis Phases of the FT-ICR MS Data Itemized in Compound Classes[a]

			CH	O1	O2	S1	S1O1	S1O2	S2	S2O1	N1	N1O1	N1S1	N1S2	N2
number of formulae	(des)	MS	-	(↗)	(↗)	-	(↗)	↗	(↘)	-	↘	-	(↘)	-	-
		MS/MS	-	↗	↗	-	-	↗	-	↗	↘	↗	(↘)	-	↘
	(pyr)	MS	-	↗	(↗)	-	↗	-	(↘)	-	(↘)	-	(↘)	-	-
		MS/MS	-	↗	↗	-	↗	↗	-	(↗)	(↘)	↗	(↘)	-	(↘)
summed intensity	(des)	MS	-	↗	-	-	-	↗	-	-	↘	-	(↘)	-	-
		MS/MS	-	↗	↗	-	↗	↗	-	↗	(↘)	(↗)	(↘)	-	-
	(pyr)	MS	-	↗	-	-	↗	-	-	-	-	-	(↘)	-	-
		MS/MS	-	↗	↗	-	↗	↗	-	↗	(↘)	↗	(↘)	-	-
intensity-weighed m/z	(des)	MS	-	(↗)	↗	-	-	-	↘	-	(↘)	-	(↘)	-	-
		MS/MS	-	↗	(↗)	-	(↗)	(↘)	-	-	-	↗	↘	-	(↘)
	(pyr)	MS	(↘)	(↗)	↗	(↘)	-	-	↘	-	(↘)	-	↘	-	-
		MS/MS	-	↗	-	-	(↗)	-	-	-	(↘)	↗	(↘)	(↘)	(↘)
intensity-weighed DBE	(des)	MS	(↘)	(↗)	↗	-	(↗)	↘	↗	-	(↘)	-	(↘)	(↘)	-
		MS/MS	(↘)	-	(↗)	-	↗	↘	-	-	(↘)	↗	(↘)	-	-
	(pyr)	MS	(↘)	(↗)	-	-	(↗)	-	-	-	(↘)	-	(↘)	-	-
		MS/MS	-	(↗)	-	-	-	-	-	-	(↘)	-	-	-	-

↗ significant increasing trend during aging
(↗) non-significant increasing trend during aging
↘ significant decreasing trend during aging
(↘) non-significant decreasing trend during aging

[a]The trends in bold are verified by the Weir *t*-test, while trends in parentheses show consistent, but nonsignificant trends. The abbreviation (des) accounts for the desorption phase, while (pyr) accounts for the pyrolysis phase.

https://dx.doi.org/10.1021/acs.energyfuels.0c01242
Energy Fuels 2020, 34, 10641−10654

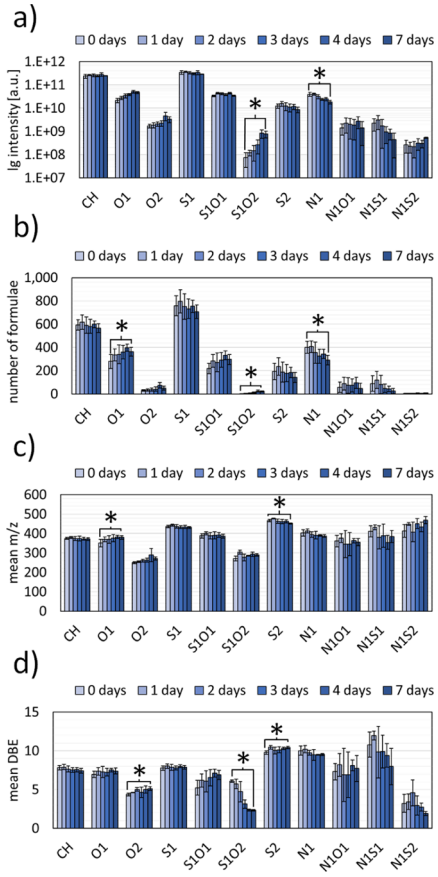

Figure 3. Overview of the considered average parameters exemplarily depicted for the desorption phase in the normal MS-mode for the model bitumen over the aging time. The shown compound classes account for over 99% of the assigned signal intensity. (a) Log(10) summed intensity for easier investigation of the aging trends of low-abundant compound classes, (b) number of calculated formulae, (c) mean intensity-weighed m/z, and (d) mean intensity-weighed DBE. The asterisks mark significant differences with a statistical reliability of 95% between the parameters in the nonaged sample and the 7 days aged model bitumen.

of the intensity-weighed mean DBE between 0.2 and 0.4 units is observed for the desorption phase and for thermal fragments in the pyrolysis phase. When previously divided into compound classes, DBE versus carbon number (#C) plots give an ideal opportunity to investigate the aging process on the molecular level because the chemical space is spanned by aromaticity (DBE) versus alkylation/molecular size (#C), and additionally, data points can be color-coded with signal intensity. Figures 4 and 5 show the DBE versus #C plots of selected compound classes for desorption and pyrolysis phases, respectively. In both figures, the aging extrema (0 days vs 7 days) are compared to underline the aging-related changes. Regions, in which aging effects occurred, are marked to facilitate the discussion. In accordance with the average parameters, the CH-class reveals no changes for the desorption phase in DBE versus #C diagrams as well. Therefore, evaporation effects can be excluded from FT-ICR MS data and molecular alterations can be attributed to chemical aging effects. GC × GC−HRTOFMS data were used for group-type analysis[63,66] of the chemical space. The relative abundance for the dominant 20 functionalities is shown in Figure 6a, which account together for 96% of the classified peak area. Information on nonpolar hydrocarbons as well as on distinct chemical structures is added to the sum formula attribution of FT-ICR MS data. The averaged abundance of alkanes, naphthenes, hopanes, benzenes, fluorenes, and three-ring aromatics show no significant alterations over the aging time. However, slight evaporation effects are observed for small hydrocarbons, especially after 7 days of aging. C13- to C16-*n*-alkanes are prevalently affected. Beyond that, after extensive aging, a slight decrease of the averaged signal intensity is observed for benzonaphthenes, naphthalenes, and biphenyls, which is attributable to the evaporation of low-boiling homologues. A slight decrease of pyrenes was observed for GC × GC−HRTOFMS data as well but could not be confirmed by a decrease of DBE 12 for the CH-class in FT-ICR MS data. Nonetheless, the reduction of condensed aromatic species during aging was observed in previous studies by Handle et al. (2017) with ESI-FT-ICR MS.[53] Generally, for both measurement techniques, desorbable CH-species show extremely low alterations, which are congruent for observations of the saturate fraction in classical SARA fractionation, considered as relatively inert against aging in the literature.[1,14,18,25]

In contrast to intact evaporable species, the pyrolysis phase obtained by TG-FT-ICR MS reveals aging-related changes for high-molecular-weight CH-compounds. As discernable in Figure 5a for the 7 days aged model bitumen, there is an increase for smaller thermal fragments with carbon numbers between 13 and 29 and DBEs of 4−12, corresponding to aromatics with low alkylation. Exemplarily, the species can be tentatively attributed to alkylated benzenes (DBE 4), tetrahydronaphthalenes (DBE 5), naphthalenes (DBE 7), fluorenes (DBE 9), anthracenes/phenanthrenes (DBE 10), or pyrenes/fluoranthenes (DBE 12). The increased detection of these low alkylated aromatics could be explained as follows. The oxidation of hydrocarbons increases their polarity, which subsequently decreases their vapor pressure shifting species from the desorption phase into the pyrolysis phase. Because of the high temperatures during pyrolysis, side chains can be cleaved off. If these chains were oxidized before, the remaining, mostly dealkylated aromatic core is detected as a pure CH-compound in the pyrolysis phase. In the MS/MS-mode in Figure 5b, a significant increase for aromatic cores with 14−31 carbons is observed, where species with DBE 13 (potentially chrysenes) and DBE 16 (potentially benzochrysenes or other aromatic isomers) are most prevalent. An increase in aromaticity and a decrease of the long-chain index are also known from other studies about bitumen aging.[9,24] As alterations are mainly found in the pyrolysis phase, it can be assumed that the thermal treatment of the model bitumen primarily affects the high-molecular-weight CH-species or may lead to their formation.

As expected for oxidative aging, the oxygen-containing classes steadily increase over the aging time. For FT-ICR MS data, the number of assigned sum formulae increases significantly for the O1-class for both measurement modes and the signal intensity grows significantly over the aging time for the desorption and pyrolysis phases. Following the same trend, the intensity-weighed mean m/z shows a significant increase for the O1-class of about 30 Da in both phases and modes and reaches approximately the same value as the CH-class after 7 days of aging, which is about 375 Da for the MS-mode and 325 Da in the MS/MS-mode in both phases. DBE versus #C plots reveal an increase in DBE and alkylation for

https://dx.doi.org/10.1021/acs.energyfuels.0c01242
Energy Fuels 2020, 34, 10641−10654

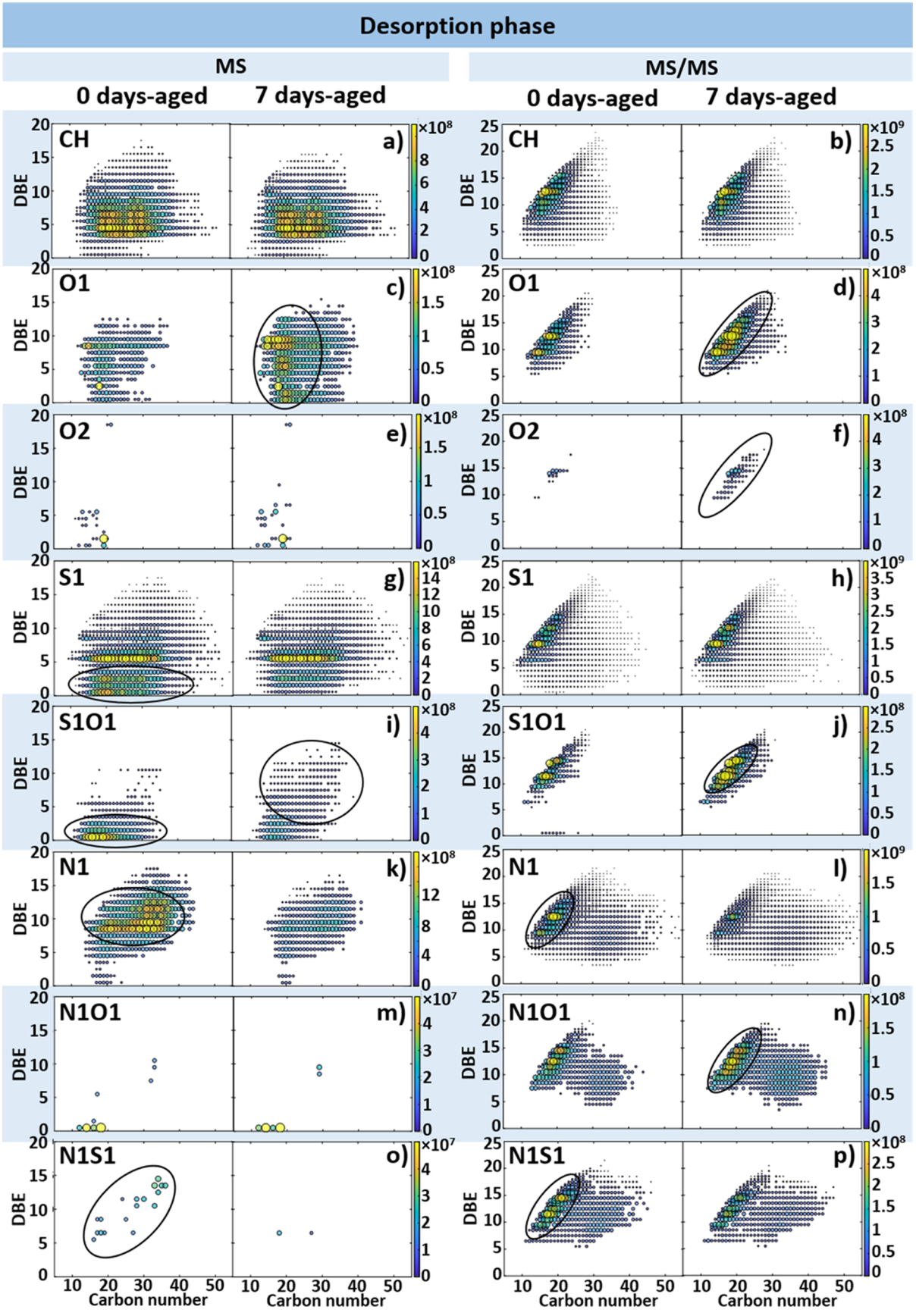

Figure 4. DBE vs the number of carbon atoms (#C) plots of different compound classes obtained from the desorption phase of the TG-FT-ICR MS data in MS- and MS/MS-modes for nonaged and 7 days aged model bitumen. The size and color of the data points correlate with the signal intensity. The shown species were found in all three replicates.

https://dx.doi.org/10.1021/acs.energyfuels.0c01242
Energy Fuels 2020, 34, 10641−10654

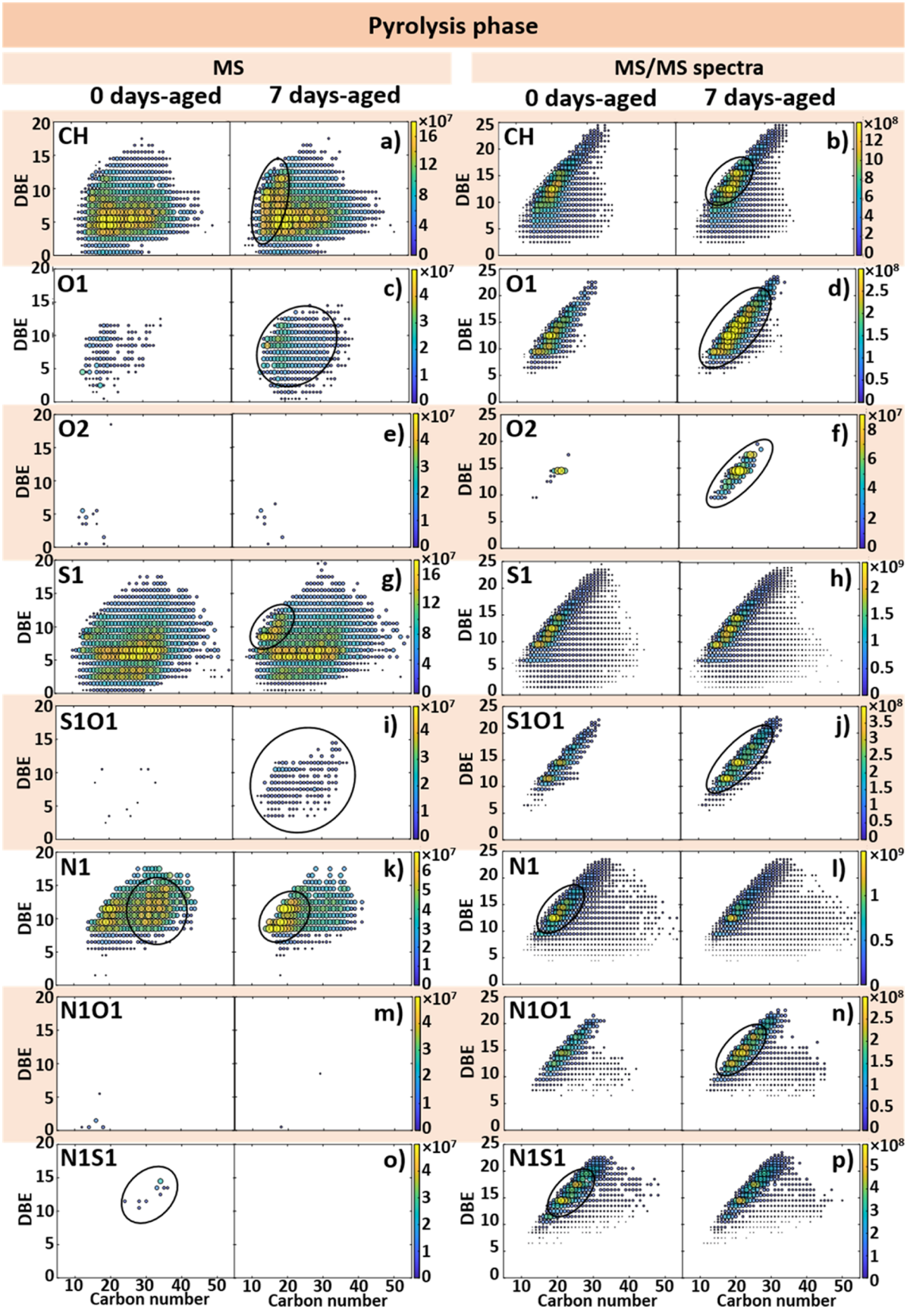

Figure 5. DBE vs the number of carbon atoms (#C) plots of different compound classes obtained from the pyrolysis phase of the TG-FT-ICR MS data in MS- and MS/MS-modes for nonaged and 7 days aged model bitumen. The size and color of the data points correlate with the signal intensity. The shown species were found in all three replicates.

https://dx.doi.org/10.1021/acs.energyfuels.0c01242
Energy Fuels 2020, 34, 10641−10654

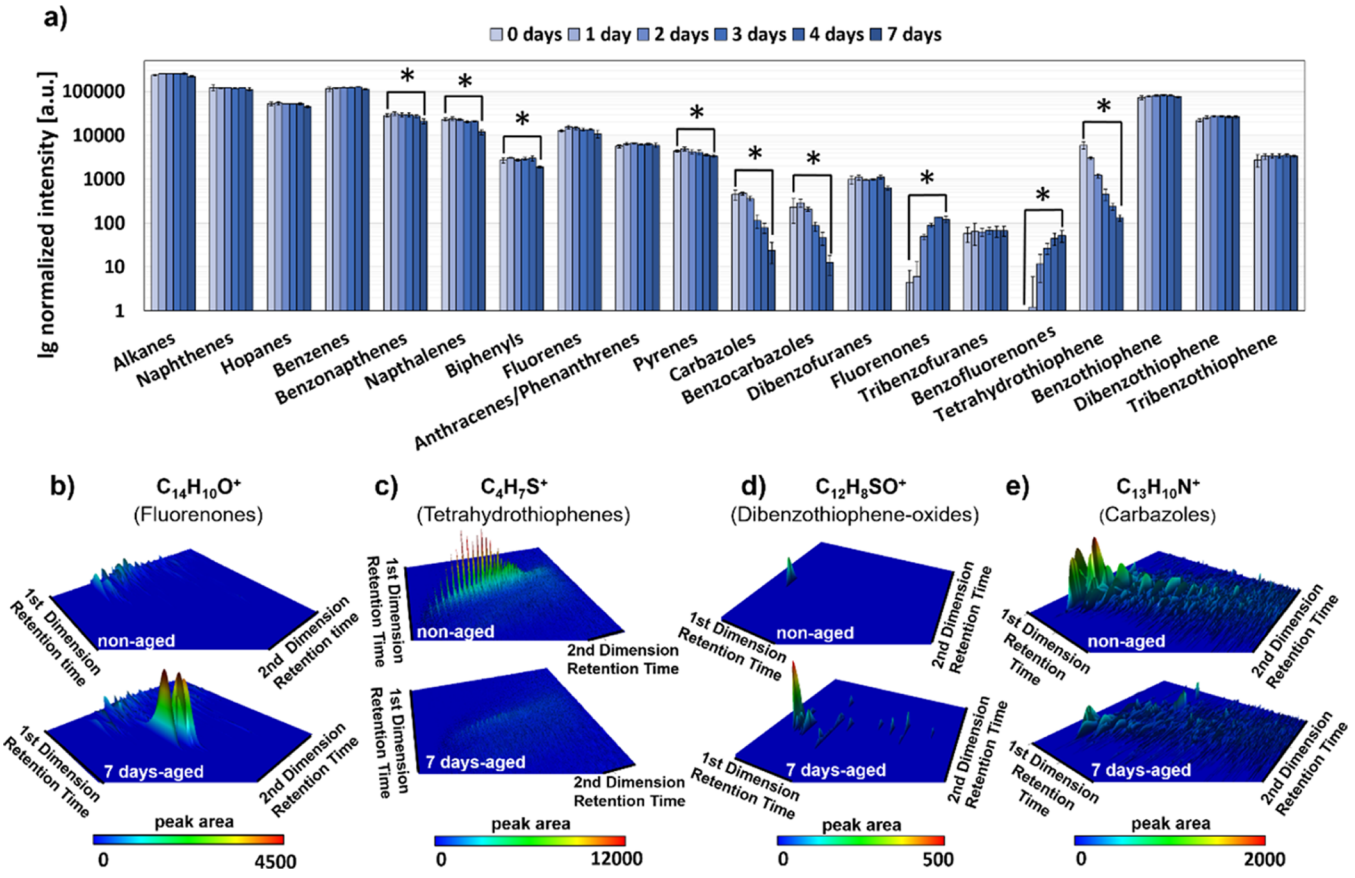

Figure 6. Compilation of GC × GC−HRTOFMS data of different aging effects on selected compound classes investigated in the model bitumen. (a) Investigated compound classes in nonaged to 7 days aged model bitumen after group-type analysis. The 20 depicted compound classes account for 96% of the classified peak area. Significant changes between nonaged and 7 days aged bitumen are marked with an asterisk. The significance with 95% statistic certainty was investigated with the Weir *t*-test. (b) Survey view of the $C_{14}H_{10}O^+$-fragment corresponding to fluorenones. After 7 days of aging, the signal intensity of the fragment is clearly increased. (c) Survey view of the $C_4H_7S^+$-fragment corresponding to tetrahydrothiophenes. Aging clearly reduces the signal intensity of the fragment. (d) Survey view of the $C_{12}H_8SO^+$-fragment corresponding to dibenzothiophene oxides. Aging increases the signal intensity of the fragment, but it remains near the detection level. (e) Survey view of the $C_{13}H_{10}N^+$-fragment corresponding to carbazoles. After 7 days of aging, the signal intensity of the fragment is clearly reduced.

the desorption and pyrolysis phases of the O1-class in both modes. In the desorption phase depicted in Figure 4c, species with 15−21 carbons show a significant increase in aromaticity, with DBE 9 (potentially oxidized biphenyls) and 10 (potentially fluorenones) being most preferred. These structural considerations are in very good accordance with GC × GC−HRTOFMS data, which show the carbonyl formation, especially on aromatics with an activated carbon atom, such as fluorenes. Chromatographic information exhibits a distinct significant increase for fluorenones and benzofluorenones corresponding to a direct oxidation of the ring. Contrarily, furans, as the investigated dibenzofurans and tribenzofurans, show no significant changes, indicating that the formation mechanism of cyclic-bound oxygen seems to be not triggered by short-term aging conditions. For desorbable species in FT-ICR MS data, a preference of oxidation on smaller molecules with a high DBE was observed. For example, species potentially attributed to fluorenones (DBE 10) show a distinct increase, especially for C1−C5 alkylation, with the C3-alkylated being most favored. A corresponding observation was revealed by GC × GC−HRTOFMS data, where C0-, C1-, and C2-alkylated fluorenones occur in an increasing order with C2-fluorenone steadily increasing during the complete aging time (Figure S7). For strongly alkylated species, FT-ICR MS data show evidence for a less favored oxidation, which could be explained by an increased steric hindrance for oxidation at the aromatic core. Long or strongly branched alkyl chains of larger molecules may protect the aromatic core against oxidation. In MS/MS-mode for the desorption phase in Figure 4d, and especially for the pyrolysis phase in Figure 5d, a substantial increase in oxidized core structures of high-molecular compounds is observed. This finding is congruent with previous studies in the literature, which reported an increase in the resin and asphaltene SARA fractions analyzed with different analytic techniques.[1,3,4,25,30,31,33] The core structures of the pyrolysis fragments observed in this study are most likely formed by species typically attributed to the resin or asphaltene fraction. Although the O2-class shows no significant changes for the MS-mode in the FT-ICR MS data, the core structures occurring in the desorption and pyrolysis phases in the MS/MS-mode reveal the same trends in signal intensity and a number of formulae, as exhibited by the O1-class. In addition, DBE versus #C plots show an increase for O2-species with a comparatively high DBE between 10 and 18 for the desorption phase and 12 and 20 for the pyrolysis phase. As a consequence, multiple oxidations seem to take place favorably at high aromatic structures. The fact that various oxidized compounds survive the fragmentation during the CID process leads to the

https://dx.doi.org/10.1021/acs.energyfuels.0c01242
Energy Fuels 2020, 34, 10641−10654

assumption that oxidation takes place at the aromatic core or at a position close to the aromatic ring, forming, most likely, a ketone.[1,13] This hypothesis is supported by Petersen et al. (1998) and Dorrence et al. (1974) who found strong evidence that carbonyls are preferentially formed at the carbon in the benzylic position.[26−28]

S_x-Classes and Oxidized S_xO_y-Classes. For FT-ICR MS data, the S1-class is the compound class with the highest signal intensity and the highest number of assigned sum formulae with a mean m/z of 430 for the MS-mode and 390−400 for the MS/MS-mode, as well as a mean DBE of 7.9−8.6 and 10.3−11.5, respectively. The discrepancy to the GC × GC−HRTOFMS data, where hydrocarbons are prevalently represented, is explicable by the application of APCI highlighting more polar compounds. The average parameters of the S1-class obtained with FT-ICR MS show no significant changes in average parameters over the aging time. Nonetheless, the comparison of the DBE versus #C plots of the desorption phase in Figure 4g reveals that compounds with DBE <4 decrease significantly. These species may involve tetrahydrothiophenes (DBE 1) measured by GC × GC−HRTOFMS, which show a significant decrease, as depicted in Figure 6a,c. In contrast, higher DBE compounds, such as benzothiophenes (DBE 6), dibenzothiophenes (DBE 9), and benzonaphthothiophenes (DBE 12), show no changes during aging in GC × GC−HRTOFMS data. The same observation was made by FT-ICR MS, where the predominant intact species with DBE 6, which can tentatively be attributed to benzothiophenes, and the major core structures with DBE 10, 12, and 13 (potentially benzylbenzothiophenes, benzonaphthothiophenes, and benzonaphthothiophenes with an attached saturated ring)[67−69] hardly reveal any alterations. Regarding the pyrolysis phase in the MS-mode in Figure 5g, a slight decrease in intensity for low-DBE S1-compounds is observed as well. However, for species with DBE 9−12 and carbon numbers between 10 and 20, an increase in signal intensity is revealed. This observation can be explained by the formation of oxidation products at the side chains of the molecules, which are cleaved off during pyrolysis leading to the detection of the nonoxidized thermal fragment. This reaction is discussed in detail for the CH-class above. Besides the S1-class, the S2-class and for MS/MS-spectra, the S3-class was also observed with low abundancies. The classes with more than one sulfur atom have, in general, a higher mean m/z and mean DBE, which are typically observed for petroleum-derived materials.[70,71] Only minor alterations are caused by aging for the classes containing two to three sulfur atoms. A significant decrease of the intensity-weighed mean m/z is observed for the S2-class in the MS-mode, indicating a reduction in alkylation. In general, our results show that nonaromatic sulfur components exhibit a higher reactivity to oxidative aging than aromatic sulfur species. Lobodin et al. (2015) already revealed that crude oil is composed of reactive (sulfides, disulfides, and thiols) and nonreactive (thiophenes and diaryl sulfides) sulfur species.[68] Furthermore, Porto et al. (2019) found evidence that asphalt concretes containing a high amount of nonaromatic sulfur compounds are prevalently affected by short-term aging.[72]

According to previous studies,[1,9,26,28] sulfoxides are one of the main functional groups formed during oxidative aging in bitumen. For FT-ICR MS data, already the average parameters for core structures in the desorption phase and for both modes in the pyrolysis phase reveal a distinct increase of the S1O1-class. At first glance, however, the average intensity as well as the number of assigned sum formulae stay consistent over the aging time for intact species in the desorption phase. Nevertheless, the in-depth investigation at the molecular level in Figure 4i reveals alterations during aging as well. In the nonaged model bitumen, S1O1-species with DBE 1−2 are prevalent, while these species are significantly reduced after 7 days of aging and higher DBE species occur. Figure S8 illustrates the DBE versus #C diagrams opposing for the O1-class and the S1O1-class for the whole aging row. While the O1-class shows a distinct increase in smaller molecules as described above, the S1O1-class shows after 1 day of aging an increase in species with a low DBE of 1−2. With the progress of the aging time, the low-DBE species decrease significantly, whereas higher DBE compounds are formed. By investigation of the DBE versus #C diagram of the S1O2-class of the desorption phase in the MS-mode, we found evidence that the reduction of the low-DBE compounds in S1O1-class correlates with an increase in low-DBE species in the S1O2-class (Figure S9). Because of very low intensity, the S2O1-class was only detected for the complete aging row in the MS/MS-mode but follows the same trend as other oxidized sulfur-containing classes. The core structures showed a significant increase in the average number of sum formulae as well as the average signal intensity. In Figure S10a, the DBE versus #C diagram of the desorption phase reveals a distinct increase in the intensity of S2O1-core structures with DBEs between 12 and 17. For desorbable oxidized sulfur-containing compounds, only a few additional structural information could be obtained with GC × GC−HRTOFMS because of the nominal proportion of this kind of components. Nonetheless, for dibenzothiophene oxides, an increase in the signal intensity was observed over the aging time, as depicted in Figure 6d.

Regarding the pyrolyzed compounds of the FT-ICR MS data in Figure 5i, only very few S1O1-species could be found in the nonaged model bitumen, but the number and signal intensity increased significantly after 7 days of aging. The MS/MS-mode reveals an increase in signal intensity for high aromatic core structures of intact S1O1-species and their pyrolysis fragments. In the desorption phase, prevalently, compounds with a DBE of 10−15 increase, while in the pyrolysis phase, species with DBE 12, DBE 15, and DBE 18 are mostly favored. The latter can be tentatively attributed to oxidized benzonaphthothiophenes and further attached fused aromatic rings. Besides the S1O1-class, the S2O1-class shows a significant increase for the average intensity in the MS/MS-mode as well. At the molecular level, the signal intensity increases predominantly for species between DBE 12 and 20 in the pyrolysis phase, as depicted in Figure S10b.

N_x-Class, NS-Class, and Oxidized NO-Classes. Although oxides and sulfoxides are often investigated with respect to bitumen aging in the literature, nitrogen-containing species are rarely considered. To the best of the authors' knowledge, only Handle et al. (2017) have reported an increase of oxidized NO_{1-9}-compounds in long-term-aged bitumen investigated by direct infusion ESI-FT-ICR MS.[33] Compatible with these results, a substantial loss of volatile N1-compounds was observed for the model bitumen in this study. The average parameters revealed by FT-ICR MS measurements exhibited a significant reduction in the number of molecular formulae and signal intensity of the N1-class during the desorption phase. Because of the very low abundance, the N2-class could only be detected in the MS/MS-mode but shows the same significant decrease as the N1-class. Regarding the DBE versus #C plots in

https://dx.doi.org/10.1021/acs.energyfuels.0c01242
Energy Fuels 2020, 34, 10641−10654

Figure 4k, nonaged bitumen shows a comparable high intensity for the intact N1-species with a DBE of 9−13, which can tentatively be attributed to benzoindoles or carbazoles (DBE 9), acridines (DBE 10), tetrahydroacridines or benzylacridines (DBE 11), indenoquinolines or benzocarbazoles (DBE 12), and benzacridines (DBE 13).[69,73,74] After 7 days of aging, the previously mentioned molecular structures are severely reduced. A similar observation was made for the MS/MS-mode of the desorption phase in Figure 4l, where a strong reduction of the dominant DBE lines of 10 and 13, potentially attributed to acridines and benzacridines, is observed. In addition, GC × GC−HRTOFMS measurements reveal a strong and distinct decrease in intact carbazolic and benzocarbazolic structures as well, partially validating the proposed structures from FT-ICR MS. The decrease for the $C_{13}H_{10}N_1^+$, which is a typical EI fragment ion of carbazoles, is highlighted in Figure 6e. However, no evidence for acridinic structures was found in the GC × GC−HRTOFMS data. Concerning the pyrolysis phase in Figure 5k,l, high-molecular thermal fragments, such as species with a DBE between 9 and 15 and carbon numbers between 26 and 38, show a distinct decrease after 7 days of aging. The same trend is observed for aromatic core structures in the MS/MS-mode as well, where compounds with a DBE of 13 (possibly benzacridines) to a DBE of 15 (possibly phenanthrocarbazoles) are prevalently reduced. However, different from the predominantly observed decrease of the N1-class, small molecular pyrolysis fragments, especially with DBE 9 (possibly carbazoles), DBE 10 (possibly acridines), and DBE 12 (possibly benzocarbazoles), are increased during aging in the MS-mode. A possibility for the observed increase is discussed in the following. The most apparent hypothesis explaining the general decrease of the N1-class is strong oxidation of the N1-containing compounds. However, the DBE versus #C plots for the MS-mode show no increase of the intact species or pyrolysis fragments of the N1O1-class. Furthermore, with GC × GC−HRTOFMS, no oxidized nitrogen-containing compounds could be detected. The absence of newly formed N1O1-compounds in the MS-mode and chromatographic measurements can be explained by the poor signal intensity of the oxidized products remaining below the detection limit. Another explanation is the decrease of the N1-class due to intermolecular reactions triggered by the high aging temperatures of about 150−160 °C. High reaction temperatures can lead, for example, to the condensation of indole derivatives on acridine-like structures obtained in high yields in the literature.[75] The condensates have a higher molecular weight and, therefore, a higher vapor pressure, converting previously evaporable species into compounds occurring in the pyrolysis phase. Evidence for this hypothesis can be abstracted from the 7 days aged N1-class in Figure 5k. In the MS-mode, smaller pyrolysis fragments with carbon numbers of 15−25 reveal an increase in signal intensity, indicating the cracking of newly formed N-containing condensates. Besides the N1-class, N2-class core structures reveal a similar decrease in signal intensity for the desorption and pyrolysis phases, which is shown in Figure S10a,b. Because of the low concentration of these species, the N2-class is hardly detectable after 7 days of aging.

Although the MS-mode reveals no increase in oxidized nitrogen-containing components, preferred oxidation of high aromatic core structures is indicated by MS/MS spectra because of a distinct increase in the number of assigned sum formulae, signal intensity, mean m/z, and mean DBE for the N1O1-class. With respect to Figures 4n and 5n, core structures with a DBE of 10−16 reveal a clear increase in intensity for N1O1-compounds in the desorption phase, while the oxidation is also pronounced for species with a DBE of up to 20 in the pyrolysis phase.

In addition to pure N-containing classes, the N1S1-class shows a slight decrease in the average signal intensity, number of sum formulae, mean m/z, and DBE as well. Equal to other classes containing more than one heteroatom, the N1S1-species show a comparably high mean DBE and are mostly detected in the MS/MS spectra as high aromatic core structures, which is explicable by the Boduszynski model. The model predicts the occurrence of N- and S-atoms in one molecule only for bigger aromatic structures in crude oil-derived materials and was proven by several FT-ICR MS studies.[52−54] With respect to the studied aging effects in the desorption phase in Figure 4p, the N1S1-class mainly shows a reduction of the DBE lines of 12, 13, and 15 of the core structures, which can tentatively be attributed to benzothienoquinolines, benzylthienoquinolines, and dibenzothienoquinolines, respectively.[69] In the pyrolysis phase, species with DBEs of 12, 15, and 18 are primarily reduced. The few species detected in the MS-mode disappeared nearly completely after 7 days of aging.

CONCLUSIONS

The combination of TG-APCI-FT-ICR MS and GC × GC−HRTOFMS revealed complementary and consistent results on different chemical changes occurring during prolonged short-term aging in a specially generated model bitumen. Polar to semipolar as well as semivolatile to pyrolyzable species were highlighted at the molecular level by TG-APCI-FT-ICR MS. The supporting GC × GC−HRTOFMS enabled the validation of FT-ICR MS data for semivolatile compounds and contributed insights about aging processes on selected molecular structures and distinct functionalities. The main changes attributed to aging can be summarized as follows:

- The CH-class is relatively inert against aging; nonetheless, pyrolysis fragments and their corresponding core structures show a shift to smaller carbon numbers with less alkylation.
- The O1-class, especially fluorenones, show a significant increase in the signal intensity. Smaller molecules of the O1-class are preferably oxidized, while the O2-class occurs primarily for high-molecular-weight structures.
- The S1-class significantly decreases for nonaromatic species (especially tetrahydrothiophenes), while aromatic sulfur components, such as thiophenic structures, reveal no changes. Pyrolysis fragments increase for species with lower carbon numbers with a comparatively high DBE, which might be attributed to dealkylation during aging. For the S1O1-class, low-DBE compounds probably decrease because of further oxidation, while high-DBE species are formed.
- One of the strongest observed effects was the depletion of nitrogen-containing structures, especially for carbazolic structures. An increase in intact oxidized N-species that evolve in the desorption phase could not be detected. Nonetheless, an increasing number of small N-species with a comparatively high DBE are formed during aging in the pyrolysis phase, potentially caused by thermally induced condensation reactions due to high

https://dx.doi.org/10.1021/acs.energyfuels.0c01242
Energy Fuels 2020, 34, 10641−10654

aging temperatures. For core structures, an increase in the amount of N1O1-species was observed.

To conclude, the macroscopic changes observed in the physical properties of bitumen may be derived from the formation of polar components such as O-, SO-, and NO-containing species, which are primarily observed for high aromatic compounds as well as the reduction of species with low aromaticity and N-containing species in general. Furthermore, the combination of both techniques can be beneficial for the analysis of a variety of analytically challenging complex mixtures, which essentially need a multimethod approach for a detailed chemical description.

The deep understanding of bitumen aging will help to improve the quality of bitumen binders and could increase the durability of the pavement. Future studies on bitumen aging will focus on how different laboratory aging methods, as well as more realistic aging,[76] further treatment, or the addition of additives affect the chemical composition of the aged material.

■ ASSOCIATED CONTENT

Supporting Information

The Supporting Information is available free of charge at https://pubs.acs.org/doi/10.1021/acs.energyfuels.0c01242.

Measurement parameters of FT-ICR MS and GC × GC−HRTOFMS; data quality proof for FT-ICR MS measurements; time-resolved FT-ICR MS spectra for nonaged and 7 days aged model bitumen; GC × GC−HRTOFMS chromatograms for nonaged and 7 days aged model bitumen as well as details showing evaporation for low-boiling components after severe aging; compound class distribution for nonaged model bitumen for both techniques; average parameters obtained by FT-ICR MS measurements for both modes and phases as well as for all examined classes; aging effect of fluorenones with different alkylation degrees, as revealed by GC × GC−HRTOFMS; and DBE versus #C diagrams of FT-ICR MS data for O1-, S1O1-, S1O2-, S2O1-, and N2-classes (PDF)

■ AUTHOR INFORMATION

Corresponding Author

Christopher P. Rüger − *Joint Mass Spectrometry Centre, Chair of Analytical Chemistry, University of Rostock, 18059 Rostock, Germany;* orcid.org/0000-0001-9634-9239; Email: christopher.rueger@uni-rostock.de

Authors

Anika Neumann − *Joint Mass Spectrometry Centre, Chair of Analytical Chemistry, University of Rostock, 18059 Rostock, Germany;* orcid.org/0000-0001-7256-3716

Uwe Käfer − *Joint Mass Spectrometry Centre, Comprehensive Molecular Analytics, Helmholtz Center Munich German Research Center for Environmental Health, 85764 Neuherberg, Germany;* orcid.org/0000-0002-4016-0661

Thomas Gröger − *Joint Mass Spectrometry Centre, Comprehensive Molecular Analytics, Helmholtz Center Munich German Research Center for Environmental Health, 85764 Neuherberg, Germany*

Thomas Wilharm − *ASG Analytik-Service Gesellschaft mbH, 86356 Neusäss, Germany*

Ralf Zimmermann − *Joint Mass Spectrometry Centre, Chair of Analytical Chemistry, University of Rostock, 18059 Rostock, Germany; Joint Mass Spectrometry Centre, Comprehensive Molecular Analytics, Helmholtz Center Munich German Research Center for Environmental Health, 85764 Neuherberg, Germany;* orcid.org/0000-0002-6280-3218

Complete contact information is available at: https://pubs.acs.org/10.1021/acs.energyfuels.0c01242

Notes

The authors declare no competing financial interest.

■ ACKNOWLEDGMENTS

Funding by the Horizon 2020 program for the EU FT-ICR MS project (European Network of Fourier-Transform Ion-Cyclotron-Resonance Mass Spectrometry Centers, grant agreement ID: 731077) is gratefully acknowledged. The authors thank the German Research Foundation (DFG) for funding the Bruker FT-ICR MS (INST 264/56). Financial support by ZIM (Zentrales Innovationsprogramm Mittelstand, Germany, grant ID: ZF4198001SL6) is gratefully acknowledged.

■ REFERENCES

(1) Petersen, J. C. *A Review of the Fundamentals of Asphalt Oxidation: Chemical, Physicochemical, Physical Property, and Durability Relationships*; Transportation Research Board: Washington, D.C., 2009.

(2) Lesueur, D. The colloidal structure of bitumen: consequences on the rheology and on the mechanisms of bitumen modification. *Adv. Colloid Interface Sci.* **2009**, *145*, 42−82.

(3) Rebelo, L. M.; de Sousa, J. S.; Abreu, A. S.; Baroni, M. P. M. A.; Alencar, A. E. V.; Soares, S. A.; Mendes Filho, J.; Soares, J. B. Aging of asphaltic binders investigated with atomic force microscopy. *Fuel* **2014**, *117*, 15−25.

(4) Chipps, J. F.; Davison, R. R.; Glover, C. J. A Model for Oxidative Aging of Rubber-Modified Asphalts and Implications to Performance Analysis. *Energy Fuels* **2001**, *15*, 637−647.

(5) Themeli, A.; Chailleux, E.; Farcas, F.; Chazallon, C.; Migault, B.; Buisson, N. Molecular structure evolution of asphaltite-modified bitumens during ageing; Comparisons with equivalent petroleum bitumens. *Int. J. Pavement Res. Technol.* **2017**, *10*, 75−83.

(6) Branthaver, J. F.; Petersen, J. C.; Robertson, R. E.; Duvall, J. J.; Kim, S. S.; Harnsberger, P. M.; Mill, T.; Ensly, E. K.; Barbour, F. A.; Scharbron, J. F. *Binder Characterization and Evaluation: Volume 2: Chemistry*; Strategic Highway Research Program. National Research Council, National Academy of Sciences, 1993.

(7) Hofko, B.; Hospodka, M. Rolling Thin Film Oven Test and Pressure Aging Vessel Conditioning Parameters: Effect on Viscoelastic Behavior and Binder Performance Grade. *Transp. Res. Rec.* **2016**, *2574*, 111−116.

(8) Hofko, B.; Cannone Falchetto, A.; Grenfell, J.; Huber, L.; Lu, X.; Porot, L.; Poulikakos, L. D.; You, Z. Effect of short-term ageing temperature on bitumen properties. *Road Mater. Pavement Des.* **2017**, *18*, 108−117.

(9) Tarsi, G.; Varveri, A.; Lantieri, C.; Scarpas, A.; Sangiorgi, C. Effects of Different Aging Methods on Chemical and Rheological Properties of Bitumen. *J. Mater. Civ. Eng.* **2018**, *30*, 04018009.

(10) Bonaquist, R.; Anderson, D. A. *Investigation of Short-Term Laboratory Aging of Neat and Modified Asphalt Binders*; National Academies Press: Washington, D.C., 2011.

(11) Bahia, H. U.; Anderson, D. A. The Pressure Aging Vessel (PAV): A Test to Simulate Rheological Changes Due to Field Aging. In *Physical Properties of Asphalt Cement Binders*; Hardin, J. C., Ed.; STP/ASTM 1241; ASTM International: Philadelphia, PA, 1995; 67-67-22.

(12) Elwardany, M. D.; Yousefi Rad, F.; Castorena, C.; Kim, Y. R. Evaluation of asphalt mixture laboratory long-term ageing methods for performance testing and prediction. *Road Mater. Pavement Des.* **2017**, *18*, 28−61.

(13) Petersen, J. C. *Binder Characterization and Evaluation*; Strategic Highway Research Program; National Research Council: Washington, D.C., 1994.
(14) Lerfald, B. O. Ageing and Degradation of Asphalt Pavements on Low Volume Roads. Ph.D. Thesis, Department of Road and Railway Engineering, The Norwegian University of Science and Technology NTNU, 2000.
(15) Noureldin, A. S. Oxidation of Asphalt Binders and its Effect on Molecular Size Distribution and Consistency. In *Physical Properties of Asphalt Cement Binders*; Hardin, J. C., Ed.; STP/ASTM 1241; ASTM International: Philadelphia, PA, 1995; 137-137-17.
(16) Ehinola, O. A.; Falode, O. A.; Jonathan, G. Softening point and Penetration Index of bitumen from parts of Southwestern Nigeria. *Nafta* **2012**, *63*, 319−323.
(17) Grilli, A.; Gnisci, M. I.; Bocci, M. Effect of ageing process on bitumen and rejuvenated bitumen. *Constr. Build. Mater.* **2017**, *136*, 474−481.
(18) Eberhardsteiner, L.; Füssl, J.; Hofko, B.; Handle, F.; Hospodka, M.; Blab, R.; Grothe, H. Towards a microstructural model of bitumen ageing behaviour. *Int. J. Pavement Eng.* **2015**, *16*, 939−949.
(19) Eberhardsteiner, L.; Füssl, J.; Hofko, B.; Handle, F.; Hospodka, M.; Blab, R.; Grothe, H. Influence of asphaltene content on mechanical bitumen behavior: experimental investigation and micromechanical modeling. *Mater. Struct.* **2015**, *48*, 3099−3112.
(20) Hofko, B.; Eberhardsteiner, L.; Füssl, J.; Grothe, H.; Handle, F.; Hospodka, M.; Grossegger, D.; Nahar, S. N.; Schmets, A. J. M.; Scarpas, A. Impact of maltene and asphaltene fraction on mechanical behavior and microstructure of bitumen. *Mater. Struct.* **2016**, *49*, 829−841.
(21) Baek, C.; Underwood, B. S.; Kim, Y. R. Effects of Oxidative Aging on Asphalt Mixture Properties. *Transp. Res. Rec.* **2012**, *2296*, 77−85.
(22) ASTM D2007-19. *Test Method for Characteristic Groups in Rubber Extender and Processing Oils and Other Petroleum-Derived Oils by the Clay-Gel Absorption Chromatographic Method*; ASTM International: West Conshohocken, PA, 2019.
(23) Mikhailenko, P.; Bertron, A.; Ringot, E. Methods for Analyzing the Chemical Mechanisms of Bitumen Aging and Rejuvenation with FTIR Spectrometry. *International Symposium on Testing and Characterization of Sustainable and Innovative Bituminous Materials*, 2016, Vol. *11*, pp 203−214.
(24) Nivitha, M. R.; Prasad, E.; Krishnan, J. M. Ageing in modified bitumen using FTIR spectroscopy. *Int. J. Pavement Eng.* **2016**, *17*, 565−577.
(25) Le Guern, M.; Chailleux, E.; Farcas, F.; Dreessen, S.; Mabille, I. Physico-chemical analysis of five hard bitumens: Identification of chemical species and molecular organization before and after artificial aging. *Fuel* **2010**, *89*, 3330−3339.
(26) Petersen, J. C.; Glaser, R. Asphalt Oxidation Mechanisms and the Role of Oxidation Products on Age Hardening Revisited. *Road Mater. Pavement Des.* **2011**, *12*, 795−819.
(27) Dorrence, S. M.; Barbour, F. A.; Petersen, J. C. Direct evidence of ketones in oxidized asphalts. *Anal. Chem.* **1974**, *46*, 2242−2244.
(28) Petersen, J. C. A dual, sequential mechanism for the oxidation of petroleum asphalts. *Pet. Sci. Technol.* **1998**, *16*, 1023−1059.
(29) Corbett, L. W. Composition of asphalt based on generic fractionation, using solvent deasphaltening, elution-adsorption chromatography, and densimetric characterization. *Anal. Chem.* **1969**, *41*, 576−579.
(30) Allen, R. G.; Little, D. N.; Bhasin, A. Structural Characterization of Micromechanical Properties in Asphalt Using Atomic Force Microscopy. *J. Mater. Civ. Eng.* **2012**, *24*, 1317−1327.
(31) Gamarra, A.; Ossa, E. A. Thermo-oxidative aging of bitumen. *Int. J. Pavement Eng.* **2016**, *19*, 641−650.
(32) Weigel, S.; Stephan, D. Modelling of rheological and ageing properties of bitumen based on its chemical structure. *Mater. Struct.* **2017**, *50*, 83.
(33) Handle, F.; Harir, M.; Füssl, J.; Koyun, A. N.; Grossegger, D.; Hertkorn, N.; Eberhardsteiner, L.; Hofko, B.; Hospodka, M.; Blab, R.; et al. Tracking Aging of Bitumen and Its Saturate, Aromatic, Resin, and Asphaltene Fractions Using High-Field Fourier Transform Ion Cyclotron Resonance Mass Spectrometry. *Energy Fuels* **2017**, *31*, 4771−4779.
(34) Le Maître, J.; Hubert-Roux, M.; Paupy, B.; Marceau, S.; Rüger, C. P.; Afonso, C.; Giusti, P. Structural analysis of heavy oil fractions after hydrodenitrogenation by high-resolution tandem mass spectrometry and ion mobility spectrometry. *Faraday Discuss.* **2019**, *218*, 417−430.
(35) Smith, D. F.; Rodgers, R. P.; Rahimi, P.; Teclemariam, A.; Marshall, A. G. Effect of Thermal Treatment on Acidic Organic Species from Athabasca Bitumen Heavy Vacuum Gas Oil, Analyzed by Negative-Ion Electrospray Fourier Transform Ion Cyclotron Resonance (FT-ICR) Mass Spectrometry. *Energy Fuels* **2009**, *23*, 314−319.
(36) McKenna, A. M.; Marshall, A. G.; Rodgers, R. P. Heavy Petroleum Composition. 4. Asphaltene Compositional Space. *Energy Fuels* **2013**, *27*, 1257−1267.
(37) Podgorski, D. C.; Corilo, Y. E.; Nyadong, L.; Lobodin, V. V.; Bythell, B. J.; Robbins, W. K.; McKenna, A. M.; Marshall, A. G.; Rodgers, R. P. Heavy Petroleum Composition. 5. Compositional and Structural Continuum of Petroleum Revealed. *Energy Fuels* **2013**, *27*, 1268−1276.
(38) Rodgers, R. P.; McKenna, A. M. Petroleum analysis. *Anal. Chem.* **2011**, *83*, 4665−4687.
(39) Hourani, N.; Andersson, J. T.; Möller, I.; Amad, M.; Witt, M.; Sarathy, S. M. Atmospheric pressure chemical ionization Fourier transform ion cyclotron resonance mass spectrometry for complex thiophenic mixture analysis. *Rapid Commun. Mass Spectrom.* **2013**, *27*, 2432−2438.
(40) Rüger, C. P.; Grimmer, C.; Sklorz, M.; Neumann, A.; Streibel, T.; Zimmermann, R. Combination of Different Thermal Analysis Methods Coupled to Mass Spectrometry for the Analysis of Asphaltenes and Their Parent Crude Oils: Comprehensive Characterization of the Molecular Pyrolysis Pattern. *Energy Fuels* **2018**, *32*, 2699−2711.
(41) Rüger, C. P.; Neumann, A.; Sklorz, M.; Schwemer, T.; Zimmermann, R. Thermal Analysis Coupled to Ultrahigh Resolution Mass Spectrometry with Collision Induced Dissociation for Complex Petroleum Samples: Heavy Oil Composition and Asphaltene Precipitation Effects. *Energy Fuels* **2017**, *31*, 13144−13158.
(42) Jennerwein, M. K.; Sutherland, A. C.; Eschner, M.; Gröger, T.; Wilharm, T.; Zimmermann, R. Quantitative analysis of modern fuels derived from middle distillates—The impact of diverse compositions on standard methods evaluated by an offline hyphenation of HPLC-refractive index detection with GC×GC-TOFMS. *Fuel* **2017**, *187*, 16−25.
(43) Jennerwein, M. K.; Eschner, M. S.; Wilharm, T.; Zimmermann, R.; Gröger, T. M. Proof of Concept of High-Temperature Comprehensive Two-Dimensional Gas Chromatography Time-of-Flight Mass Spectrometry for Two-Dimensional Simulated Distillation of Crude Oils. *Energy Fuels* **2017**, *31*, 11651−11659.
(44) Dutriez, T.; Courtiade, M.; Thiébaut, D.; Dulot, H.; Hennion, M.-C. Improved hydrocarbons analysis of heavy petroleum fractions by high temperature comprehensive two-dimensional gas chromatography. *Fuel* **2010**, *89*, 2338−2345.
(45) Pollo, B. J.; Alexandrino, G. L.; Augusto, F.; Hantao, L. W. The impact of comprehensive two-dimensional gas chromatography on oil & gas analysis: Recent advances and applications in petroleum industry. *Trends Anal. Chem.* **2018**, *105*, 202−217.
(46) Vanini, G.; Pereira, V. B.; Romão, W.; Gomes, A. O.; Oliveira, L. M. S. L.; Dias, J. C. M.; Azevedo, D. A. Analytical advanced techniques in the molecular-level characterization of Brazilian crude oils. *Microchem. J.* **2018**, *137*, 111−118.
(47) Ávila, B. M. F.; Vaz, B. G.; Pereira, R.; Gomes, A. O.; Pereira, R. C. L.; Corilo, Y. E.; Simas, R. C.; Nascimento, H. D. L.; Eberlin, M. N.; Azevedo, D. A. Comprehensive Chemical Composition of Gas Oil Cuts Using Two-Dimensional Gas Chromatography with Time-of-Flight Mass Spectrometry and Electrospray Ionization Coupled to

https://dx.doi.org/10.1021/acs.energyfuels.0c01242
Energy Fuels 2020, 34, 10641−10654

Fourier Transform Ion Cyclotron Resonance Mass Spectrometry. *Energy Fuels* **2012**, *26*, 5069−5079.
(48) Tessarolo, N. S.; Silva, R. C.; Vanini, G.; Pinho, A.; Romão, W.; de Castro, E. V. R.; Azevedo, D. A. Assessing the chemical composition of bio-oils using FT-ICR mass spectrometry and comprehensive two-dimensional gas chromatography with time-of-flight mass spectrometry. *Microchem. J.* **2014**, *117*, 68−76.
(49) Tessarolo, N. S.; Silva, R. V. S.; Vanini, G.; Casilli, A.; Ximenes, V. L.; Mendes, F. L.; de Rezende Pinho, A.; Romão, W.; de Castro, E. V. R.; Kaiser, C. R.; et al. Characterization of thermal and catalytic pyrolysis bio-oils by high-resolution techniques: 1 H NMR, GC × GC-TOFMS and FT-ICR MS. *J. Anal. Appl. Pyrolysis* **2016**, *117*, 257−267.
(50) Huba, A. K.; Huba, K.; Gardinali, P. R. Understanding the atmospheric pressure ionization of petroleum components: The effects of size, structure, and presence of heteroatoms. *Sci. Total Environ.* **2016**, *568*, 1018−1025.
(51) Gaspar, A.; Zellermann, E.; Lababidi, S.; Reece, J.; Schrader, W. Impact of different ionization methods on the molecular assignments of asphaltenes by FT-ICR mass spectrometry. *Anal. Chem.* **2012**, *84*, 5257−5267.
(52) Chacón-Patiño, M. L.; Rowland, S. M.; Rodgers, R. P. The Compositional and Structural Continuum of Petroleum from Light Distillates to Asphaltenes: The Boduszynski Continuum Theory As Revealedby FT-ICR Mass Spectrometry. In *The Boduszynski Continuum: Contributions to the Understanding of the Molecular Composition of Petroleum*; Ovalles, C., Moir, M. E., Eds.; ACS Symposium Series 1282; American Chemical Society: Washington DC, 2018; pp 113−171.
(53) McKenna, A. M.; Blakney, G. T.; Xian, F.; Glaser, P. B.; Rodgers, R. P.; Marshall, A. G. Heavy Petroleum Composition. 2. Progression of the Boduszynski Model to the Limit of Distillation by Ultrahigh-Resolution FT-ICR Mass Spectrometry. *Energy Fuels* **2010**, *24*, 2939−2946.
(54) McKenna, A. M.; Purcell, J. M.; Rodgers, R. P.; Marshall, A. G. Heavy Petroleum Composition. 1. Exhaustive Compositional Analysis of Athabasca Bitumen HVGO Distillates by Fourier Transform Ion Cyclotron Resonance Mass Spectrometry: A Definitive Test of the Boduszynski Model. *Energy Fuels* **2010**, *24*, 2929−2938.
(55) *The Boduszynski Continuum: Contributions to the Understanding of the Molecular Composition of Petroleum*; Ovalles, C.; Moir, M. E., Eds.; ACS Symposium Series 1282; American Chemical Society: Washington DC, 2018.
(56) Boduszynski, M. M.; Altgelt, K. H. Composition of heavy petroleums. 4. Significance of the extended atmospheric equivalent boiling point (AEBP) scale. *Energy Fuels* **1992**, *6*, 72−76.
(57) ASTM D2892-18. *Test Method for Distillation of Crude Petroleum (15-Theoretical Plate Column)*; ASTM International: West Conshohocken, PA, 2018.
(58) Rüger, C. P.; Miersch, T.; Schwemer, T.; Sklorz, M.; Zimmermann, R. Hyphenation of Thermal Analysis to Ultrahigh-Resolution Mass Spectrometry (Fourier Transform Ion Cyclotron Resonance Mass Spectrometry) Using Atmospheric Pressure Chemical Ionization For Studying Composition and Thermal Degradation of Complex Materials. *Anal. Chem.* **2015**, *87*, 6493−6499.
(59) Zhang, L.; Zhang, Y.; Zhao, S.; Xu, C.; Chung, K. H.; Shi, Q. Characterization of heavy petroleum fraction by positive-ion electrospray ionization FT-ICR mass spectrometry and collision induced dissociation: Bond dissociation behavior and aromatic ring architecture of basic nitrogen compounds. *Sci. China: Chem.* **2013**, *56*, 874−882.
(60) Qian, K.; Edwards, K. E.; Mennito, A. S.; Freund, H.; Saeger, R. B.; Hickey, K. J.; Francisco, M. A.; Yung, C.; Chawla, B.; Wu, C.; et al. Determination of structural building blocks in heavy petroleum systems by collision-induced dissociation Fourier transform ion cyclotron resonance mass spectrometry. *Anal. Chem.* **2012**, *84*, 4544−4551.
(61) Mikhailenko, P.; Webber, G.; Baaj, H. Evaluation of solvents for asphalt extraction. *Road Mater. Pavement Des.* **2019**, 1−12.
(62) Käfer, U.; Gröger, T.; Rohbogner, C. J.; Struckmeier, D.; Saraji-Bozorgzad, M. R.; Wilharm, T.; Zimmermann, R. Detailed Chemical Characterization of Bunker Fuels by High-Resolution Time-of-Flight Mass Spectrometry Hyphenated to GC × GC and Thermal Analysis. *Energy Fuels* **2019**, *33*, 10745−10755.
(63) Jennerwein, M. K.; Eschner, M.; Gröger, T.; Wilharm, T.; Zimmermann, R. Complete Group-Type Quantification of Petroleum Middle Distillates Based on Comprehensive Two-Dimensional Gas Chromatography Time-of-Flight Mass Spectrometry (GC×GC-TOFMS) and Visual Basic Scripting. *Energy Fuels* **2014**, *28*, 5670−5681.
(64) Weir, J. B. D. V. Significance of the Difference between Two Means when the Population Variances may be Unequal. *Nature* **1960**, *187*, 438.
(65) Marshall, A. G.; Rodgers, R. P. Petroleomics: chemistry of the underworld. *Proc. Natl. Acad. Sci. U.S.A.* **2008**, *105*, 18090−18095.
(66) Weggler, B. A.; Gröger, T.; Zimmermann, R. Advanced scripting for the automated profiling of two-dimensional gas chromatography-time-of-flight mass spectrometry data from combustion aerosol. *J. Chromatogr. A* **2014**, *1364*, 241−248.
(67) Müller, H.; Andersson, J. T.; Schrader, W. Characterization of high-molecular-weight sulfur-containing aromatics in vacuum residues using Fourier transform ion cyclotron resonance mass spectrometry. *Anal. Chem.* **2005**, *77*, 2536−2543.
(68) Lobodin, V. V.; Robbins, W. K.; Lu, J.; Rodgers, R. P. Separation and Characterization of Reactive and Non-Reactive Sulfur in Petroleum and Its Fractions. *Energy Fuels* **2015**, *29*, 6177−6186.
(69) Hughey, C. A.; Rodgers, R. P.; Marshall, A. G.; Walters, C. C.; Qian, K.; Mankiewicz, P. Acidic and neutral polar NSO compounds in Smackover oils of different thermal maturity revealed by electrospray high field Fourier transform ion cyclotron resonance mass spectrometry. *Org. Geochem.* **2004**, *35*, 863−880.
(70) Jarrell, T. M.; Jin, C.; Riedeman, J. S.; Owen, B. C.; Tan, X.; Scherer, A.; Tykwinski, R. R.; Gray, M. R.; Slater, P.; Kenttämaa, H. I. Elucidation of structural information achievable for asphaltenes via collision-activated dissociation of their molecular ions in MSn experiments: A model compound study. *Fuel* **2014**, *133*, 106−114.
(71) Klein, G. C.; Kim, S.; Rodgers, R. P.; Marshall, A. G.; Yen, A. Mass Spectral Analysis of Asphaltenes. II. Detailed Compositional Comparison of Asphaltenes Deposit to Its Crude Oil Counterpart for Two Geographically Different Crude Oils by ESI FT-ICR MS. *Energy Fuels* **2006**, *20*, 1973−1979.
(72) Porto, C. F. C.; Pinto, F. E.; Souza, L. M.; Madeira, N. C. L.; Neto, Á. C.; de Menezes, S. M. C.; Chinelatto, L. S.; Freitas, C. S.; Vaz, B. G.; Lacerda, V.; et al. Characterization of organosulfur compounds in asphalt cement samples by ESI(+)FT-ICR MS and 13C NMR spectroscopy. *Fuel* **2019**, *256*, 115923.
(73) Qian, K.; Rodgers, R. P.; Hendrickson, C. L.; Emmett, M. R.; Marshall, A. G. Reading Chemical Fine Print: Resolution and Identification of 3000 Nitrogen-Containing Aromatic Compounds from a Single Electrospray Ionization Fourier Transform Ion Cyclotron Resonance Mass Spectrum of Heavy Petroleum Crude Oil. *Energy Fuels* **2001**, *15*, 492−498.
(74) Zhu, X.; Shi, Q.; Zhang, Y.; Pan, N.; Xu, C.; Chung, K. H.; Zhao, S. Characterization of Nitrogen Compounds in Coker Heavy Gas Oil and Its Subfractions by Liquid Chromatographic Separation Followed by Fourier Transform Ion Cyclotron Resonance Mass Spectrometry. *Energy Fuels* **2011**, *25*, 281−287.
(75) Chiron, J.; Galy, J.-P. Reactivity of the Acridine Ring: A Review. *Synthesis* **2004**, 313−325.
(76) Mirwald, J.; Werkovits, S.; Camargo, I.; Maschauer, D.; Hofko, B.; Grothe, H. Understanding bitumen ageing by investigation of its polarity fractions. *Constr. Build. Mater.* **2020**, *250*, 118809.

https://dx.doi.org/10.1021/acs.energyfuels.0c01242
Energy Fuels 2020, 34, 10641−10654

Investigation of aging processes in bitumen at the molecular level with high resolution Fourier transform ion cyclotron mass spectrometry and two-dimensional gas chromatography mass spectrometry

Supplemental material

Table S 1: Weighed portion of sample material for all measurements as well as the amount of non-evaporable residues weighed after the measurements. The red-marked sample "MP200 1D replicate 1" showed a negative value for the residue after the measurement and was considered as outlier.

Bitumen sample	crucible	sample	volatiles		residue	
	[mg]	[mg]	[mg]	[%]	[mg]	[%]
MP 200 original Replicate 1	22.44	1.00	0.84	84	0.16	16
MP 200 original Replicate 2	22.68	0.92	0.78	85	0.14	15
MP 200 original Replicate 3	22.31	1.05	0.91	87	0.14	13
MP 200 1D Replicate 1	21.92	0.98			-0.08	
MP 200 1D Replicate 2	22.30	1.09	0.89	82	0.20	18
MP 200 1D Replicate 3	22.20	0.96	0.82	85	0.14	15
MP 200 2D Replicate 1	22.39	1.09	0.89	82	0.20	18
MP 200 2D Replicate 2	22.40	1.02	0.82	80	0.20	20
MP 200 2D Replicate 3	22.56	1.14	0.94	82	0.20	18
MP 200 3D Replicate 1	22.56	1.04	0.91	87	0.13	13
MP 200 3D Replicate 2	22.37	1.00	0.86	86	0.14	14
MP 200 3D Replicate 3	22.48	1.14	0.88	77	0.26	23
MP 200 4D Replicate 1	22.54	1.04	0.91	87	0.13	13
MP 200 4D Replicate 2	22.35	1.10	0.91	83	0.19	17
MP 200 4D Replicate 3	22.46	1.10	0.93	85	0.17	15
MP 200 7D Replicate 1	22.24	1.06	0.85	80	0.21	20
MP 200 7D Replicate 2	22.28	1.12	0.86	77	0.26	23
MP 200 7D Replicate 3	22.35	0.98	0.71	72	0.27	28

Table S 2: GC×GC-HRTOF MS parameters.

Injection volume	1 µL (20 % wt solutions)
Injection temperature (PTV)	40°C – 2 °C/s – 400 °C (5 min hold)
Split flow	50 mL/min
Column flow	1.2 mL/min
Carrier gas	Helium (5.0)
1st Dimension Column	Phenomenex Zebron ZB-35HT Inferno (30 m × 0.25 mm; film: 0.1 µm)
2nd Dimension Column	SGE BPX1 (1.5 m × 0.1 mm; film: 0.1 µm)
Transferline	Agilent deactivated fused silica (0.8 m × 0.1 mm)
Modulation time	6 s (Hot pulses 2.5 s; Cold pulses: 0.5 s)
Primary oven temperature program	80 °C (5 min hold) – 2K/min – 400 °C (15 min hold)
Secondary oven temperature program	90 °C (5 min hold) – 1.95 K/min – 400 °C (15 min hold)
Modulator temperature program	105 °C (5 min hold) – 1.9 K/min – 400 °C (15 min hold)
Transferline Temperature	350 °C
MS acquisition delay	500 s
MS Acquisition rate	80 Hz
Mass range	40-800 m/z
Extraction frequency	1.5 kHz
Ion source temperature	300 °C
Ionization energy (EI)	70 eV
Mass calibration	PFTBA valve open during the whole run

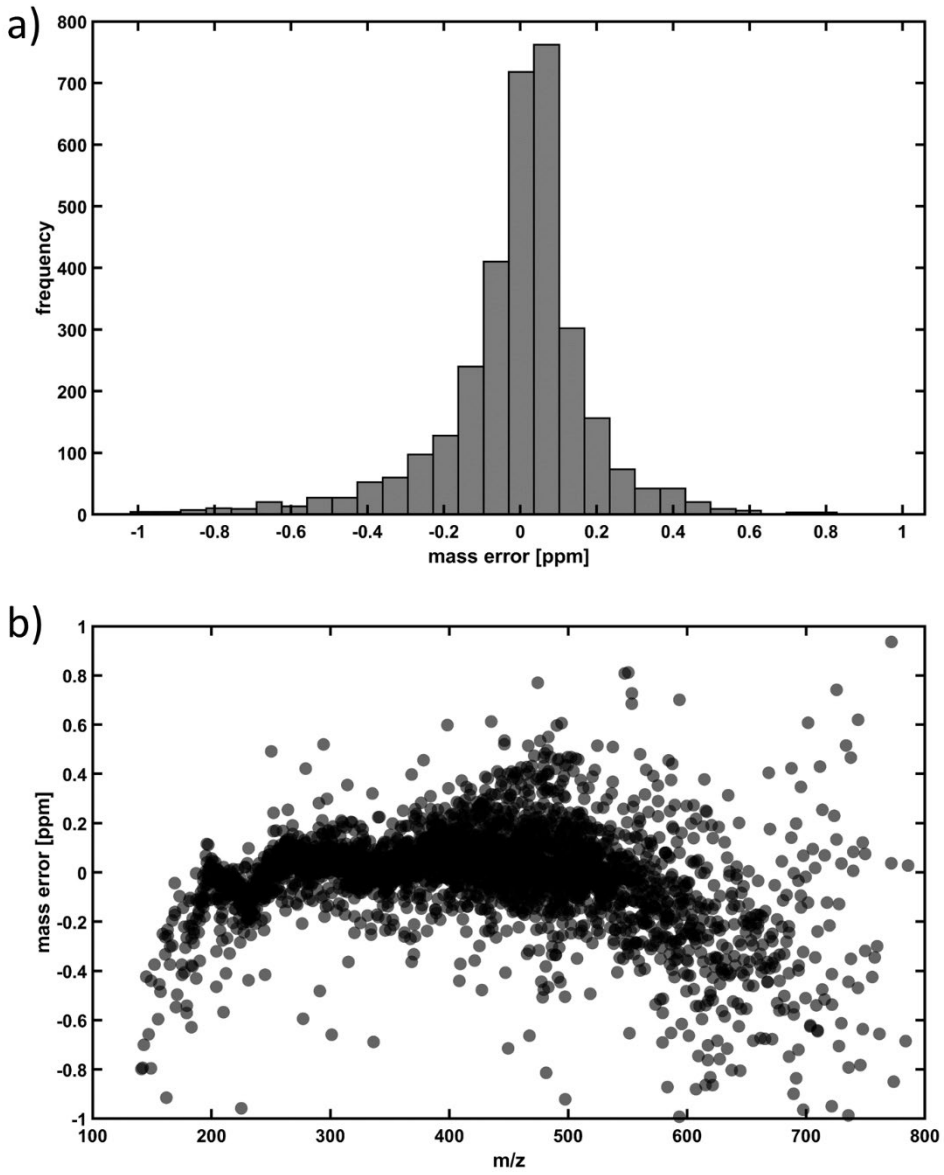

Figure S 1 Data quality of TG-FT-ICR MS data. a) Error histogram of the sum formula assignment exemplarily depicted for non-aged model bitumen. The error border for elemental composition calculation was set to 1 ppm. b) Mass error in ppm versus m/z. Generally, the root mean square error was below 0.28 ppm for MS-mode and below 0.31 ppm for MSMS-mode.

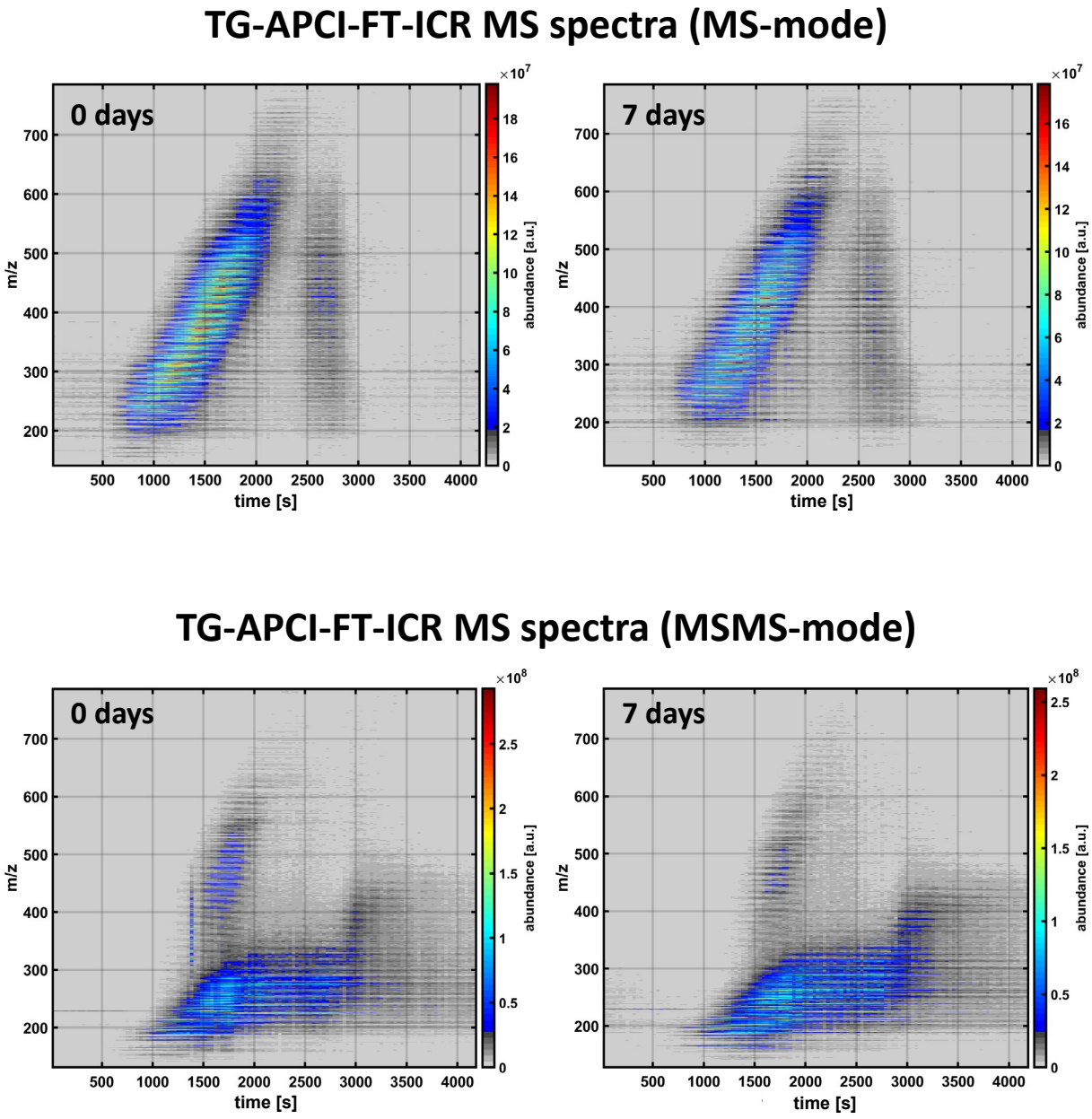

Figure S 2: Time resolved mass spectra of the TG-FT-ICR MS measurements for non-aged and 7 days-aged model bitumen. (top) Mass spectra obtained from intactly desorbed species and thermal fragments of pyrolyzed compounds. (bottom) CID-spectra of the alternating MSMS-mode.

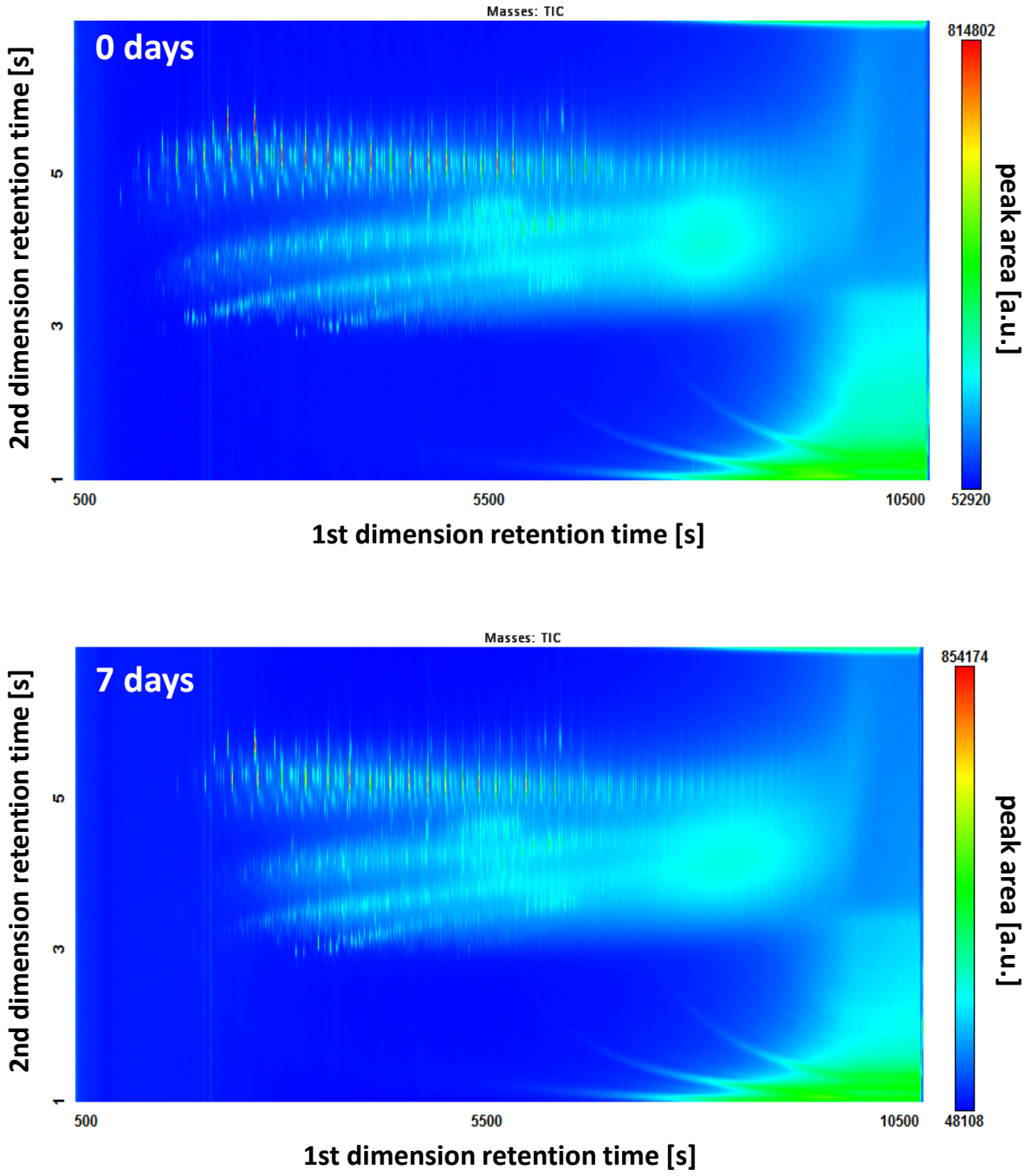

Figure S 3: Two-dimensional gas chromatograms obtained by GC×GC-HRTOF MS for non-aged and 7 days-aged model bitumen.

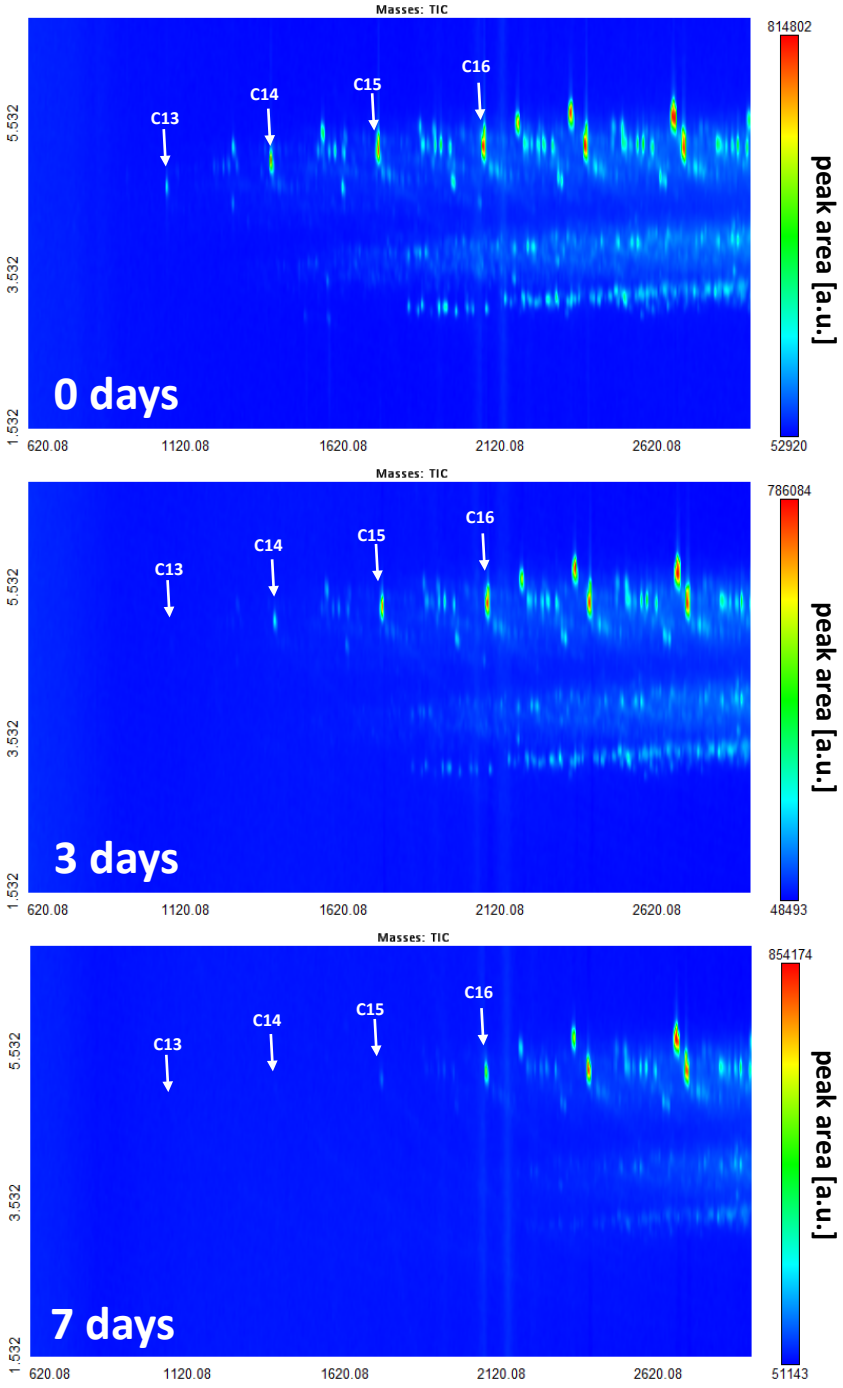

Figure S 4: Zoom in the region for low-boiling components of the GC×GC-HRTOF MS measurements. After severe aging, slight evaporation effects occur.

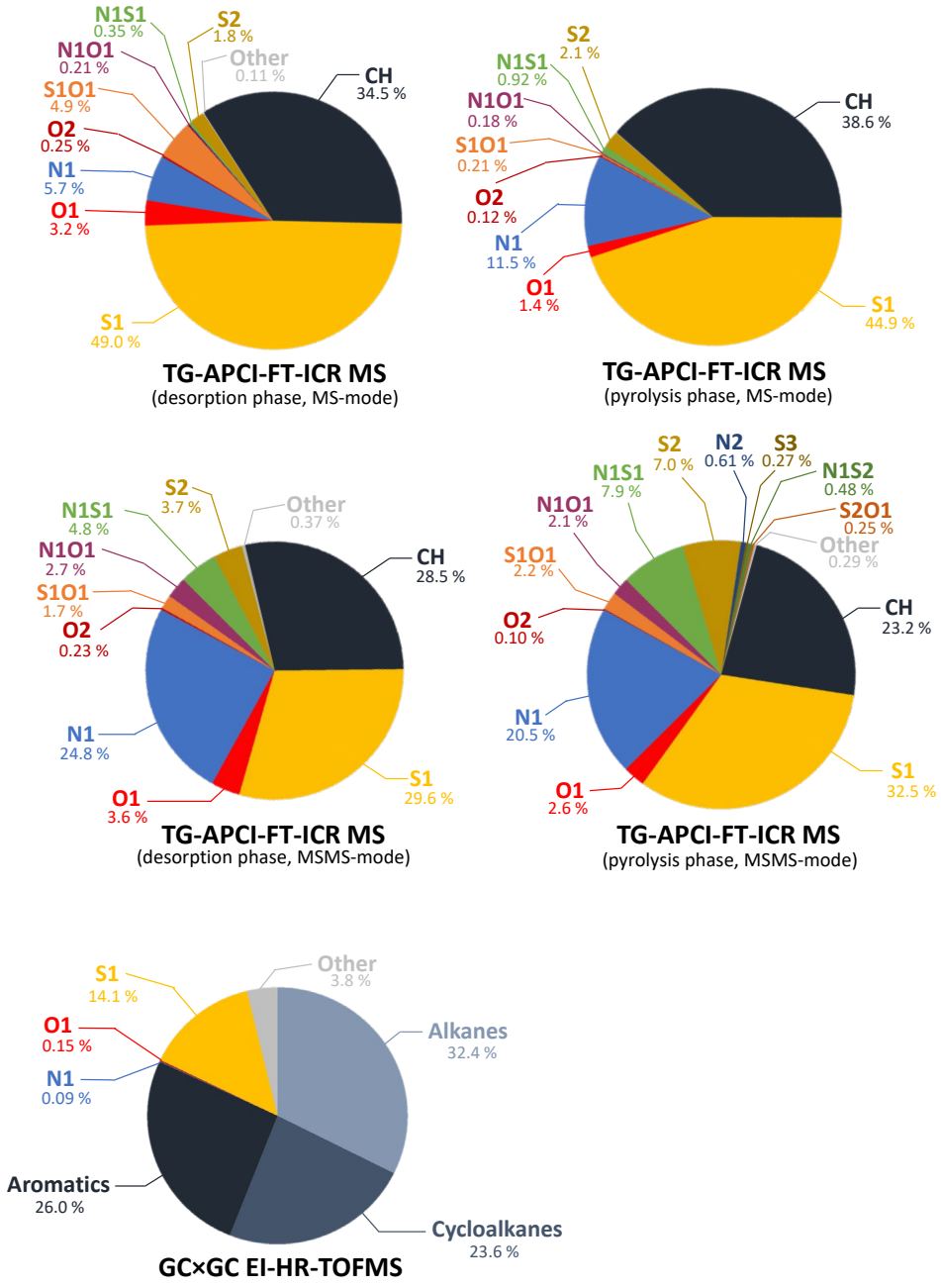

Figure S 5: Class distribution for non-aged model bitumen (average of three replicates) obtained by TG-APCI-FT-ICR MS and GC×GC-EI-HRTOF MS.

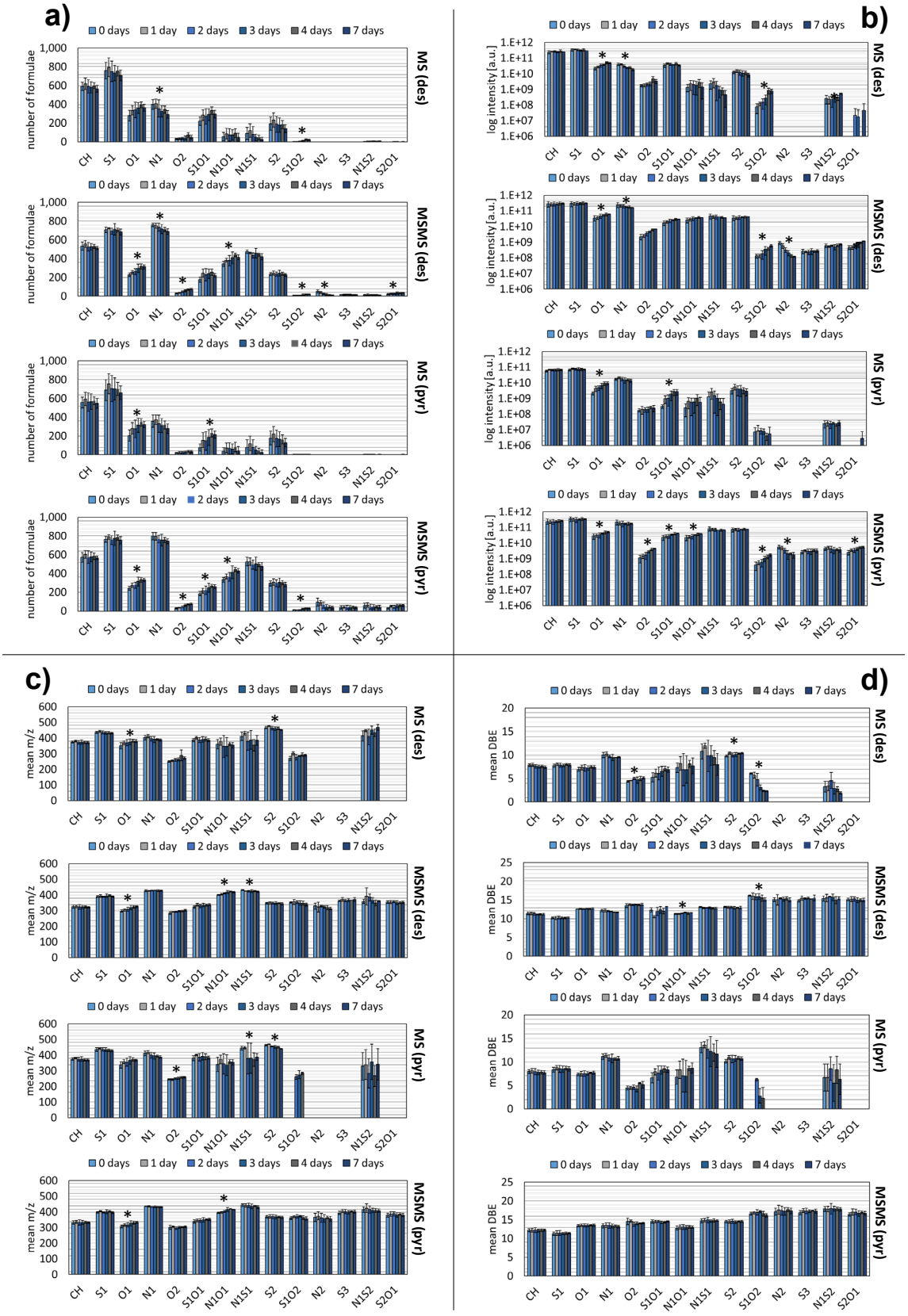

Figure S 6: Collection of average parameters for desorption and pyrolysis phase for MS and MSMS-mode. a) number of calculated sum formula, b) common logarithm for summed intensity, c) intensity-weighed mean m/z and d) intensity-weighed mean DBE.

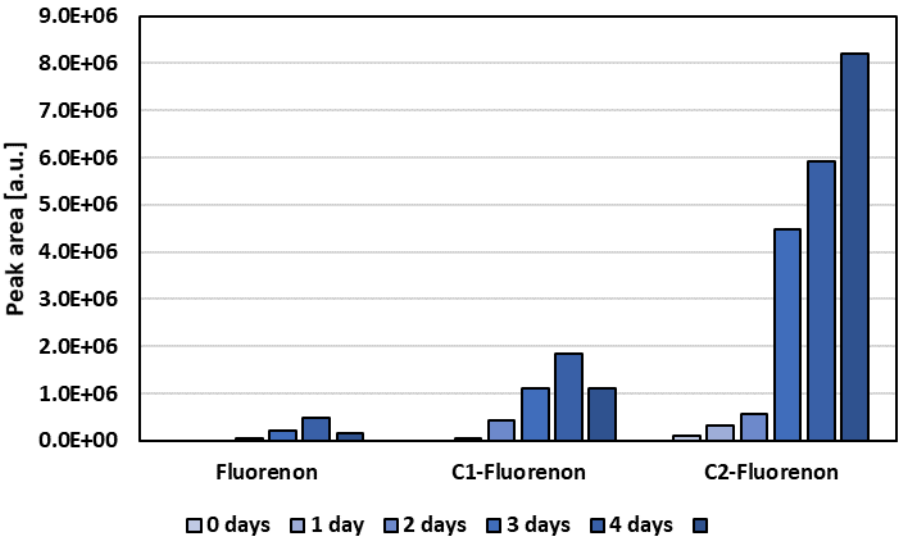

Figure S 7: Summed peak area of fluorenones with different alkylation degree revealed by GC×GC-HRTOF MS for all aging stages.

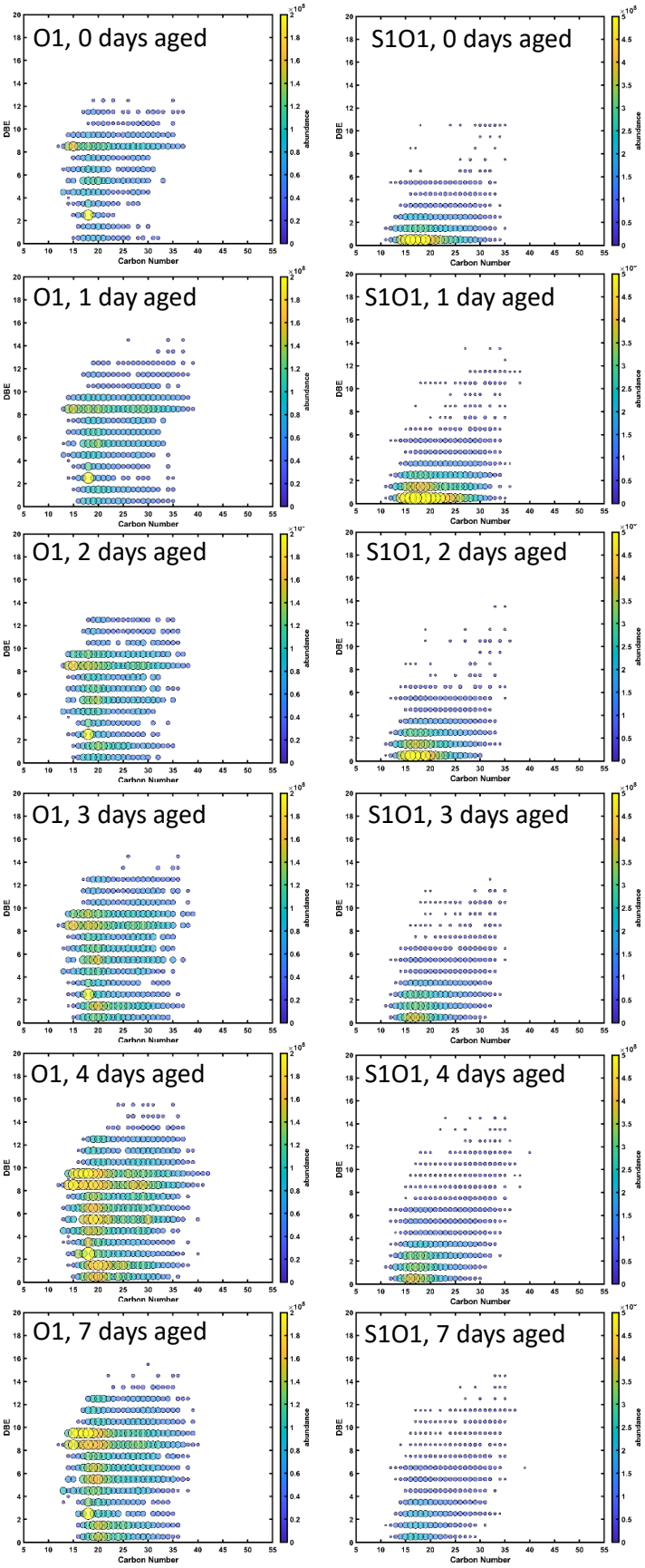

Figure S 8: Complete aging row for the O1- and S1O1-class of the desorption phase in MS-mode. While the O1-class shows a distinct increase for species with carbon numbers of 10 to 25 and a DBE of 1 to 10, the S1O1-class reveals a different behaviour. Species with DBE 1 to 2 in the S1O1-class show a slight increase after 1 day of aging and start to decrease after 2 days of aging. At the same time, species with higher DBEs are increasing.

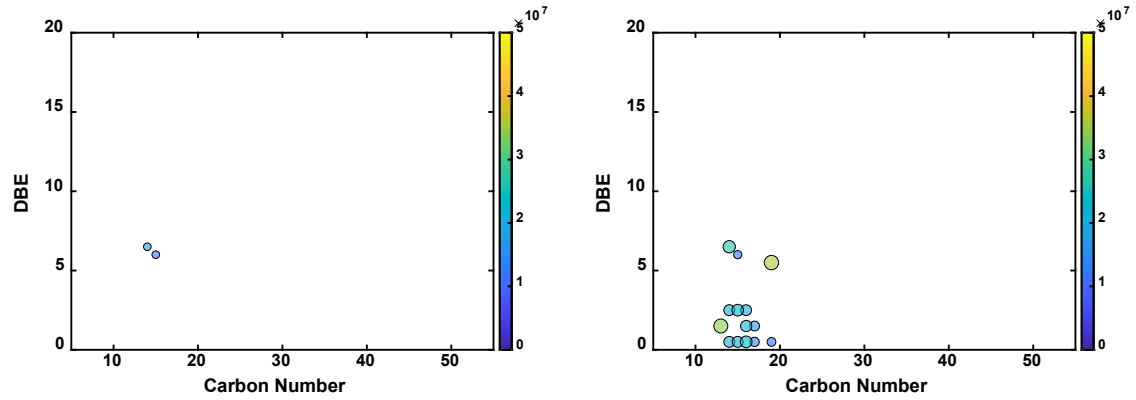

Figure S 9: Comparison of the S1O2-class for the desorption phase of the non-aged model bitumen (left) and 7 days-aged model bitumen (right). The increase in low DBE-species during aging may arise from the decrease of low DBE species observed in the S1O1-class due to further oxidation.

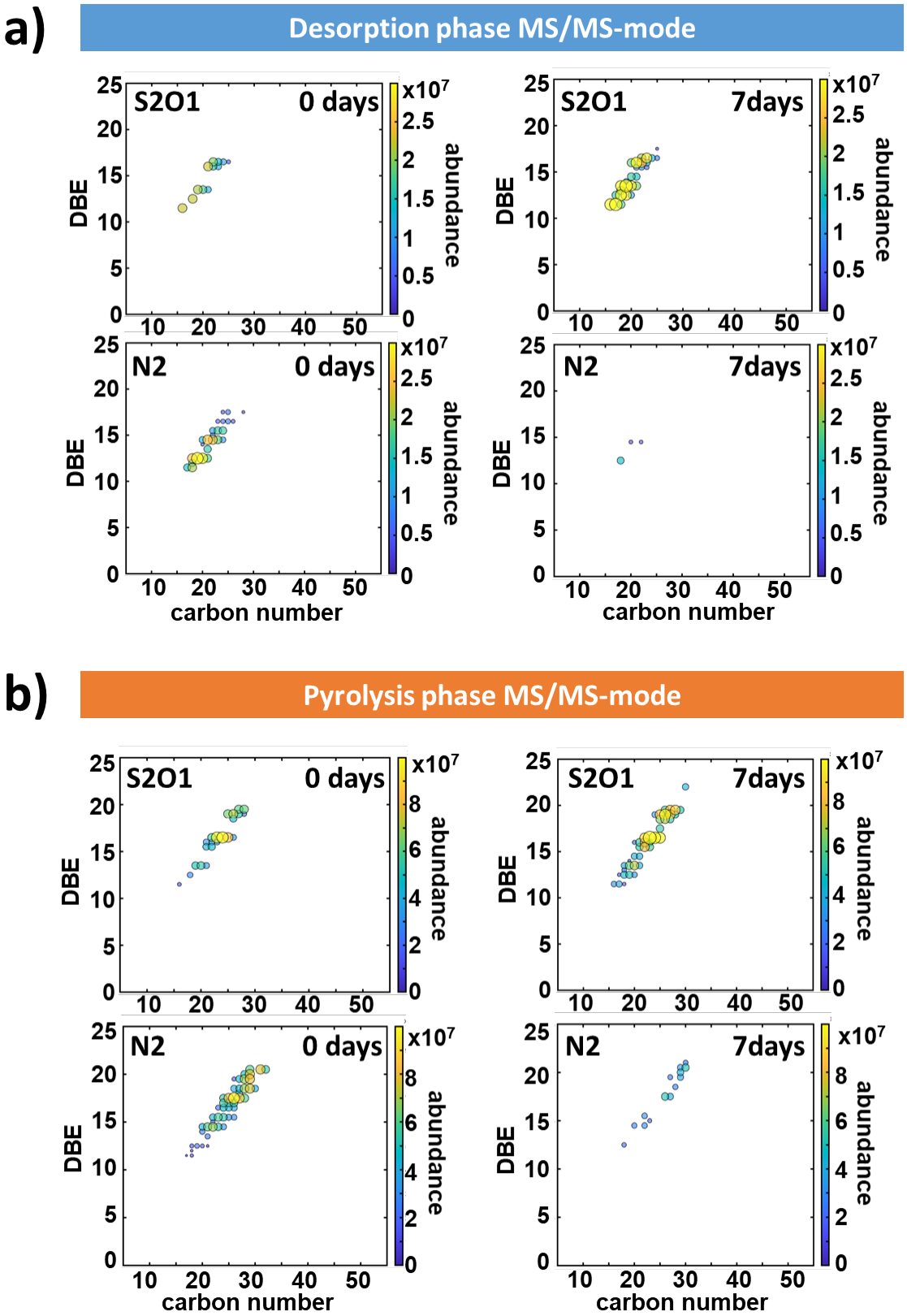

Figure S 10: DBE vs. #C diagrams of the S2O1- and N2-class for the desorption and pyrolysis phase. Due to very low intensity, both classes are only detected in MS/MS-mode.

Publication 5

Investigation of island/ single core and archipelago/ multicore enriched asphaltenes and their solubility fractions by thermal analysis coupled to high resolution Fourier transform ion cyclotron resonance mass spectrometry

by

Anika Neumann, Martha Liliana Chacón-Patiño, Ryan P. Rodgers, Christopher P. Rüger, Ralf Zimmermann

Energy and Fuels, 2021, 35 (5), S. 3808–3824

DOI: 10.1021/acs.energyfuels.0c03751

Publication 6

Atmospheric pressure single photon laser ionization (APSPLI) mass spectrometry using a 157 nm Fluorine excimer laser for sensitive and selective detection of non-polar to semi-polar hydrocarbons

by

Rüger, Christopher P.; Neumann, Anika; Sklorz, Martin; Zimmermann, Ralf

Analytical Chemistry, 93 (8), S. 3691-3697

DOI: 10.1021/acs.analchem.0c04740